NASA/CR-96- 206507

Final Technical Report

NASA Contract #: NAG 3 – 1539

**Report Title: Comparison of the Aeroacoustics of Two Small-Scale Supersonic Inlets**

Principal Investigator

Wing Ng

September 1996

# Comparison of the Aeroacoustics of Two Small-Scale Supersonic Inlets

by

Kevin C. Miller

Dr. W. F. Ng, Chairman

Mechanical Engineering

(ABSTRACT)

An aerodynamic and acoustic investigation was performed on two small-scale supersonic inlets to determine which inlet would be more suitable for a High Speed Civil Transport (HSCT) aircraft during approach and takeoff flight conditions. The comparison was made between an axisymmetric supersonic P inlet and a bifurcated two-dimensional supersonic inlet. The 1/14 scale model supersonic inlets were used in conjunction with a 4.1 in (10.4 cm) turbofan engine simulator. A bellmouth was utilized on each inlet to eliminate lip separation commonly associated with airplane engine inlets that are tested under static conditions. Steady state measurements of the aerodynamic flowfield and acoustic farfield were made in order to evaluate the aeroacoustic performance of the inlets. The aerodynamic results show the total pressure recovery of the two inlets to be nearly identical, 99% at the approach condition and 98% at the takeoff condition. At the approach fan speed (60% design speed), there was no appreciable difference in the acoustic performance of either inlet over the entire 0° to 110° farfield

measurement sector. The inlet flow field results at the takeoff fan speed (88% design speed), show the average inlet throat Mach number for the P inlet (Mach 0.52) to be approximately 2 times that of the 2D inlet (Mach 0.26). The difference in the throat Mach number is a result of the smaller throughflow area of the P inlet. This reduced area resulted in a "soft choking" of the P inlet which lowered the tone and overall sound pressure levels of the simulator in the forward sector by an average of 9 dB and 3 dB, respectively, when compared to the 2D inlet.

# Acknowledgments

I would like to take this opportunity to thank the many individuals who have contributed to this thesis and made my graduate studies a very memorable experience. My sincere thanks to professors Dr. Ricardo A. Burdisso, Dr. Clinton L. Dancey, and Dr. Wing F. Ng for giving their valuable time and insight while serving on my advisory committee. I want to express a special thanks to Dr. Wing F. Ng for providing me with this opportunity and for his encouragement and patience.

I would also like to thank Dr. Todd Ninneman, David White, Tom Leitch, Zhenguo Yuan, Kevin Detwiler, Rob Wagner, Jeff Kozak, and Dikran Akseraylian. They made my graduate experience much more enjoyable and helped me out during hard times. I truly value their friendship and company. A special thanks to Todd Ninneman , David White, and Tom Leitch for their invaluable advice and hard work.

I also wish to thank my parents, Tom and Barbara, my brother, Ben, and my sister Kelley, for their continuous support and encouragement throughout my engineering studies. Finally, I would like to thank all of my friends back home for their support during my entire college experience.

# Table of Contents

**1.0 Introduction** ..... **1**

**2.0 Background** ..... **7**

2.1 Previous Research ..... 7

2.2 Understanding Fan Noise ..... 9

**3.0 Experiment** ..... **13**

3.1 Turbofan Engine Simulator ..... 13

3.2 Supersonic Inlets ..... 15

3.2.1 Axisymmetric P Inlet ..... 16

3.2.2 Bifurcated Two-Dimensional Inlet ..... 20

3.2.3 Geometry Comparison of the P Inlet and 2D Inlet ..... 24

3.3 Research Facility ..... 29

3.4 Aerodynamic Measurements ..... 31

3.4.1 Instrumentation ..... 32

3.4.2 Aerodynamic Setup ..... 32

3.5 Acoustic Measurements ..... 36

3.5.1 Instrumentation ..... 36

3.5.2 Acoustic Setup ..... 37

3.6 Test Matrix ..... 39

**4.0 Results and Discussion ..... 43**

4.1 Aerodynamic Results ..... 43

4.1.1 Inlet Cowl Lip Separation ..... 44

4.1.2 Fan Operating Condition ..... 46

4.1.3 Throat Station ..... 48

4.1.4 Inlet Flow Distortion ..... 54

4.1.5 Inlet Pressure Recovery ..... 62

4.2 Acoustic Results ..... 68

4.2.1 Soft Choking Effect ..... 69

4.2.2 Radiated Noise Levels ..... 72

4.2.3 Narrowband Noise Spectra ..... 80

4.2.4 Modal Analysis ..... 83

**5.0 Conclusions** ..... **89**

**Appendix A. Bellmouth Test** ..... **92**

**Appendix B. Fan Exit Area Test** ..... **97**

**Appendix C. Circumferential Distortion Method** ..... **102**

**Appendix D. Acoustic Measurement Plane Comparison** ..... **115**

**References** ..... **121**

**Vita** ..... **124**

# List of Illustrations

Figure 3.1 Turbofan Engine Simulator ..... 14

Figure 3.2 NASA P Inlet ..... 17

Figure 3.3 Axisymmetric P Inlet in Research Facility ..... 18

Figure 3.4 Isometric Views of the P Inlet ..... 19

Figure 3.5 NASA Bifurcated Two-Dimensional Inlet ..... 21

Figure 3.6 Bifurcated 2D Inlet in Research Facility ..... 22

Figure 3.7 Isometric Views of the 2D Inlet ..... 23

Figure 3.8 Front Face Views of the Inlets ..... 25

Figure 3.9 Rear Face Views of the Inlets ..... 26

Figure 3.10 Cutaway Profile of the P Inlet and 2D Inlet Comparing Throughflow Area ..... 27

Figure 3.11 Throughflow Area Comparison Graph of the P Inlet and 2D Inlet ..... 28

Figure 3.12 Research Facility ..... 30

Figure 3.13 P Inlet Aerodynamic Measurement Locations ..... 34

Figure 3.14 2D Inlet Aerodynamic Measurement Locations ..... 35

Figure 3.15 Microphone Positions, Plane View ..... 38

Figure 3.16 P Inlet Acoustic Measurement Planes ..... 40

Figure 3.17 2D Inlet Acoustic Measurement Planes ..... 41

Figure 4.1 Total Pressure Recovery Profiles at the Lip Station, 60 PNC and 88 PNC ..... 45

Figure 4.2 Fan Performance Map ..... 47

Figure 4.3 Inlet Throat Mach Number vs. Blade Tip Speed ..... 50

Figure 4.4 Inlet Throat Mach Number Profiles at the Throat Station, 60 PNC and 88 PNC ..... 52

Figure 4.5 Total Pressure Recovery Profiles at the Throat Station, 60 PNC and 88 PNC ..... 53

Figure 4.6 Hypothetical Gradients of Axial Velocity Distortion at the Fan Face ..... 56

Figure 4.7 Mach Number Distribution at the Fan Face, 60 PNC ..... 57

Figure 4.8 Mach Number Distribution at the Fan Face, 88 PNC ..... 59

Figure 4.9 Wake Profile Traverse Stations ..... 60

Figure 4.10 Wake Profile Behind Strut, 60 PNC and 88 PNC ..... 61

Figure 4.11 Total Pressure Recovery Distribution at the Fan Face, 60 PNC ..... 63

Figure 4.12 Total Pressure Recovery Distribution at the Fan Face, 88 PNC ..... 65

Figure 4.13 Inlet Throat Mach Number and Tone Sound Pressure Level vs. Blade Tip Speed at the 20° Microphone Location ..... 70

Figure 4.14 Inlet Throat Mach Number and Overall Sound Pressure Level vs. Blade Tip Speed at the 20° Microphone Location ..... 71

Figure 4.15 Directivity Plots at 60 PNC (Approach Condition) ..... 73

Figure 4.16 Sideline Estimates for Blade Passing Tone, 60 PNC ..... 76

Figure 4.17 Directivity Plots at 88 PNC (Takeoff Condition) ..... 78

Figure 4.18 Sideline Estimates for Blade Passing Tone, 88 PNC ..... 79

Figure 4.19 Sample Spectra at the 0° Microphone Location, 60 PNC ..... 81

Figure 4.20 Sample Spectra at the 20° Microphone Location, 60 PNC ..... 82

Figure 4.21 Sample Spectra at the 0° Microphone Location, 88 PNC ..... 84

Figure 4.22 Sample Spectra at the 20° Microphone Location, 88 PNC ..... 85

Figure 4.23 Example of Acoustic Lobe Radiation Pattern ..... 88

Figure A.1 Total Pressure Recovery Profiles at the Lip Station of the P Inlet and the Throat Station of the 2D Inlet With and Without Bellmouth, 88 PNC ..... 94

Figure A.2 Directivity Plots of the P Inlet With and Without Bellmouth, 88 PNC ..... 95

Figure A.3 Sample Spectra at the 20° Microphone Location of the P Inlet With and Without Bellmouth, 88 PNC ..... 96

Figure B.1 Mach Number and Total Pressure Recovery Profiles for P Inlet at the 45° Circumferential Fan Face Station Comparing New and Old Fan Exit Area, 88 PNC ..... 99

Figure B.2 Directivity Plots of the P Inlet Comparing New and Old Fan Exit Area, 88 PNC ..... 100

Figure B.3 Sample Spectra at the 20° Microphone Location of the P Inlet Comparing New and Old Fan Exit Area, 88 PNC. ..... 101

Figure D.1 Directivity Plots of the P Inlet at 60 PNC Comparing Acoustic Planes ..... 117

Figure D.2 Directivity Plots of the P Inlet at 88 PNC Comparing Acoustic Planes ..... 118

Figure D.3 Directivity Plots of the 2D Inlet at 60 PNC Comparing Acoustic Planes .. 119

Figure D.4 Directivity Plots of the 2D Inlet at 88 PNC Comparing Acoustic Planes .. 120

# List of Tables

Table 4.1 Fan Pressure Ratio ..... 48

Table 4.2 Average Throat Mach Numbers ..... 49

Table 4.3 Fan Face Area Averaged Total Pressure Recovery ..... 66

Table 4.4 Total Pressure Circumferential Distortion Intensities ..... 68

Table 4.5 2D Inlet Modal Analysis ..... 87

Table A.1 Fan Face Area Averaged Total Pressure Recovery With and Without Bellmouth ..... 93

Table B.1 Fan Pressure Ratio for the 2D Inlet, Old and New Fan Exit Area ..... 97

Table B.2 Fan Pressure Ratio for the P Inlet, Old and New Fan Exit Area ..... 98

# Nomenclature

| | |
|---|---|
| BPT | Blade Passing Tone |
| BPF | Blade Passing Frequency |
| dB | Decibel, sound pressure level, reference pressure $20 \times 10^{-6}$ Pascal |
| Hz | Hertz, frequency |
| FFT | Fast Fourier Transform |
| RPM | Revolutions Per Minute |
| PNC | Percent Corrected Fan Speed |
| $K$ | Acoustic Wave Number |
| SPL | Sound Pressure Level |

# 1.0 Introduction

Over 20 years ago, the Concorde entered air service under the collaboration of British Airways and Air France. They were the first to develop a supersonic cruise aircraft for commercial transportation. Shifting from subsonic flight to supersonic flight was a big step for any commercial airline to take. However, supersonic flight became more and more necessary as economic markets expanded globally, creating a demand for faster long distance transportation. Supersonic planes significantly reduce the amount of time it takes to travel on long distance flights and the businesses of today see this as an increasingly attractive feature. Unfortunately, the Concorde failed to reach its economic projections partly due to its unacceptable airport community noise levels and the overland sonic boom that follows the aircraft at supersonic speeds. Recently, NASA initiated a High Speed Civil Transport (HSCT) research program to develop a supersonic passenger aircraft and investigate its feasibility for commercial transportation.

Boeing Commercial Airplane Group and McDonnell Douglas Aerospace have teamed together under a NASA contract to develop technologies for a 21st Century high-speed passenger jet. The proposed airliner will be able to fly 300 passengers to Europe or

the Pacific Rim at 2.4 times the speed of sound, cutting existing travel time by more than half. It will be able to fly faster than the Concorde and twice as far, carrying three times as many passengers at a lower cost. The development is now in Phase II, which focuses on moving technology concepts out of the laboratory and into practical applications. Phase II will concentrate on developing and providing the technology necessary to make the future supersonic airliner economically practical as well as environmentally acceptable. The principal objective of the aerodynamic effort is to develop technology to increase supersonic and subsonic cruise performance [Carden, 1994].

The environmental impact of a supersonic transport (SST) has an important role in the design of the aircraft. If a supersonic plane is going to be successful the impact on the environment has to be significantly reduced compared to the Concorde. Two major environmental factors of the SST are airport community noise and atmospheric emissions. The noise levels of the engine will have to meet the FAR 36 Stage 3 noise regulations to provide acceptable airport community noise. The emissions of a supersonic aircraft at altitudes coincident with the highest concentration of atmospheric ozone will require reducing $NO_x$ emissions to levels that have no significant impact on the Earth's ozone layer. These technical challenges are currently being investigated to determine how their impact on the environment can be minimized.

A major effort is being applied to the SST's ability to meet the restrictions on airport community noise. The noise levels of an aircraft reach their peak on landing approach and takeoff. Although jet noise is expected to be the predominant noise source

for SST aircraft, previous analysis by Trefny and Sofrin shows that "forward propagating fan noise is a significant noise component during takeoff and approach." The design of an engine inlet determines many of the properties of the forward propagated fan noise. In this case, the supersonic inlet of the SST has to be carefully examined. The purpose of a supersonic engine inlet is to compress supersonic flow entering the engine to nearly a sonic Mach number at the throat and then diffuse the flow to a subsonic speed at the fan face, while minimizing pressure losses [Sauders et. al., 1991]. Supersonic inlets require many more complex features than the conventional subsonic inlets because the engine has to be able to perform at both supersonic and subsonic flight speeds. Supersonic inlets typically include auxiliary inlet doors, boundary layer bleed systems, and translating or variable geometry centerbodies to change the throat area for different flight conditions. These features are currently being investigated to determine the effects on the fan radiated engine noise.

The NASA Lewis research center began to investigate low speed aeroacoustic performance of a supersonic inlet in 1983 under the Supersonic Cruise Aircraft Research program. Testing was performed in the NASA Lewis 9x15 foot anechoic wind tunnel with a 1/3 scale model of an axisymmetric, mixed-compression supersonic inlet that was coupled with a 0.4 scale JT8D refan simulator. The wind tunnel airspeeds ranged from Mach 0.0 to 0.2 for the test cases to simulate low airspeeds.

NASA is currently investigating two different supersonic inlet designs. One is given the term axisymmetric P inlet and the other is the bifurcated two-dimensional inlet. Each inlet has several advantages and disadvantages for a supersonic aircraft. Currently, the P inlet was NASA's first choice and the design is very simple and lighter in weight than the 2D inlet. During supersonic operation, the P inlet is prone to an unstart condition. However, at transonic conditions the throat area of the P inlet is not large enough for the engine operation and the auxiliary doors may have to be opened. On the contrary, the 2D inlet has a larger throat area due to the centerbody design and the transition from a rectangular opening to a circular cross section at the engine fan face. This inlet is very stable when compared to the P inlet because of the large throughflow area. Therefore, the 2D inlet will not have as big of an engine unstart problem as the P inlet. In summary, it is not clear at this point which inlet may be better, and research is needed to characterize the aeroacoustic performance of the two inlets.

Several years ago, the Virginia Tech noise research program for supersonic inlets was initiated to provide preliminary aerodynamic and acoustic results for future detailed full scale tests. The objective of the research was to examine the generation and radiation of turbomachinery fan noise from a supersonic inlet. The experiment was performed by using a 1/14 scale supersonic inlets coupled with a 4.1 in (10.4 cm) turbofan engine simulator. A lower experimental cost is a great benefit to the research program, therefore the small scale inlets and simulator used at Virginia Tech were valuable. With the complexity of the supersonic inlet, the test matrix can be extremely large. This small-

scale experimental test program will provide initial results on how the inlets may reduce the impact of a supersonic aircraft on airport community noise. Previous studies on supersonic inlet noise have been performed by Nuckolls, Detwiler, Pande, and Wagner under this research program.

The current research by Virginia Tech focuses on evaluating a NASA axisymmetric P inlet configuration and a NASA bifurcated 2D inlet configuration at simulated approach and takeoff conditions. The two inlets can be directly compared since both are setup for the appropriate flight conditions. The evaluation is performed by comparing the sound pressure levels radiated in the farfield, inlet pressure losses, and inlet Mach numbers. The tests were performed in the Virginia Tech anechoic chamber at static conditions without a wind tunnel providing in flight effects. However, both inlets were equipped with a bellmouth to eliminate flow separation at the cowl lip. The bellmouth reduced the cowl lip separation regions that were experienced during previous tests of the inlets. The supersonic inlet testing procedure was developed by Nuckolls and Ng and was used in the current research.

This thesis is organized into five chapters. The next chapter explains previous research and gives a basic understanding of the generation of fan noise. Chapter Three describes the test procedures and facilities by detailing the two supersonic inlets, turbofan simulator, and measurement techniques. Chapter Four provides the aeroacoustic performance comparison of the P inlet and the 2D inlet. Conclusions from the investigation are discussed in Chapter Five. Finally, the bellmouth effects, turbofan

simulator exit area effects, pressure related fan face distortion calculations, and acoustic plane comparisons of the individual inlets are presented in Appendices A through D.

# 2.0 Background

This chapter consists of two sections. The first section presents some previous research conducted on the axisymmetric P inlet and the bifurcated two-dimensional inlet. The second section describes the causes of noise generation and propagation in turbofan engines.

## 2.1 Previous Research

Nuckolls and Ng developed the Virginia Tech supersonic inlet research program by using the axisymmetric, mixed compression P inlet designed by NASA. Their research program, which involved the testing of a new auxiliary door geometry, was directed at reducing the noise from the inlet at a subsonic fan speed of 50,000 RPM (60 PNC) simulating aircraft landing approach conditions. Detwiler and Ng used the same P inlet configuration, except they studied the auxiliary door geometry at a fan speed of 70,000 RPM (88 PNC) simulating takeoff conditions. In both test cases, the results

showed a reduction of the blade passing frequency tone due to the choking effect of the auxiliary doors. These test were performed without the use of a bellmouth to reduce cowl lip separation commonly experienced in a static test environment. Further tests, using a bellmouth on the P inlet, are needed to explain the aeroacoustic performance of the inlet in more detail at approach and takeoff conditions.

Wagner and Ng were the first to evaluate the aeroacoustic performance of a bifurcated two-dimensional, mixed compression supersonic inlet, designed by NASA, under the Virginia Tech research program. These results were not appropriate for approach and takeoff conditions because large cowl lip separation regions were experienced. The effects of the lip separation in the 2D inlet experiments proved to be very substantial to the flow distortion at the fan face. For these reasons, a bellmouth needed to be designed for the 2D inlet before any additional experiments could be conducted. Kozak and Ng investigated the 2D inlet to determine the extent of inlet flow distortions at the fan face. They used 3D CFD code to establish a model of the inlet flow field. The numerical simulation performed was modeled without cowl lip separation. The results showed the flow throughout the inlet was well behaved. Anderson, et al. (1994) and Saunders, et al.(1991) have performed several computational analyses on the 2D inlet at supersonic cruise speeds. Now there is a growing need to test the aerodynamic and acoustic performance of bifurcated two-dimensional inlets at approach and takeoff conditions and compare them to their axisymmetric counterparts. The only acoustic performance testing done on the 2D inlet was by Wagner and Ng without a

bellmouth. Therefore, the next step in the research program is to compare the two different supersonic inlets directly for the approach and takeoff flight conditions and examine the overall areoacoustic performance.

## 2.2 Understanding Fan Noise

There are three distinct types of noise generated by a fan which can be identified in the acoustic far field. They are know as pure tone fan noise, combination tone noise, and broadband noise. The predominant noise is the pure tone fan noise, occurring at the fundamental blade passing frequency (BPF). Tyler and Sofrin have shown that high pure tone fan noise for subsonic and supersonic rotors is due to the interaction between the rotating fan blades and the stationary vanes. Pure tone fan noise is generated at a frequency equal to $BN$, where $B$ is the number of fan blades and $N$ is the rotational speed of the fan. Combination tone fan noise is caused when the fan blade tip velocity becomes supersonic relative to the flow entering the fan. This noise is comprised of a series of tones located at integer multiples of the fan rotational speed ($f_k=kN,\ k=1,2,3...$). Each of the fan blades will shed shock waves in the upstream flow direction that vary in intensity due to small differences in the blade profiles. As these waves propagate, they will coalesce and cancel to form a combination tone frequency spectrum. The combination tones will occur in addition to the blade passing frequency generated by the sonic portion of the rotating fan blades. The broadband noise forms the spectral background between

the tones. There is generally no way of knowing whether the noise originates in the rotor or stators, whether it is produced by incident turbulence interacting with the blade rows, or whether it is random unsteadiness produced in the blade rows themselves [Oates (1985)]. All three types of noise have a significant effect on the far field acoustic spectrum recorded from the fan.

Tyler and Sofin have theoretically explained the generation and propagation of pressure modes in annular ducts. The blade passing tone results from the interaction of the rotating fan blades and the stationary disturbances. This interaction produces spinning pressure patterns that propagate in a spiraling fashion in the duct. The pressure pattern will either propagate out of the duct or decay to a negligible level. Each pressure pattern consists of a number of lobes, $m$ or cycles of pressure variations. Where the only allowable values of $m$ are given by:

$$m = nB \pm kV$$

$n$: Harmonic of blade passing frequency

$B$: Number of fan blades

$k$: Spatial harmonic of the distortion produced by the disturbance $\pm 1,2,3\ldots$

$V$: Number of stationary disturbances

In this research, the Model 460 turbofan simulator (See Section 3.1) has 18 rotor blades ($B$=18) and experiences two apparent circumferential distortions. The row of stator vanes ($V$=26) behind the fan and either the P inlet's centerbody support struts ($V$=4) or the 2D inlet's centerbody trailing edge ($V$=2) are the two distortions the fan will see. Each of the disturbances can produce an infinite number of modal pressure patterns, but only a finite number of patterns will propagate out of the duct without decaying. The propagation of a generated pressure mode in a duct is determined by the wave number, $K_{x\mu}$:

$$K_{x\mu} = \frac{2\pi}{c}\sqrt{f^2 - f_{m\mu}{}^2}$$

where, $f$ is the frequency of the blade passing tone, $f_{m\mu}$ is the cut-off frequency of the $(m,\mu)$ mode, $m$ is the number of circumferential lobes, $\mu$ is the radial order of the mode, and $c$ is the speed of sound. From the above equation, a modal pattern is considered cut-off if the axial wave number has an imaginary value ($f_{m\mu}>f$). Cut-off is a condition in which the amplitude of the level of the modal pattern will decay rapidly to negligible levels in the duct. For a modal pattern to propagate through the duct, the cut-off frequency of the mode must be less than the blade passing frequency of the tone. If the modal pattern propagates out of the duct, it is termed cut-on.

The equation for the wave number, $K_{x\mu}$ can be put in terms of the circumferential Mach number for a particular mode and critical Mach number at the outer wall:

$$K_{x\mu} = \frac{m}{b}\sqrt{\left|M_m^{\,2} - \left(\frac{k_{m\mu}^{(\sigma)}}{m}\right)^2\right|}$$

$\sigma = \frac{a}{b}$: Hub-tip ratio ($a$=hub radius, $b$=tip radius)

$M_m = \frac{nB}{m} M_{tip}$: Circumferential tip Mach number

$M_{tip}$: Blade tip Mach number

$\left(\frac{k_{m\mu}^{(\sigma)}}{m}\right) = M_m^*$ : Critical circumferential tip Mach number

$k_{m\mu}^{(\sigma)}$: Characteristic number associated with the E-functions describing the radial pressure distribution for a given hub-tip ratio

The transition from decay to propagation occurs when the circumferential tip Mach number, $M_m$, equals the value of the critical circumferential tip Mach number, $M_m^*$. Therefore, the transmission characteristics can be summed up as follows:

$M_m < M_m^*$ mode decays

$M_m > M_m^*$ mode propagates

A mode cut-off ratio can be defined such that $\xi = \frac{M_m}{M_m^*}$

$\xi < 1$ mode decays

$\xi > 1$ mode propagates

For the Model 460 turbofan simulator used in this research, the cut-off ratios for the test speeds of 50,000 RPM (60 PNC) and 70,000 RPM (88 PNC) where greater than 1 for all of the higher order modes of the rotor-stator interaction for the 2D inlet and P inlet. This proved that the generated pressure modes would be cut-on and propagate from the inlet to the farfield.

# 3.0 Experiment

This chapter describes the experimental setup. The first section presents the turbofan simulator. The second section describes the two small scale supersonic inlets. The test facility is described in section three. The next two sections explain the instrumentation and setup used to measure the aeroacoustics of the inlets. The last section outlines the test matrix.

## 3.1 Turbofan Engine Simulator

A Model 460 turbofan engine simulator, manufactured by Tech Development, was use in conjunction with the supersonic inlets in the experiment. The simulator is used to drive the inlet airflow and produce engine noise signals of a turbofan engine. Figure 3.1 shows a picture of the turbofan simulator and its rotating components. The simulator has a single-stage fan section consisting of 18 fan blades (4.1 inch diameter) and 26 stator blades. The fan is powered by a single-stage turbine with 29 blades and driven by compressed air. The Model 460 has a design speed of 80,000 RPM and is

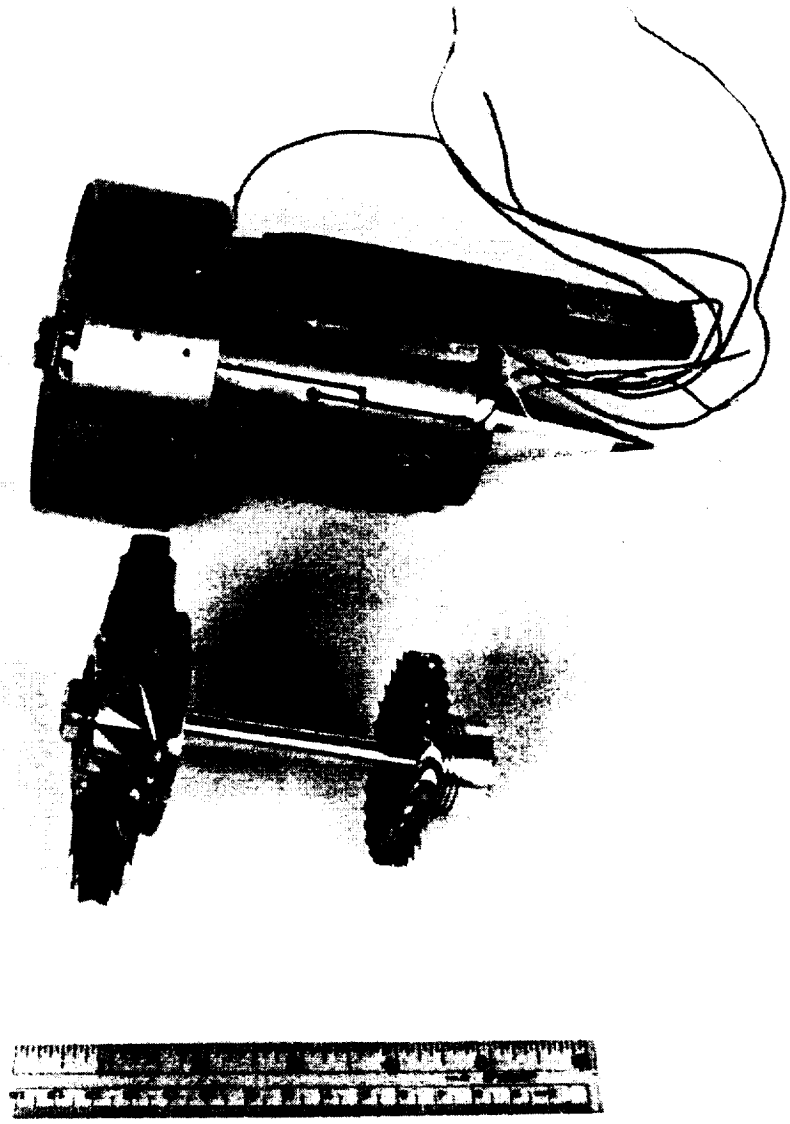

**Figure 3.1 Turbofan Engine Simulator**

capable of producing a fan pressure ratio of 1.60 with a maximum mass flow rate of 1.23 kg/sec (2.72 lbm/sec). The fan simulator is equipped with thermocouples to monitor the bearing temperatures in case of bearing failure. The magnetic-pickup tachometer allows the speed of the simulator to be displayed. The Model 460 turbofan simulator performs like a full scale fan in a typical high bypass ratio engine.

The turbofan simulator reaches supersonic fan tip velocity at a rotational speed of approximately 65,000 RPM (80 PNC). At rotational speeds of 65,000 RPM and higher, the fan will generate combination tones in the acoustic spectrum. For the simulated aircraft approach condition, the simulator was operated at 50,000 RPM (60 PNC). This simulator speed will not generate fan noise with a combination tone spectrum. However, at the simulated aircraft takeoff condition, the simulator was tested at a fan speed of 70,000 RPM (88 PNC) providing the combination tone spectra that is representative of a full-size aircraft engine.

## 3.2 Supersonic Inlets

The main objective of this research is to obtain the aeroacoustic data for the axisymmetric P inlet and the bifurcated two-dimensional inlet at approach and takeoff conditions for comparison. The following three subsections describe and compare the inlets and their features.

### 3.2.1 Axisymmetric P Inlet

A mixed-compression axisymmetric inlet system has been shown to meet the requirements of operating over a wide range of Mach numbers for a supersonic aircraft. This inlet, given the name P inlet, was first tested by NASA Lewis in 1983 to determine the aeroacoustic performance of a representative supersonic cruise inlet. Figure 3.2 shows a cutaway drawing of the NASA P inlet. This supersonic inlet is designed for a cruising speed of Mach 2.65 and has several variable features such as a translating centerbody, boundary layer bleed systems, and auxiliary inlet doors. The translating centerbody is used to adjust the throat area to maintain the correct shock structure inside the inlet at supersonic cruise speeds and to change the mass flow rate to the engine at subsonic speeds. The bleed systems are used to prevent boundary layer buildup on the inlet walls. At aircraft cruise speeds, the boundary layer needs to be minimized to avoid shock-boundary layer interaction problems. The auxiliary doors are required to provide a specific mass flow rate to the engine at certain flight conditions.

Figure 3.3 shows the VPI test axisymmetric P inlet in the test facility. The test inlet has a bellmouth attached to the front cowl lip to reduce cowl lip separation for static testing (See Appendix A). This inlet is a small scale model of the NASA P inlet, except for the boundary layer bleed systems. The aerodynamic results of [Ball et. al., 1984] show the bleed systems to be negligible at low flight speeds. The concerns of shock-boundary layer interaction do not apply to subsonic flight conditions. For these reasons,

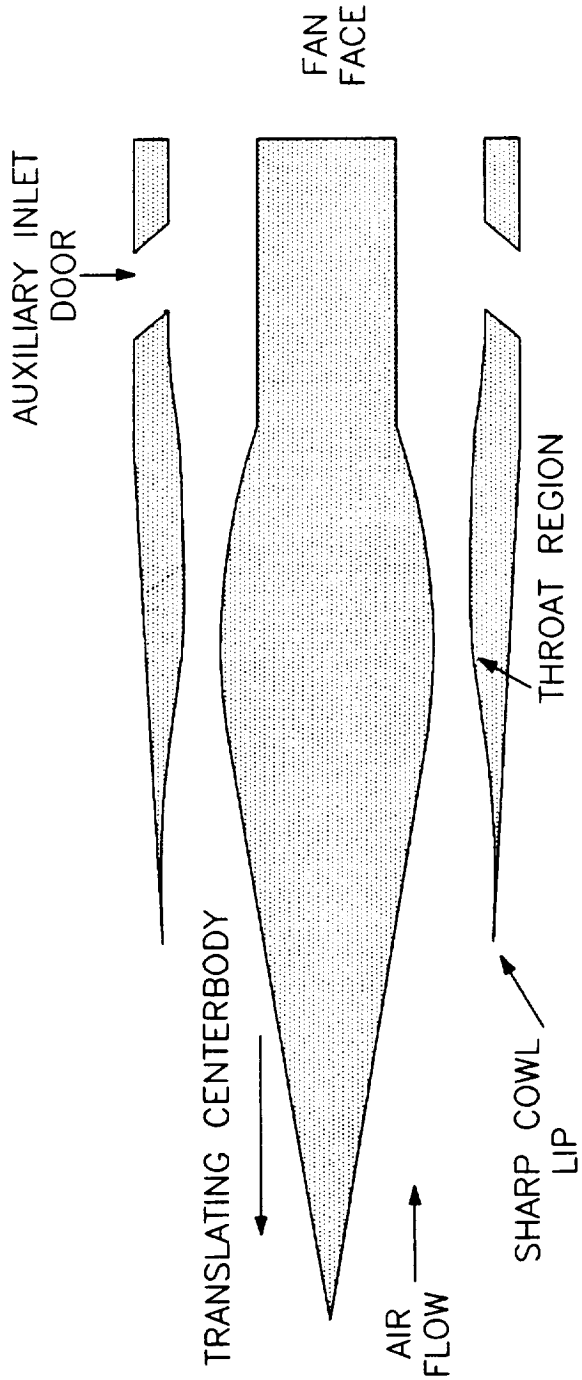


**Figure 3.2 NASA P Inlet (Ball et. al., 1984)**

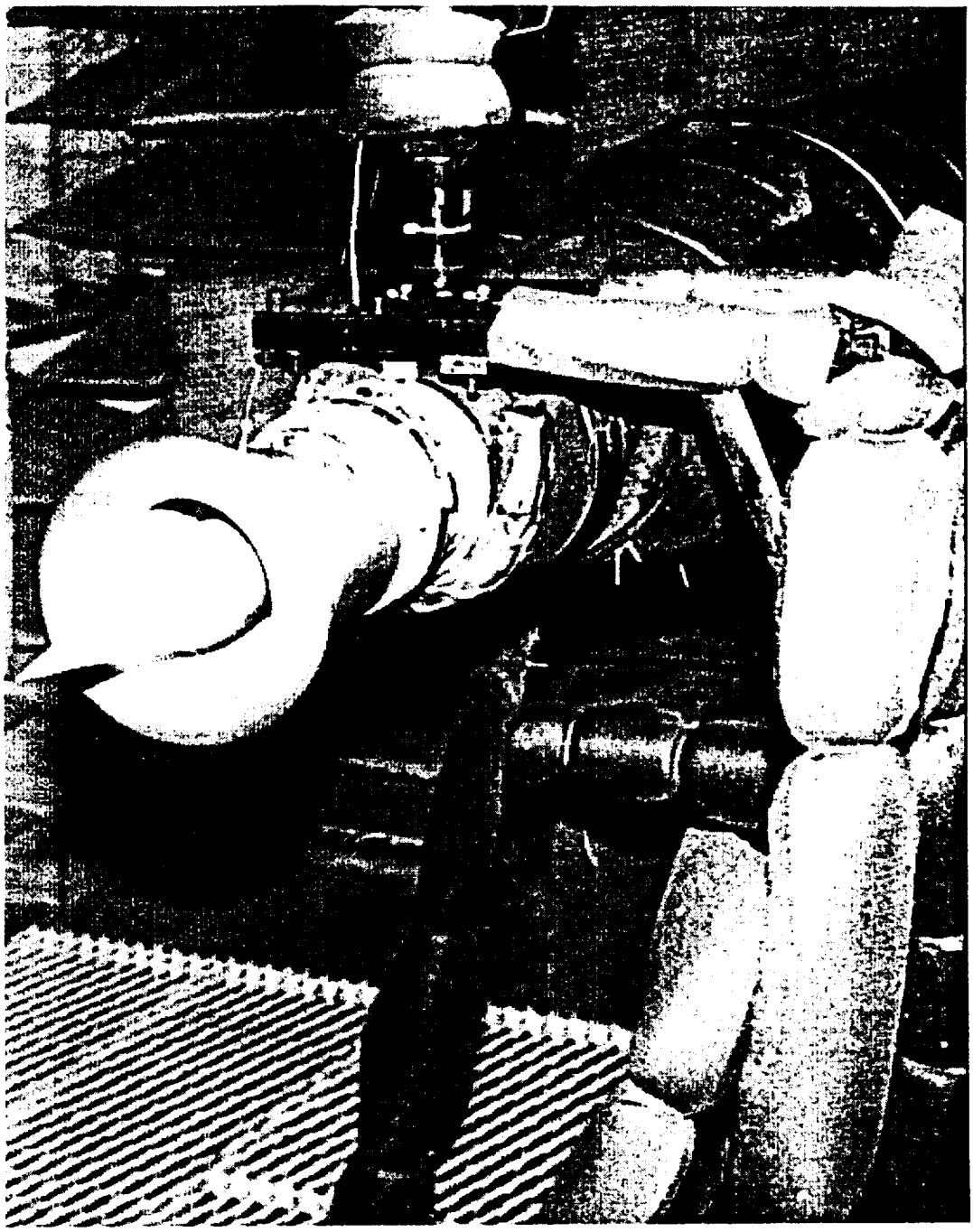

**Figure 3.3 Axisymmetric P Inlet in Research Facility**

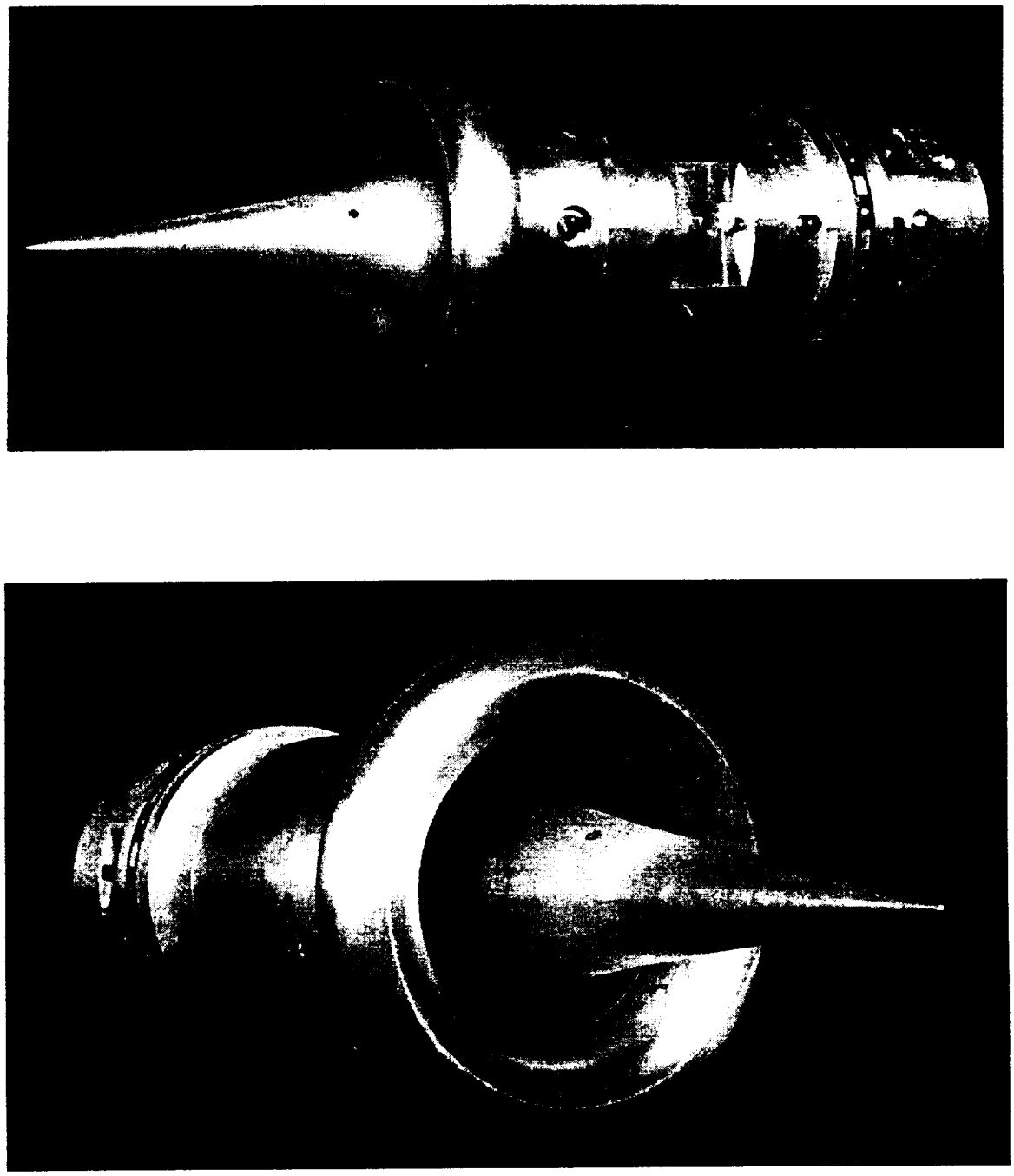

**Figure 3.4 Isometric Views of the P Inlet**

the bleed systems were not incorporated into the design of the current test P inlet. However, the translating centerbody assembly was configured into the P inlet. The centerbody has to be supported by support struts. The inlet requires four equally spaced supports position at 90° circumferential intervals directly upstream of the engines fan face. For this experiment, the centerbody was fully extended 100% forward to the approach and takeoff conditions. The auxiliary doors on the inlet remained closed throughout the testing procedure in this experiment. Figure 3.4 shows isometric views of the VPI test axisymmetric P inlet.

### 3.2.2 Bifurcated Two-dimensional Inlet

The bifurcated inlet is designed for a supersonic cruise aircraft and incorporates several important features such as reduced spillage, bypass and cowl drag, and boundary layer bleed drag. A cutaway drawing of NASA bifurcated two-dimensional (external and mixed compression) supersonic inlet is shown in Figure 3.5. The inlet is designed for cruise speeds of Mach 2.7 and has a collapsible and expandable centerbody. The changing centerbody allows the throat area to be varied to keep the correct shock structure during supersonic flight and to change the mass flow rate to the engine at subsonic flight conditions. Figure 3.6 shows the VPI test bifurcated 2D inlet in the test facility. The 2D inlet used in this experiment has the centerbody fixed in the fully collapsed position because this is the position of the centerbody during approach and

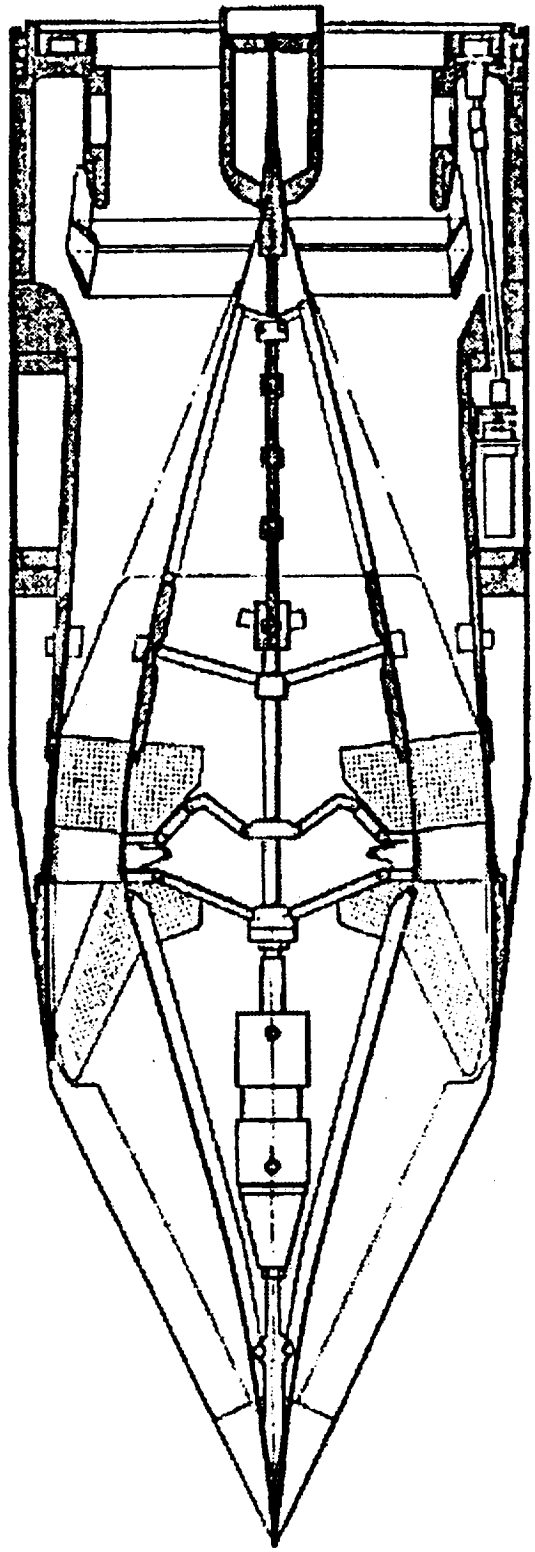

**Figure 3.5 NASA Bifurcated Two-Dimensional Inlet (NASA Report, 1977)**

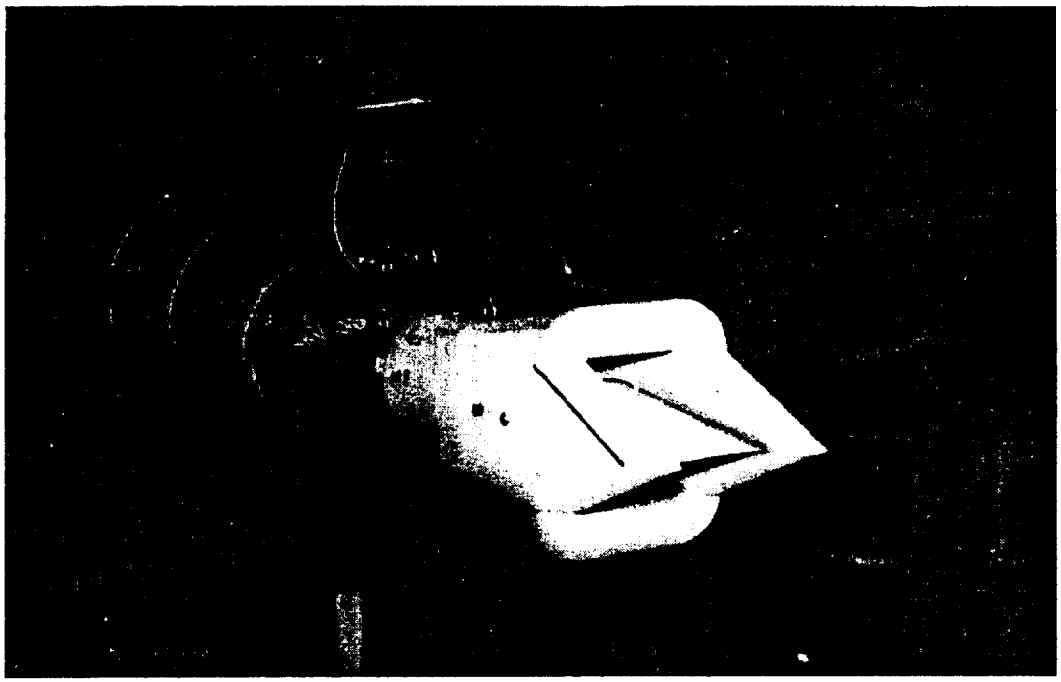

**Figure 3.6 Bifurcated 2D Inlet in Research Facility**

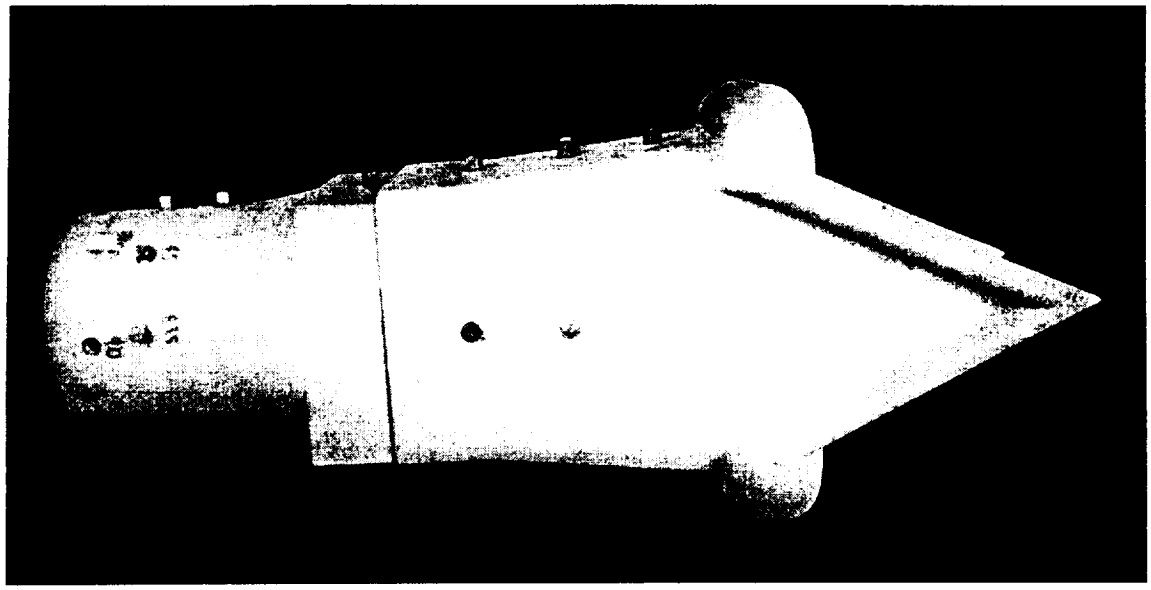

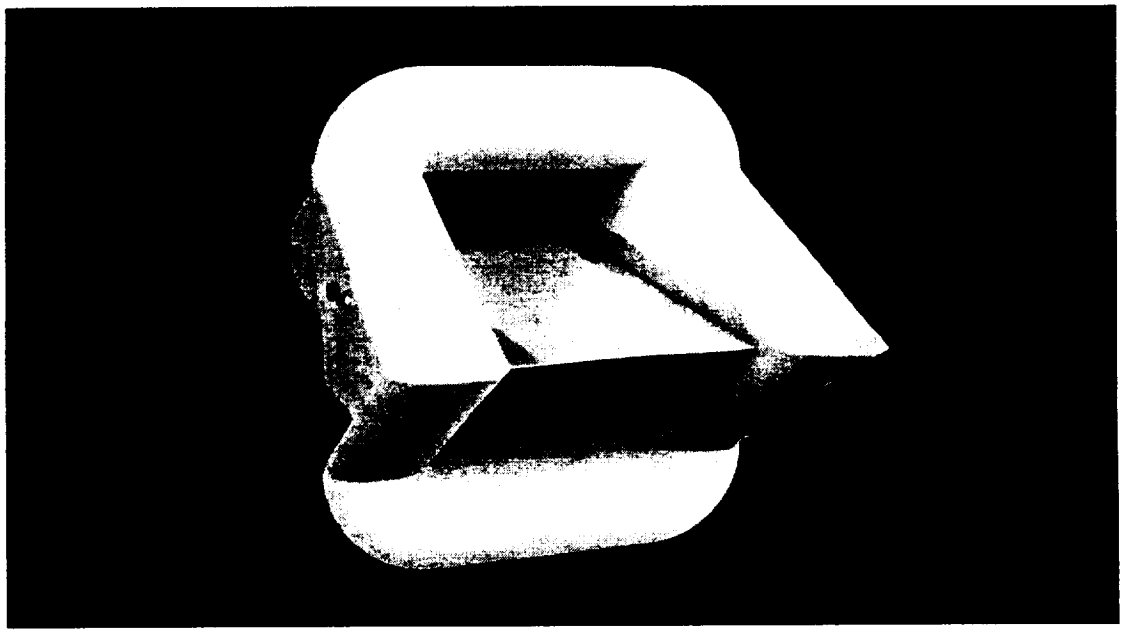

**Figure 3.7 Isometric Views of the 2D Inlet**

takeoff conditions. The 2D inlet has a cowl transition from a rectangular capture area at the front of the inlet to a circular cross section at the fan face and a boundary layer bleed system to reduce boundary layer growth on the outside cowl wall. This reduces the problem of shock/boundary layer interaction in the inlet at supersonic speeds. The boundary layer bleed system is not incorporated into the test inlet since the effects are negligible at subsonic airspeeds. The test inlet has a bellmouth attached to the front cowl lip to reduce cowl lip separation for static testing (See Appendix A). Figure 3.7 shows isometric views of the VPI test axisymmetric P inlet.

### 3.2.3 Geometry Comparison of the P Inlet and 2D Inlet

The previous two sections described the features of the different inlets. This section will compare the two inlets directly. Figure 3.8 shows the front face views of the P inlet and 2D inlet. Notice how the P inlet has an annular opening and the 2D inlet has two separate rectangular openings. The rear face views of both of the inlets are pictured in Figure 3.9 and show the different centerbody support features. The P inlet has four support struts and the 2D inlet has a nose cone with two splitter plate edges. Figure 3.10 shows a cutaway profile of the two inlets comparing the throughflow areas. The throughflow areas are graphed in Figure 3.11 and illustrate the large differences in the cross-sectional area traveling from the cowl lip to the fan face. The 2D inlet graph starts with a large area due to the rectangular openings and then transitions down to the smaller

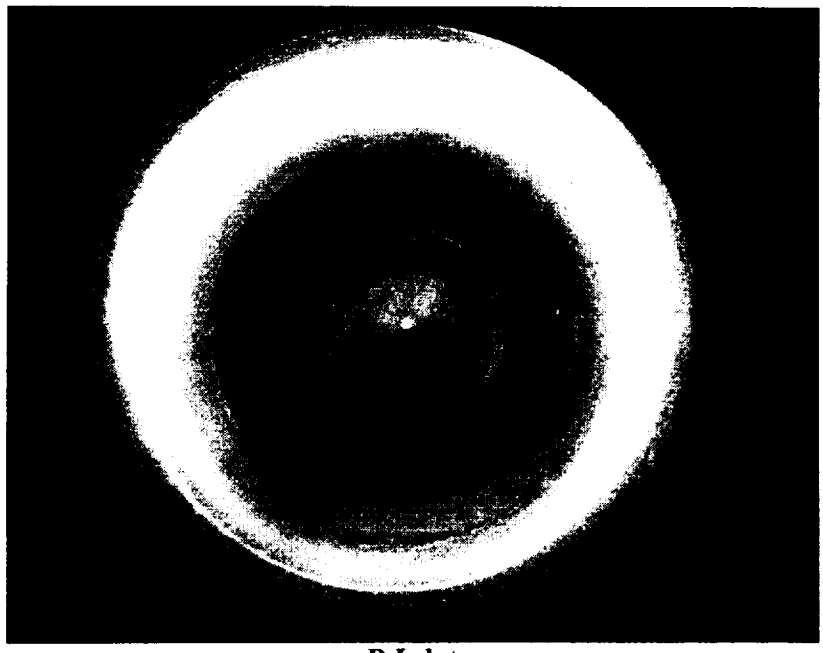

**P Inlet**

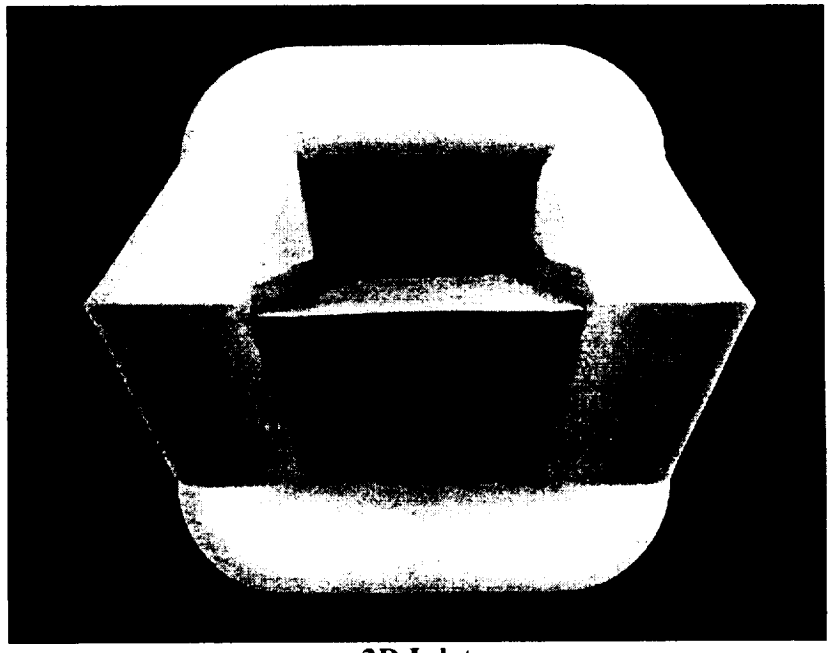

**2D Inlet**

**Figure 3.8 Front Face Views of the Inlets**

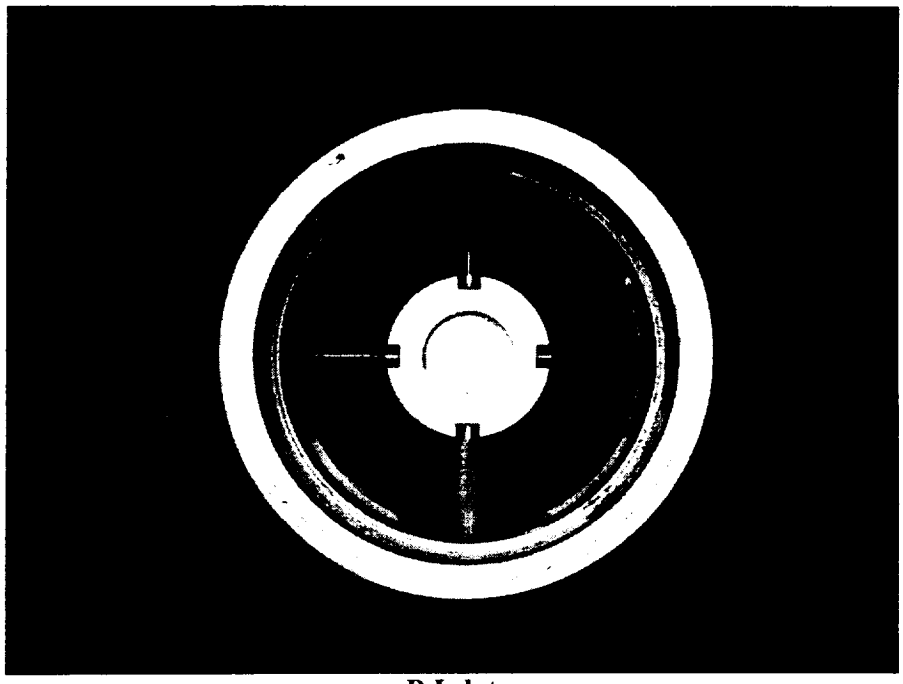

**P Inlet**

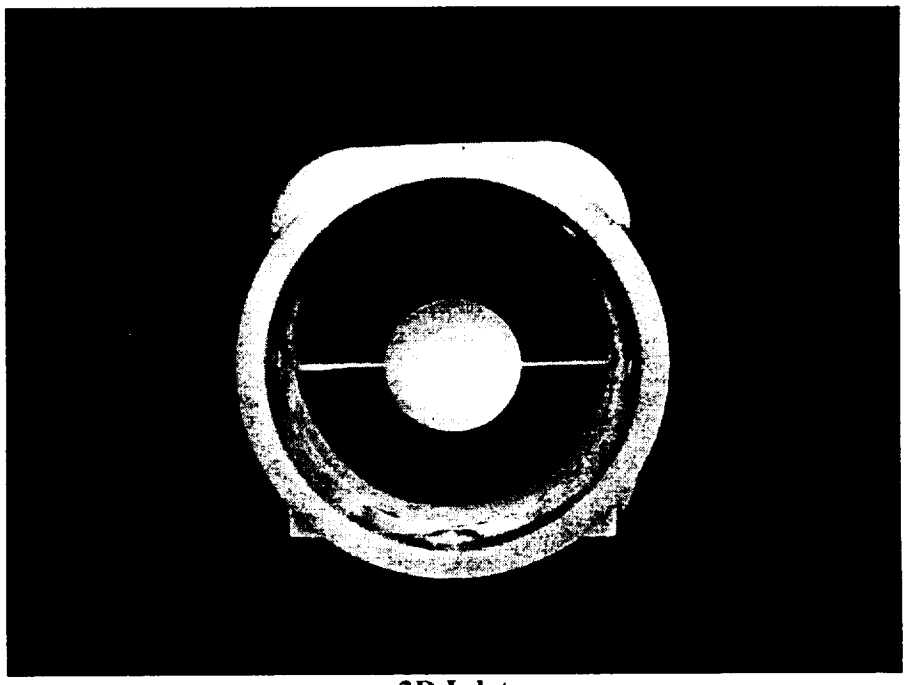

**2D Inlet**

**Figure 3.9 Rear Face Views of the Inlets**

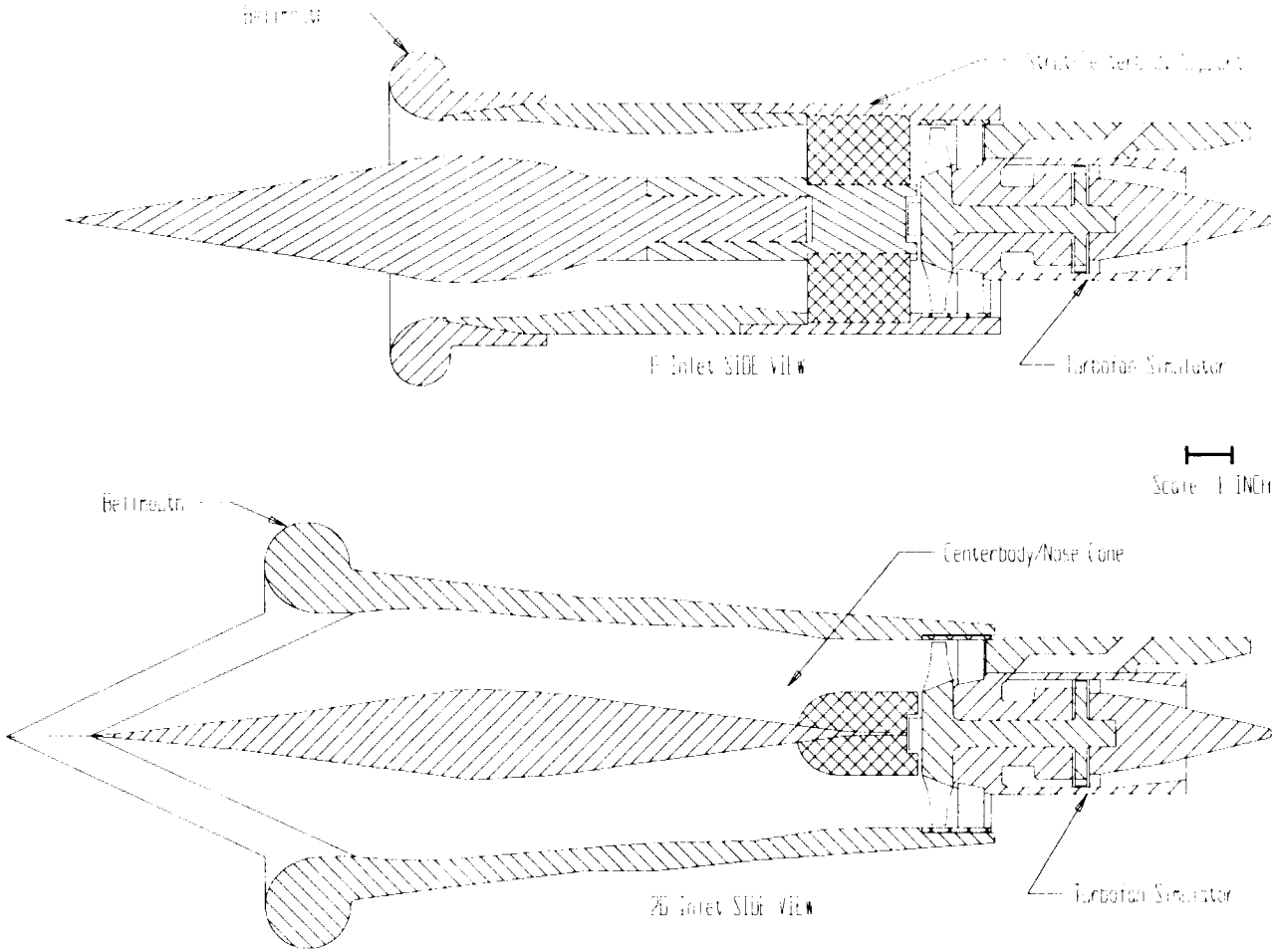


**Figure 3.10 Cutaway Profile of the P Inlet and 2D Inlet Comparing Throughflow Area**

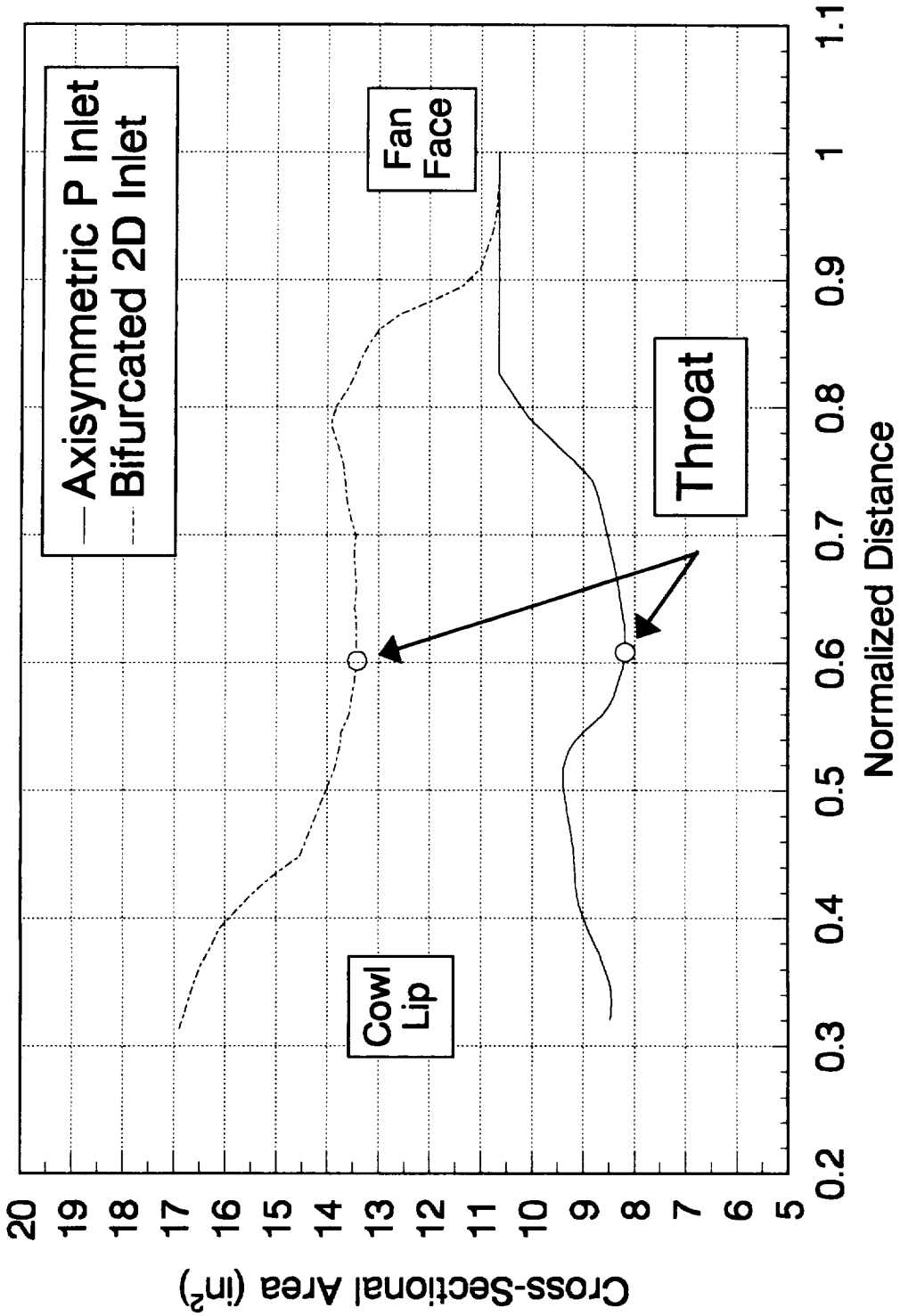


**Figure 3.11 Throughflow Area Comparison Graph of the P Inlet and 2D Inlet**

circular fan face area. The P inlet begins with a small capture area then increase slightly before decreasing to the throat area and continuing back up to the fan face area. It is important to see the large difference in the throat areas because they influence the throat Mach number. The throat Mach number will have an important impact in the level of noise radiation from the fan simulator.

## 3.3 Research Facility

All tests for this research was performed at the Virginia Tech Anechoic Chamber in the Vibration and Acoustics Lab. Figure 3.12 shows an earlier model of the sharp cowl lip axisymmetric P inlet on the test bed in the anechoic chamber. The chamber is 4.0 x 2.7 x 2.2 meters and all surfaces are made of Owens-Corning Type 705 industrial fiberglass wedges approximately 0.91 meters thick. The elevated floor of the chamber is constructed of a metal grate just above the fiberglass wedges to minimize sound reflection and provide a working surface in the chamber. The facility is considered to be anechoic above frequencies of 200 Hz and has proven to have an acceptable ambient noise level of approximately 30 dB which is on the average 80 dB below the fan spectrum noise levels.

The supersonic inlets are coupled with the turbofan engine simulator and located in the center of the anechoic chamber mounted on a test stand 48 in (122 cm) above the elevated grate floor to reduce the possibility of creating ground vortices. The turbine in

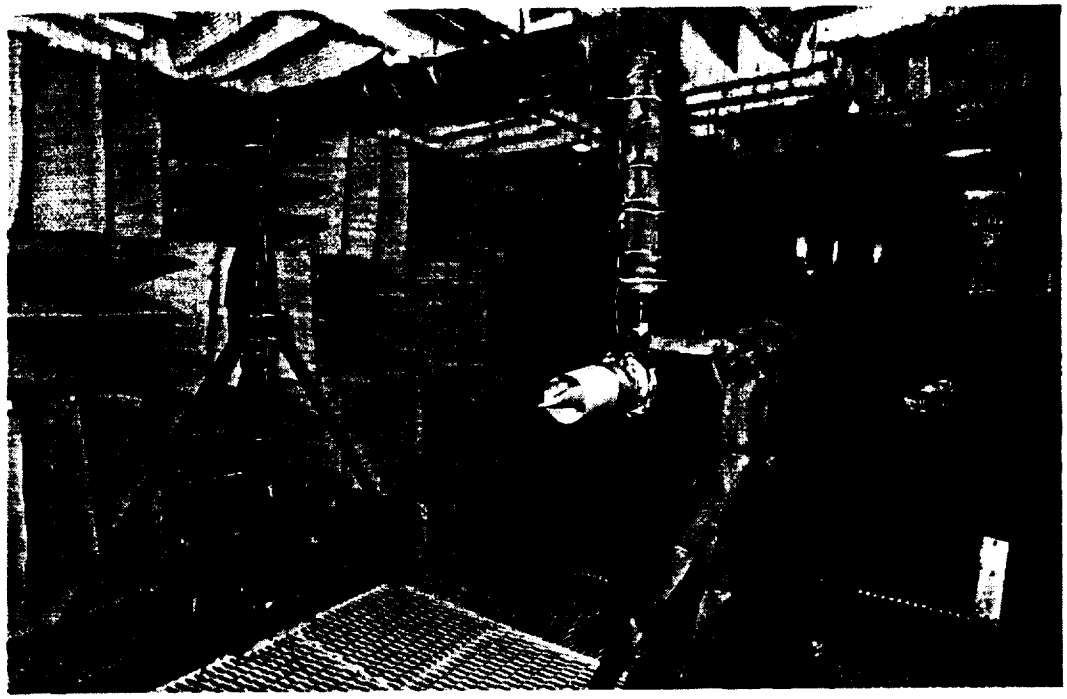

**Figure 3.12 Research Facility**

the simulator is driven by compressed air fed in through a 2 inch pipe and the exhaust is ducted away by a 12 inch tube out the rear wall of the chamber. The door to the chamber has an 18 inch hole cut in it to provide air to the fan of the simulator and has been acoustically treated. The stand supports, supply piping, and exhaust ducting are all covered with acoustic foam to reduce the sound reflection from their surfaces. A valve outside of the chamber is used to control the compressed air supply line to the simulator for adjusting the speed. These test are run under static conditions in which air is drawn into the inlet by the turbofan simulator. Since static conditions allow for more variable noise levels than in-flight conditions, multiple acoustic readings were averaged for each microphone location and inlet configuration in an effort to compensate for random atmospheric turbulence in the test area.

## 3.4 Aerodynamic Measurements

Total pressure recovery and flow distortion measurements were used to compare the overall aerodynamic performance of the axisymmetric P inlet and bifurcated two-dimensional inlet. The aerodynamic measurements have an important role in the interpretation of the acoustic results. The acoustic performance of an aircraft engine is closely related to the aerodynamic behavior of the supersonic inlet. Understanding the influence of aerodynamics on the acoustic performance of the inlets is one of the objectives of this research.

### 3.4.1 Instrumentation

All aerodynamic measurements were made using two conventional probes. A 1/8 in (3.2 mm) diameter Kiel probe was used to measure total pressure recovery at the fan face and exit because of its high tolerance of flow angularity. A 1/16 in (1.6 mm) diameter pitot-static probe was used for static and total pressure measurements at the cowl lip, throat, and fan face stations. The Mach number was then calculated from the static and total pressures assuming isentropic flow.

### 3.4.2 Aerodynamic Setup

Total pressure and Mach number measurements were made at four probe stations along the length of both inlets. The locations are described as the cowl lip, throat, fan face, and fan exit stations. In previous experiments conducted by Nuckolls and Ng using the P inlet, it was determined that flow upstream of the support struts was axisymmetric, therefore only one circumferential measurement location was made based on this condition at the throat and cowl lip stations. For the 2D inlet the axisymmetric condition does not exist, however the CFD results have shown there is little variation in flow across the width of the throat and cowl lip stations except very close to the walls where boundary layer growth occurs. Therefore, an accurate flow profile of the throat and cowl

lip station could be made by measuring only along the center of the passage way. A total of seven equally spaced radial measurements were made from the hub wall to the tip wall on both inlets at the throat and cowl lip

Figure 3.13 shows all the measurement locations on the P inlet. On the P inlet, the flow field at the fan face is axisymmetric. The measurements were made at five circumferential positions and seven equally spaced radial locations to survey the effect of the strut. The circumferential positions were equally spaced between 0° (directly behind strut) and 45° (center of coreflow) and the radial positions equally spaced from the hub to the tip of the fan blades. The fan exit station required seven radial positions from hub to tip at one circumferential location due to the mixing of the flow after passing through the stator blades. Mach number measurements were made perpendicular to the trailing edge and at the centerline of a strut to define the wakes shed by each of the centerbody support struts. The strut wake traverse station is detailed on the fan face probe grid in Figure 3.13.

Figure 3.14 shows all the measurement locations on the 2D inlet. The 2D inlet's centerbody trailing edge and nose cone distort the flow field at the fan face. The measurement grid at the fan face has to be more detailed than the P inlet's fan face measurement grid. A total of six circumferential positions with seven radial locations equally spaced from hub to tip had to be made at the fan face station. This grid covers a circumferential sector from 0° (center of coreflow) to 90° (directly behind strut). In order to measure the wakes shed by the centerbody splitter plate, a traverse was made

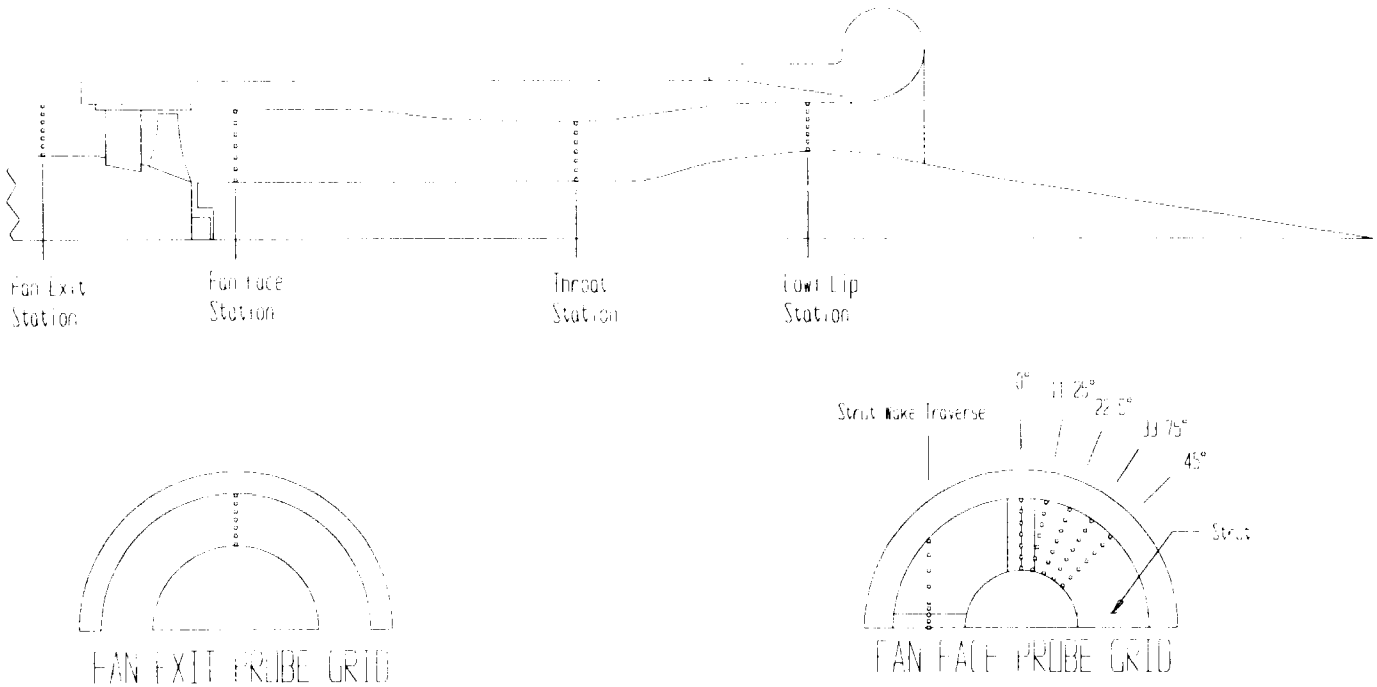


**Figure 3.13 P Inlet Aerodynamic Measurement Locations**

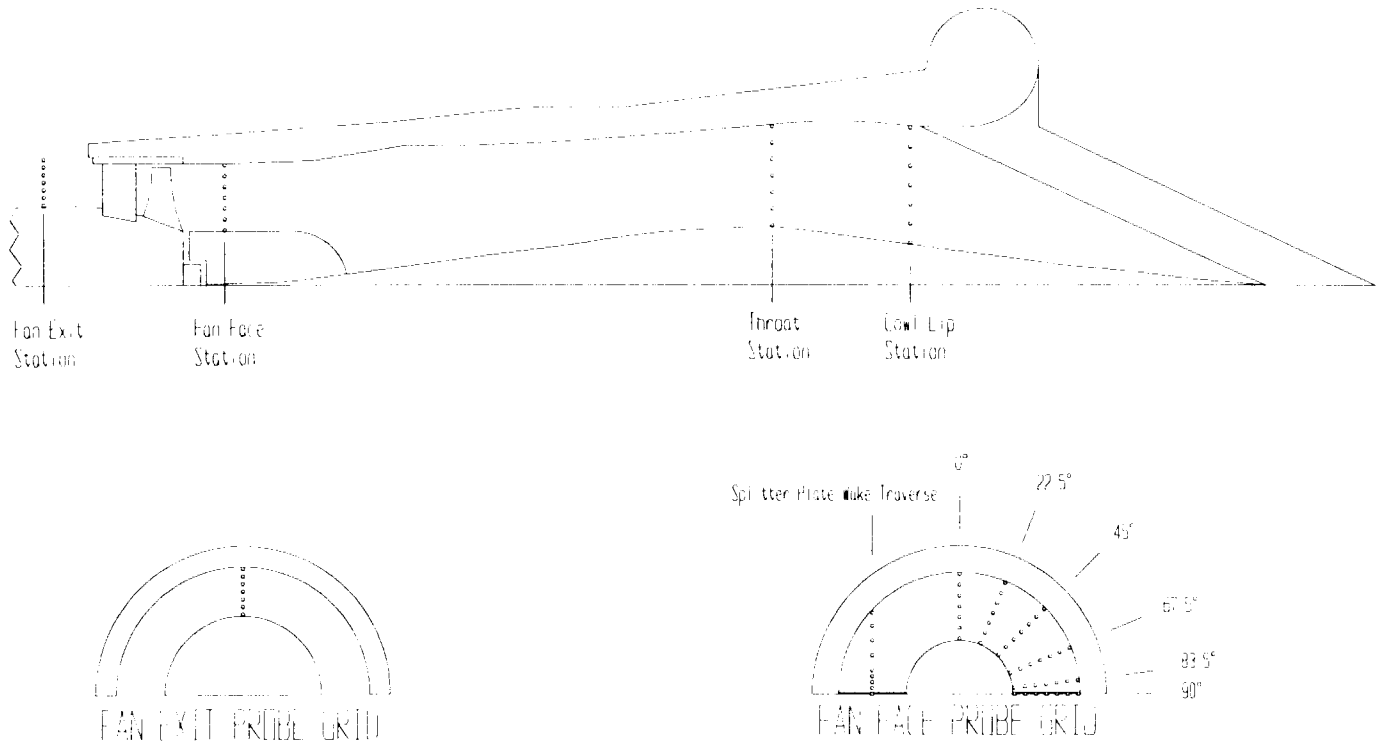


**Figure 3.14 2D Inlet Aerodynamic Measurement Locations**

perpendicular to the trailing edge of the centerbody and at the centerline of one of the two trailing edges of the splitter plate. The Mach number was measured to define the wakes at the splitter plate wake traverse station shown on the fan face probe grid in Figure 3.14.

## 3.5 Acoustic Measurements

The acoustic measurements were used to compare the overall noise levels of the axisymmetric P inlet and bifurcated two-dimensional inlet. The acoustic performance is influenced by the aerodynamic results because of the different flow fields in the two supersonic inlets. Determining how the acoustic performance is related to the aerodynamics of the inlets is another objective of this research.

### 3.5.1 Instrumentation

A Bruel and Kjaer model 4136 condenser microphone was used to measure the acoustic farfield of the P inlet and 2D inlet. The microphone has a 0.25 in (6.4 mm) diameter sensing diaphragm and provides linear responses for frequencies up to 30 kHz. The microphone was connected to a preamplifier and then to a battery operated dual channel Bruel and Kjaer power supply. The output from the power supply was connected to a Bruel and Kjaer 2030 dual channel spectrum analyzer to analyze the signal from the

microphone. The microphone was calibrated prior to testing by using a Bruel and Kjaer pistophone which produced a 114.2 dB signal at 994 Hz.

The spectrum analyzer used a narrow-bandwidth Fast-Fourier Transform (FFT) to convert the microphone signal into a frequency domain. The upper frequency limit on the measurements was 25.6 kHz with a bandwidth of 32 Hz for a total of 800 data points. The spectrum analyzer output was used to record the full frequency spectrum, blade passing frequency (BPF), and the overall sound pressure level (OASPL). The OASPL is an integration of the noise over the entire frequency spectrum from 0 to 25.6 kHz. The sample noise spectra data was transferred to a personal computer for permanent storage. To compensate for speed fluctuations and random atmospheric turbulence, the spectrum analyzer was setup to calculate the linear average of 20 consecutive noise spectra. In addition, five consecutive measurements of the average BPF and OASPL levels were recorded at each microphone location.

### 3.5.2 Acoustic Setup

Figure 3.15 shows were the acoustic measurements were made in respect to the inlets. The microphones were placed at twelve different angular positions along a circular arc centered at the intersection of the vertical plane at the cowl lip and the inlet center line at a radius of 48 in (122 cm). The radius was chosen to provide acoustic measurements in the farfield (i.e. $KL>>1$) where $K$ is the wave number ($K=\omega/c$) and $L$ is

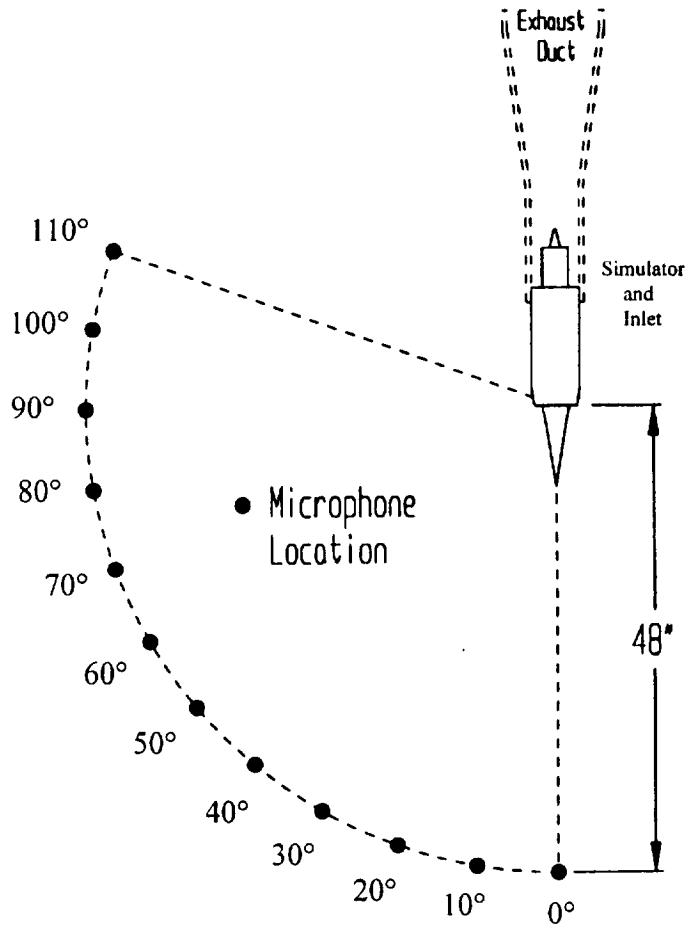


**Figure 3.15 Microphone Positions, Plane View**

the distance from the noise source to the microphone ( $L$ = 48 in). In the experimental setup, $K$ = 275/m at a fan speed of 50,000 RPM and $K$ = 385/m at a fan speed of 70,000 RPM. The microphone locations were along the angular radius from 0° to 110° at 10° increments. The microphone was mounted on a stand 48 in (122 cm) above the floor of the anechoic chamber with the diaphragm pointing directly towards the intersection of the inlet centerline and the cowl lip vertical plane. The axisymmetric P inlet was measured on two acoustic planes shown in Figure 3.16: one centered on a centerbody support strut (0°) and the other halfway between two struts (45°). The bifurcated two-dimensional inlet was tested at three acoustic planes shown in Figure 3.17: horizontal plane (0°), mid plane (45°), and vertical plane (90°). These planes had to be measured because the radiation field around the inlets was three dimensional. Only the primary acoustic planes are compared and presented in the body of this document. The primary acoustic plane for the P inlet is the 0° plane and for the 2D inlet is the vertical plane (90°). A direct plane comparison for each to the individual inlets is presented in Appendix D.

## 3.6 Test Matrix

The tests performed on the axisymmetric P inlet and the bifurcated 2D inlet were conducted at two different flight conditions. This research focuses on aircraft approach and takeoff conditions. The approach flight conditions require the simulator to run at 50,000 RPM (blade tip speed = 895ft/s) or 60% corrected fan speed (PNC) and the

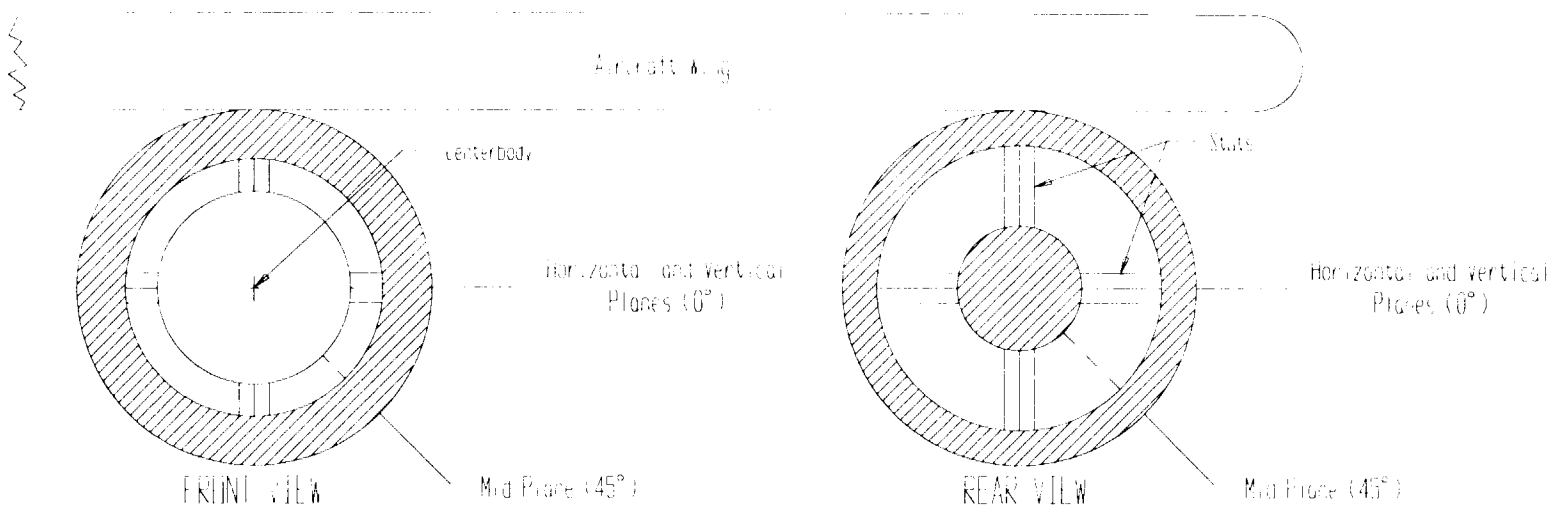


**Figure 3.16 P Inlet Acoustic Measurement Planes**

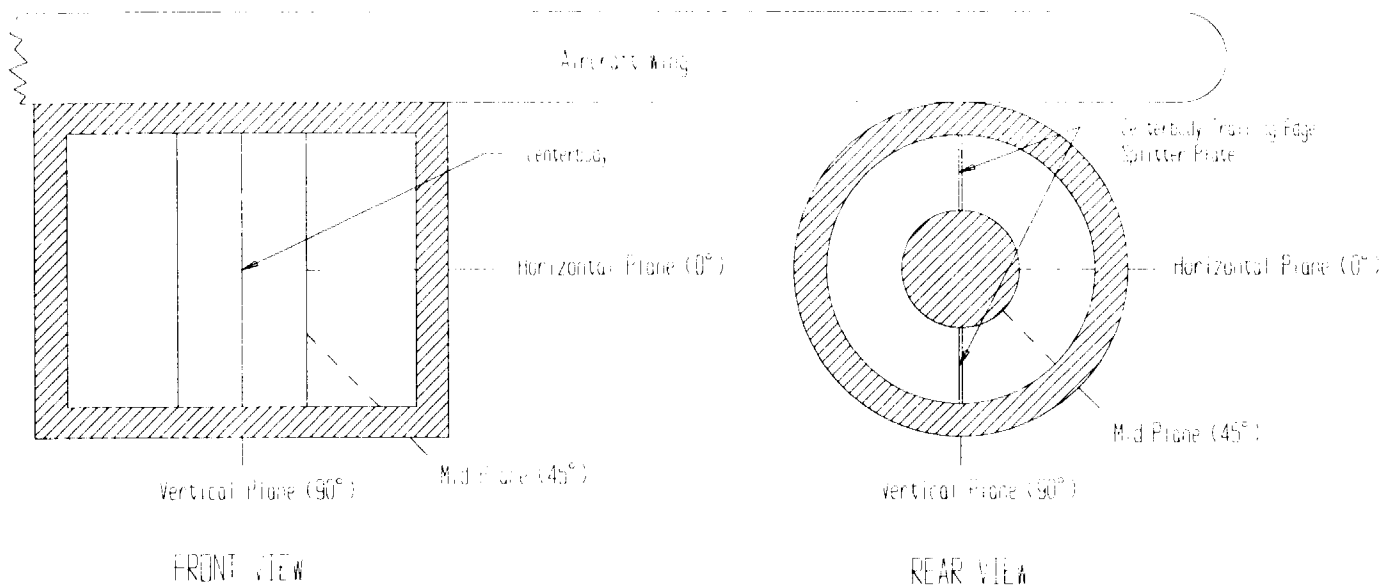


**Figure 3.17 2D Inlet Acoustic Measurement Planes**

centerbody fully extended to meet the approach and takeoff conditions. The 2D inlet has the auxiliary inlet doors closed and the centerbody fully collapsed to meet the approach and takeoff conditions. The aeroacoustics of both inlets were tested at the two conditions in order to get a direct comparison between them. The Mach number was then measured at the center of the throat station for test speeds of 30,000 RPM up to 70,000 RPM by 5,000 RPM increments on both inlets. Each inlet was also tested by varying the speed of the simulator, from 50,000 RPM up to 70,000 RPM by 2,000 RPM increments, while keeping a microphone at the 20° microphone position and recording the blade passing tone and overall sound pressure levels.

# 4.0 Results and Discussion

This chapter is divided into aerodynamic and acoustic sections. The first section investigates the overall aerodynamic performance of the bifurcated two-dimensional inlet and the axisymmetric P inlet. The aerodynamics of the inlet play an important role in influencing its acoustic performance. The acoustic results are presented in the second section. This section focuses on the acoustic performance of the inlets by showing the characteristics of the radiated noise.

## 4.1 Aerodynamic Results

The aerodynamic measurements were made at the cowl lip, throat, and fan face stations. The cowl lip and throat measurements were made along an axis perpendicular to the inlet's centerline axis. Due to the symmetry of the inlets, radial traverses at only one circumferential position were needed. However at the fan face station, several circumferential rakes had to be made over a specific sector because of the geometric differences. The bifurcated two-dimensional inlet measurements were made over a 0° to

90° sector and the axisymmetric P inlet measurements were made over a 0° to 45° sector. Using symmetry, these measurements were then mirrored over the complete fan face to give a better illustration of the flow field.

### 4.1.1 Inlet Cowl Lip Separation

The sharp edge cowl lip on both inlets created a large region of separated flow downstream of the lip when performing test under static conditions. Static test conditions are associated with varying degrees of lip separation. However, in flight test conditions can be met by using a bellmouth at the cowl lip. A bellmouth was coupled to each inlet to reduce the lip separation region. The cowl lip separation was reduced significantly for the static test conditions of this experiment. Appendix A illustrates how the bellmouth changed the flow field in the P inlet and 2D inlet. The total pressure profiles from the inlets cowl lip station, shown in Figure 4.1, provide a good indication that the separation at the mouth of the inlets has almost been completely eliminated. The profiles for the 2D inlet with the bellmouth show only a very minor separation region near the tip region of the passage at 88% of the fan speed. The P inlet profiles with the bellmouth show no separation near the cowl lip region. The results show that the separation was not evident in either case and the inlets were performing as if they had forward velocity. The bellmouths remained in use on both inlets throughout the testing procedures of the experiment.

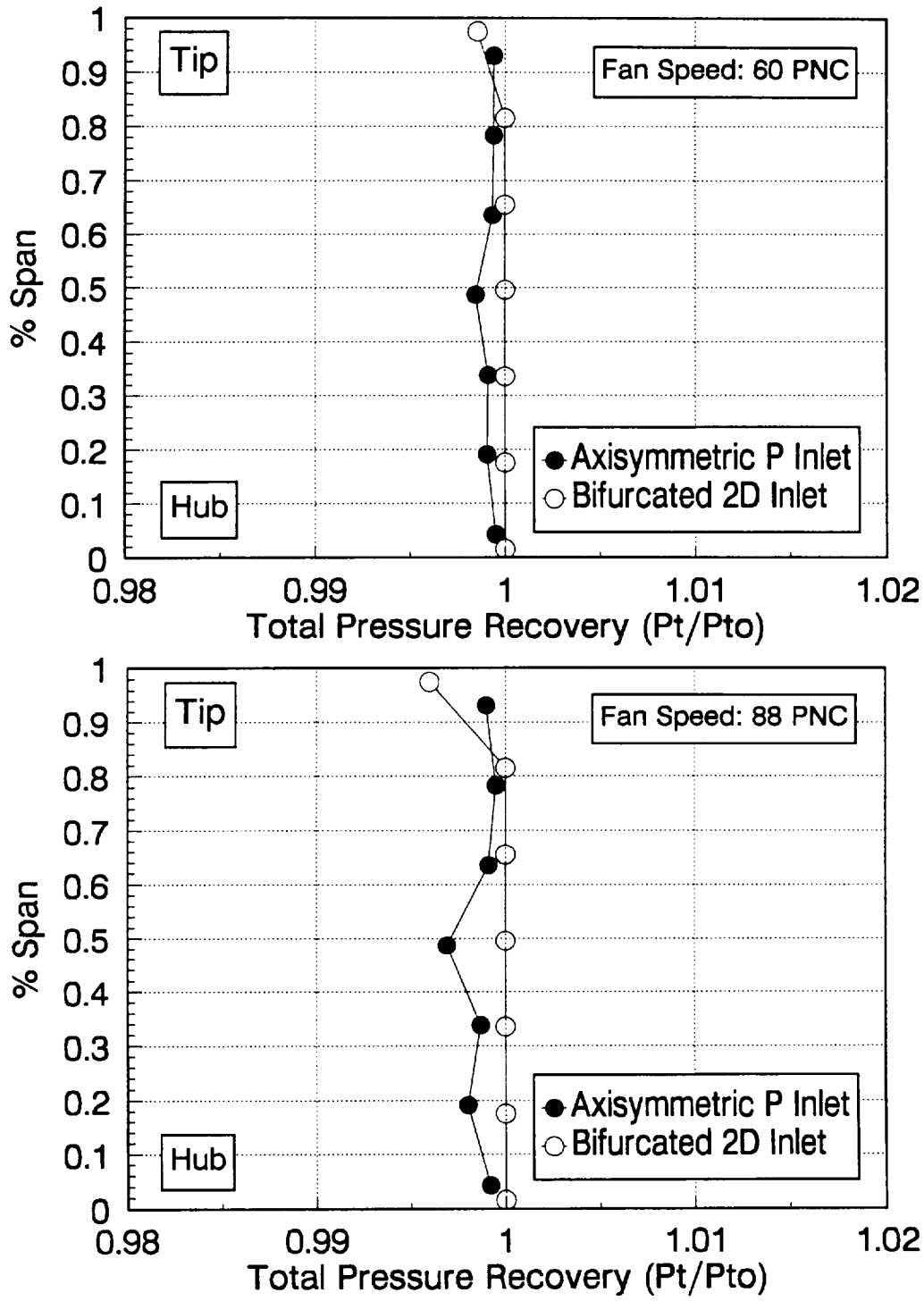


**Figure 4.1 Total Pressure Recovery Profiles at the Lip Station, 60 PNC and 88 PNC**

### 4.1.2 Fan Operating Condition

The fan pressure ratio for the turbofan simulator engine depends heavily on the average total pressure recovery at the exit of the fan. Aerodynamic measurements were made at the fan exit in order to determine the fan pressure ratio. Table 4.1 presents the fan pressure ratio for both inlets at approach and takeoff conditions. The fan pressure ratio for the bifurcated two-dimensional inlet and axisymmetric P inlet were discovered to be approximately the same for the test speeds. The same pressure ratio for both inlets indicates that the fan loading was the same for both inlets. Since noise generation is a function of fan loading, this condition is necessary in order to compare the inlets. The ratio is used in conjunction with the fan exit area to determine the operating point of the engine on the simulator performance map. Figure 4.2 shows that the fan pressure ratios fell within the normal operating range for the Model 460 turbofan simulator ensuring that the fan was performing like a typical engine.

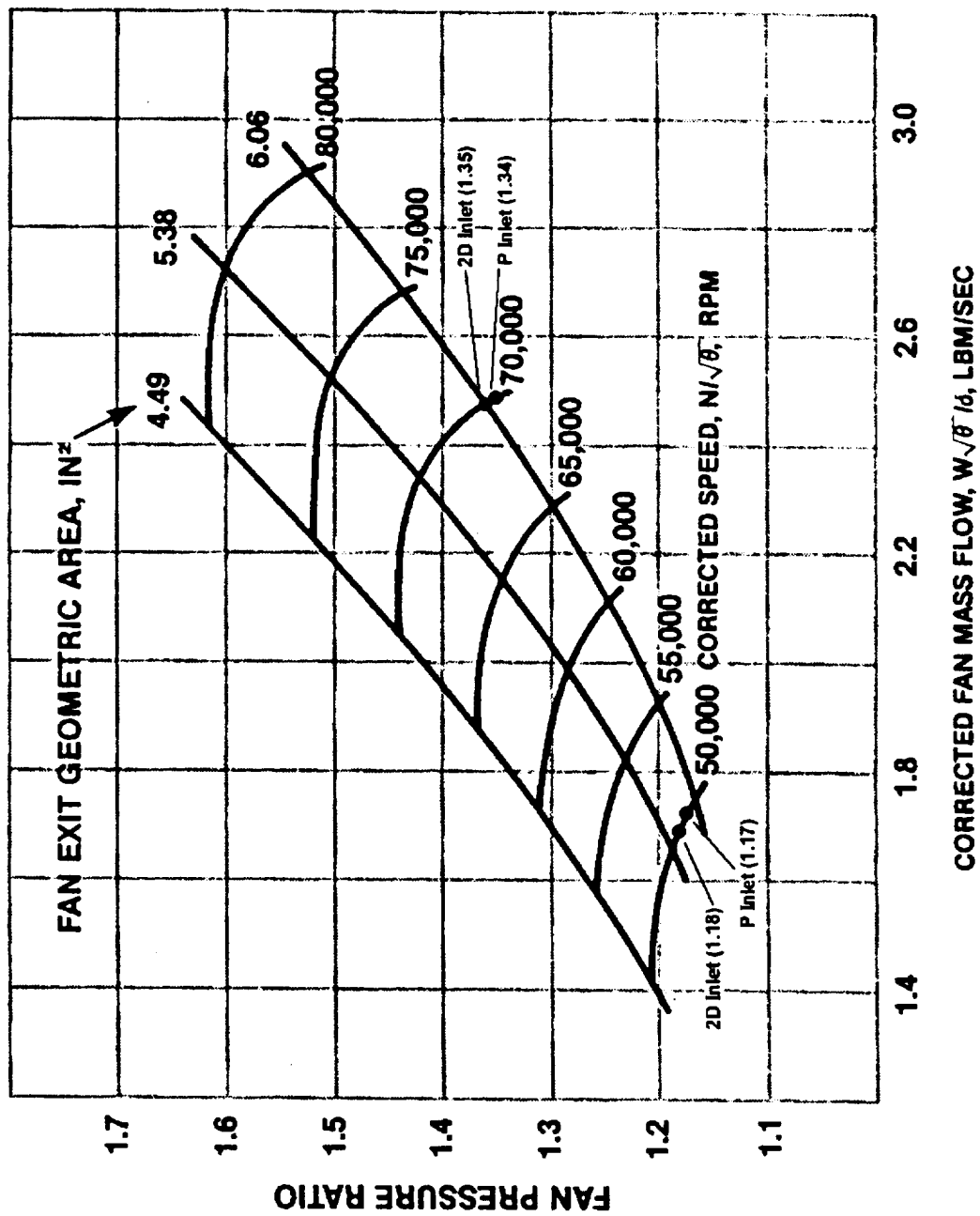


Figure 4.2 Fan Performance Map

**Table 4.1 Fan Pressure Ratio**

| Fan Speed 50,000 RPM (60 PNC) | Fan Pressure Ratio |
|---|---|
| Bifurcated two-dimensional Inlet | 1.18 |
| Axisymmetric P Inlet | 1.17 |
| **Fan Speed 70,000 RPM (88 PNC)** | **Fan Pressure Ratio** |
| Bifurcated two-dimensional Inlet | 1.35 |
| Axisymmetric P Inlet | 1.34 |

### 4.1.3 Throat Station

The throat region of a supersonic inlet has a considerable effect on the noise propagation properties. The inlet flow field is important in determining how the noise will propagate down the inlet to the front opening. High inlet throat Mach numbers increase the amount of time it takes for the noise signal to travel upstream. During this time period the spiraling pressure pattern dissipates signal energy. When the flow Mach number exceeds 0.5, this noise attenuating characteristic becomes present and is referred to as a soft choking effect. The soft choking effect will be further discussed later in Section 4.2.1. Table 4.2 shows the area averaged throat Mach numbers for both inlets at approach and takeoff conditions.

**Table 4.2 Average Throat Mach Numbers**

| Inlet Type | Throat Mach Number 50,000 RPM (60 PNC) | Throat Mach Number 70,000 RPM (88 PNC) |
|---|---|---|
| Bifurcated 2D Inlet | 0.18 | 0.26 |
| Axisymmetric P Inlet | 0.33 | 0.52 |

The throat Mach numbers for the bifurcated two-dimensional inlet and the axisymmetric P inlet have a significant difference. At the approach speed (60 PNC), the axisymmetric P inlet has a throat Mach number that is 1.8 times larger than the 2D inlet. At the takeoff speed (88 PNC), the axisymmetric P inlet has a throat Mach number that is 2.0 times larger than the 2D inlet. The reason for the large difference in throat Mach numbers is due to the difference in the throat areas of the two inlets (See Figures 3.10 and 3.11 in Section 3.2.3). The 2D inlet has a throat area of 13.42 $in^2$ and the P inlet has a smaller throat area of 8.18 $in^2$. The 2D inlet's larger throat area will cause the acoustic performance to suffer since the soft choking effect was not be evident.

The inlet throat Mach number versus the blade tip speed is presented for both inlets in Figure 4.3. At the approach speed of 60 PNC (895 ft/s), the P inlet and the 2D inlet are not exceeding a throat Mach number of 0.5. At the takeoff speed of 88 PNC (1250 ft/s), the axisymmetric P inlet surpasses a Mach number of 0.5 and the soft choking effect starts to become a factor in attenuating the noise propagating to the front of the inlet. The contrast in throat velocities will give each inlet different acoustic properties. The throat of the bifurcated two-dimensional inlet, with a Mach number only

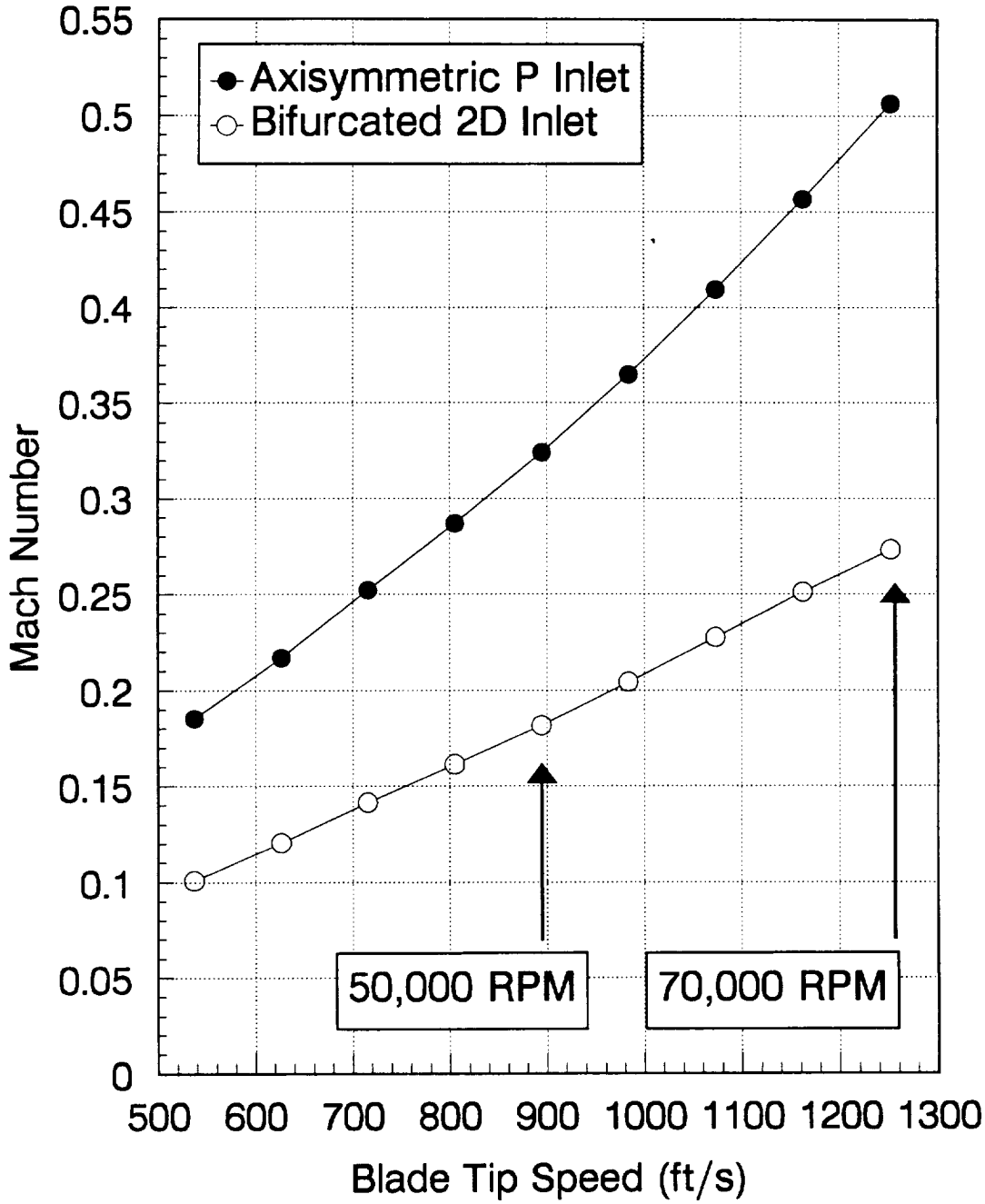


**Figure 4.3 Inlet Throat Mach Number vs. Blade Tip Speed**

of 0.26, is not expected to show any significant sign of reducing the propagating fan noise at the takeoff speed.

The Mach number distributions at the throat stations are illustrated in Figure 4.4 for both inlets at the test speeds of 60 PNC and 88 PNC. At takeoff conditions of 88 PNC, the noise propagation should be reduced for the P inlet since the core flow Mach number at the throat reaches 0.53. The attenuated noise reduction will not happen for the 2D inlet because the highest Mach number at the throat station only reaches 0.28. The axisymmetric P inlet shows lower flow velocities at the tip and hub regions whereas the 2D inlet has a more uniform flow field. The lower Mach number regions near the hub for the P inlet are a consequence of the high core flow Mach number. The high Mach numbers resulted in an increased boundary layer growth on the centerbody and the tip region. The larger the boundary layer becomes the more loss that will occur at the throat station. As the losses increase, the performance of the inlet will decrease making the inlet less desirable.

The measurements of the total pressure recovery at the throat station of both inlet configurations are shown in Figure 4.5. At the hub wall, the P inlet shows an increased area of losses which is not present on the 2D inlet. The losses indicate the presence of a measurable boundary layer. The growth of the boundary layer at the tip wall is evident on both inlets. The P inlet shows a boundary layer at the hub wall because the throat measuring station is located beyond the rear downward slope of the centerbody (See Figure 3.13 in Section 3.4.2). This causes the boundary layer to grow greater than that of

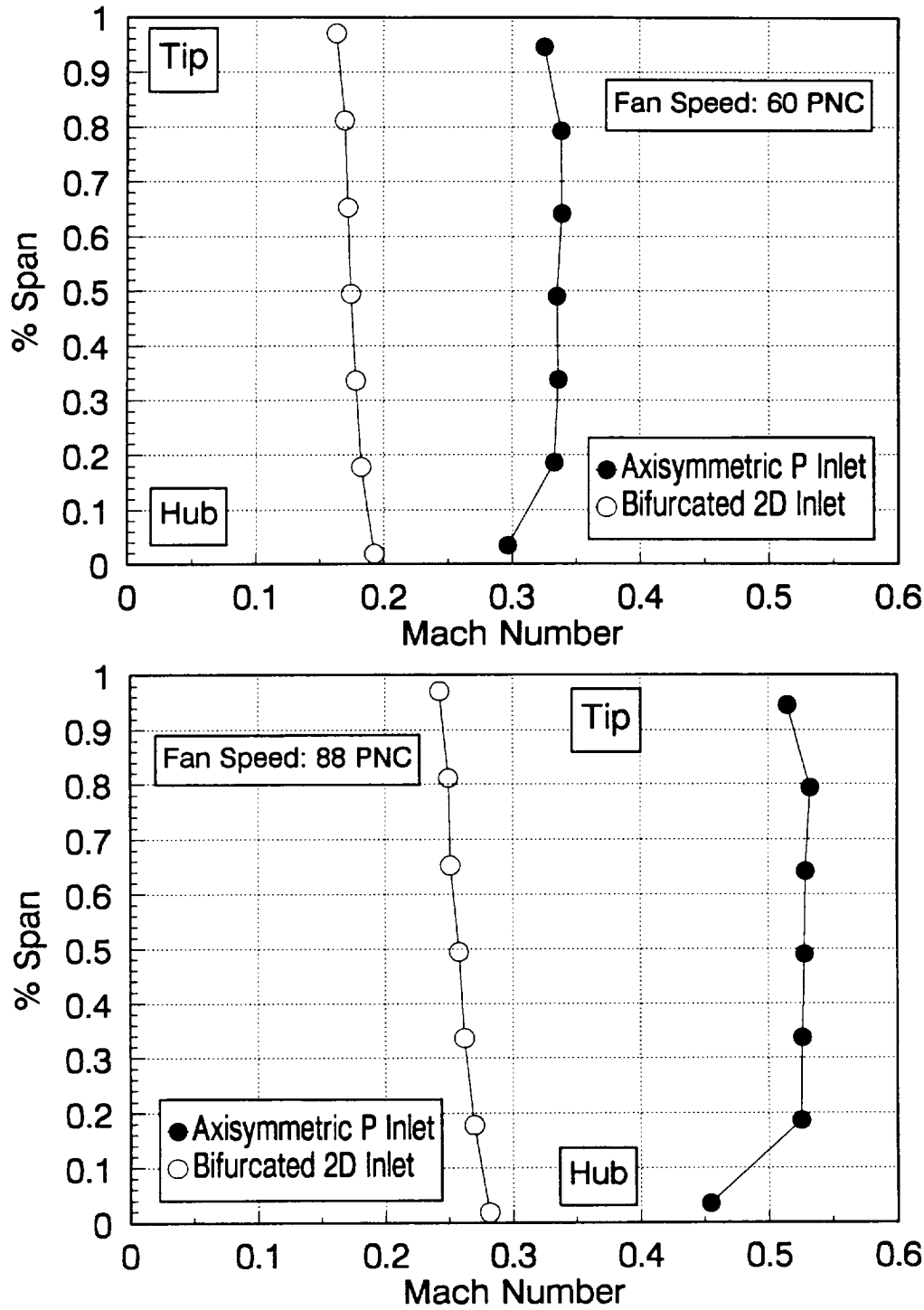


**Figure 4.4 Inlet Mach Number Profiles at the Throat Station, 60 PNC and 88 PNC**

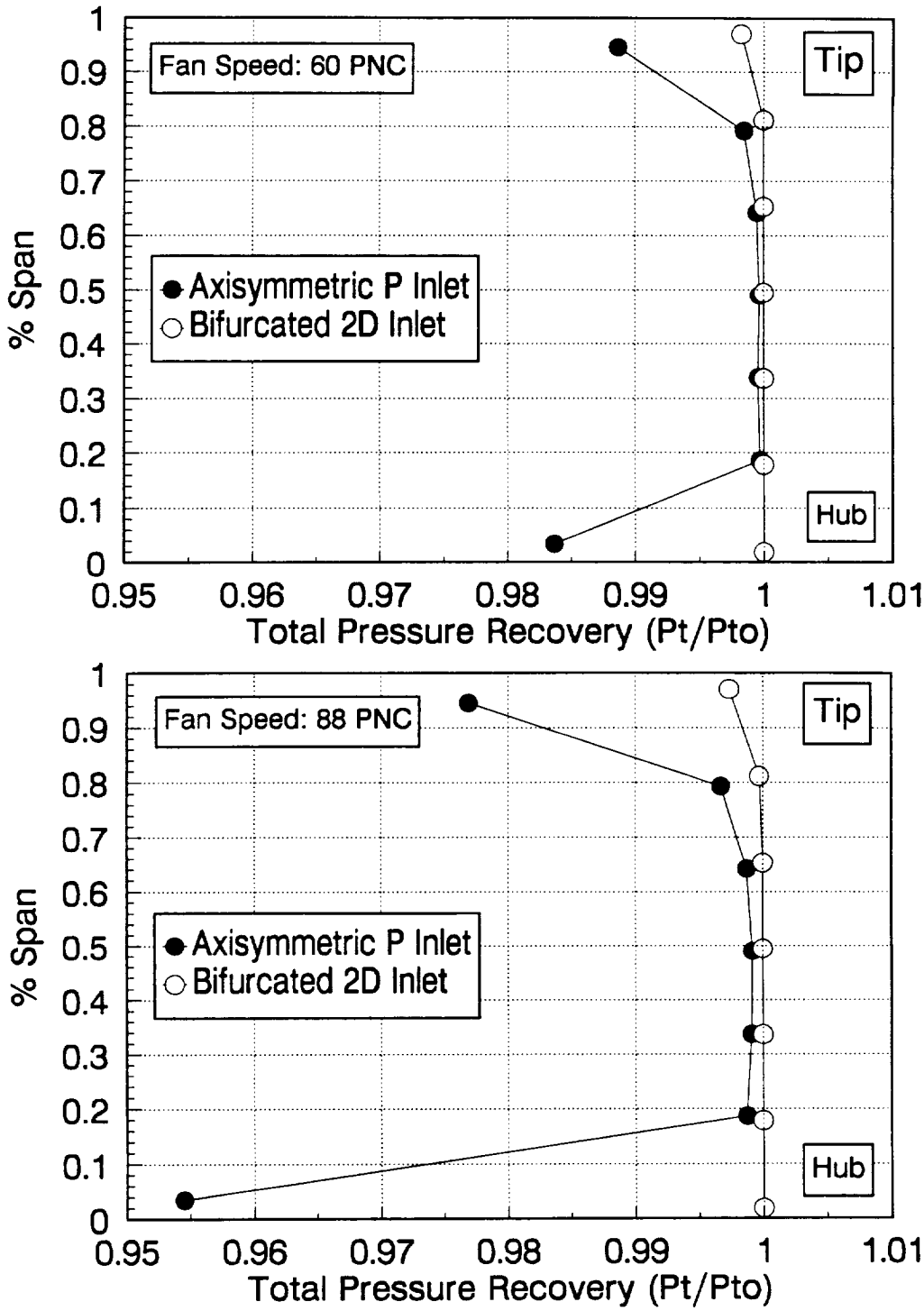


**Figure 4.5 Total Pressure Recovery Profiles at the Throat Station, 60 PNC and 88 PNC**

the 2D inlet. The 2D inlet profile shows no boundary layers because they are too small to be measured at the throat station. These profiles show the flow to be behaving normally without any extreme pressure losses or boundary layers

### 4.1.4 Inlet Flow Distortion

The design of aircraft engine inlets depends strongly on the inlet flow distortion. Distorted flow at the fan face of an engine will decrease the stall margin and increase noise generation. Supersonic inlets are very different from the conventional subsonic inlets because they require the use of a centerbody that has to be supported in some way. Typically, support struts have to be located directly upstream of the engine face in the middle of the air flow. The axisymmetric P inlet has a total of four struts to support its centerbody. The bifurcated two-dimensional inlet does not have support struts, but it is important to note the splitter plate centerbody that creates comparable flow distortions. The centerbody on the 2D inlet causes the fan face to see two regions of wake while the centerbody on the P inlet creates four regions of wake. This section compares the Mach number distributions at the fan face stations of the 2D inlet and the P inlet to evaluate the differences in the inlet distortions.

First, it is important to show the types of flow distortions that affect the acoustic performance of an aircraft engine. Noise generation is influenced by radial and circumferential gradients of Mach number and pressure distortions at the fan face of an

engine. Figure 4.6 illustrates two hypothetical examples of flow distortions. The first contour plot depicts flow distortions with gradients in the radial direction only. In a velocity field of this nature, each of the rotating fan blades in the engine will see a constant axial velocity at a given radius. Therefore, at a given radius the fan blades are uniformly loaded and the noise generation is minimal. The second contour plot shows axial velocity gradients in the circumferential direction only. In this velocity distribution, the fan blades will see periodic fluctuations as they rotate. The loading on the fan blade depends on its angular position. As the blades pass through the slower flow, the pressure in that region fluctuates. At a constant rotational fan speed, the periodic velocity change can generate noise in the far field at multiples of the blade passing frequency. Thus, large circumferential flow gradients in engine inlets can be expected to increase the noise generation when compared to an inlet with only radial distortions.

The measured Mach number distributions at the fan face of the 2D inlet and the P inlet at 60 PNC are shown in Figure 4.7. These contours represent the annular inlet passage at the entrance of the fan. The axial Mach number contours show areas of low velocities directly behind the trailing edge of the 2D inlet centerbody and the support struts of the P inlet. These regions of slow flow create steep circumferential gradients of velocity flow in the region of the fan. The contour plots illustrate how the Mach number distribution at the fan face is effected by having four or two circumferential distortions. The contours show low Mach numbers near the hub as well as at the tip wall on both

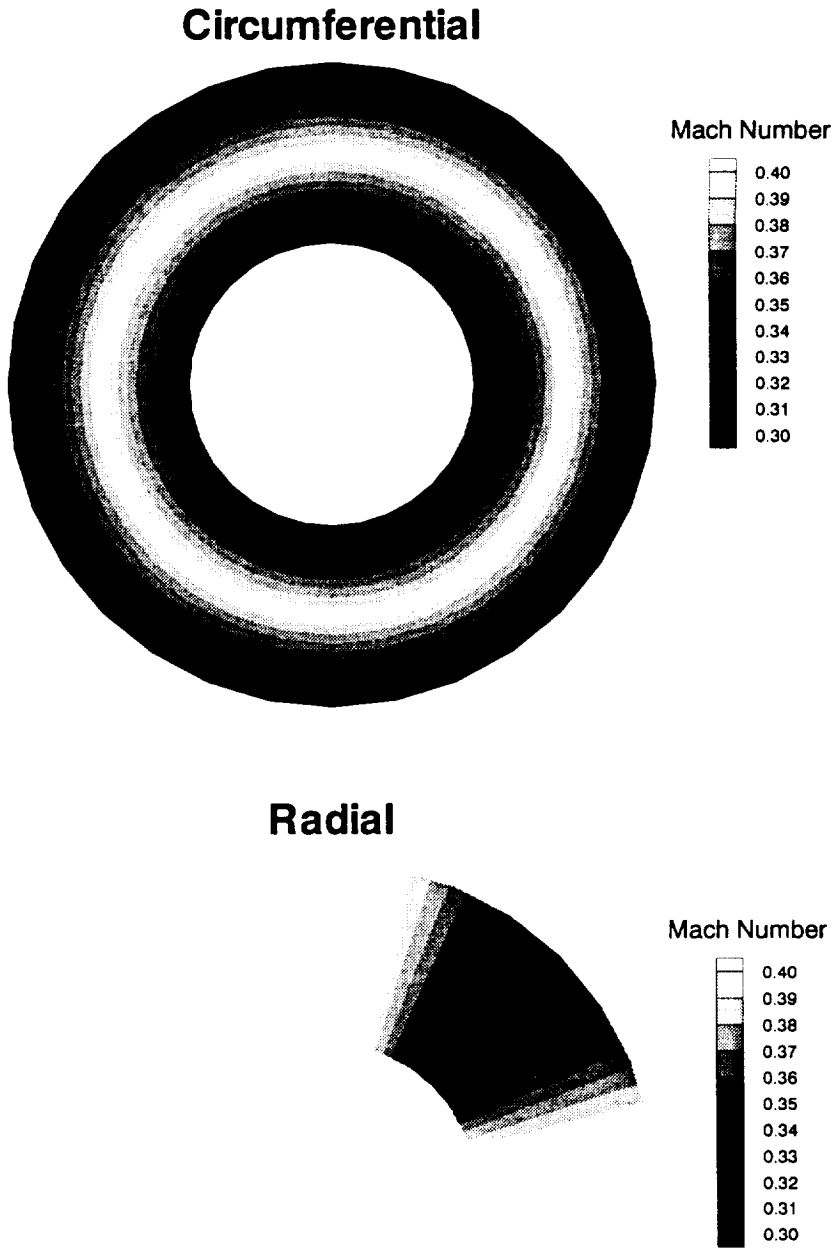


**Figure 4.6 Hypothetical Gradients of Axial Velocity Distortion at the Fan Face**

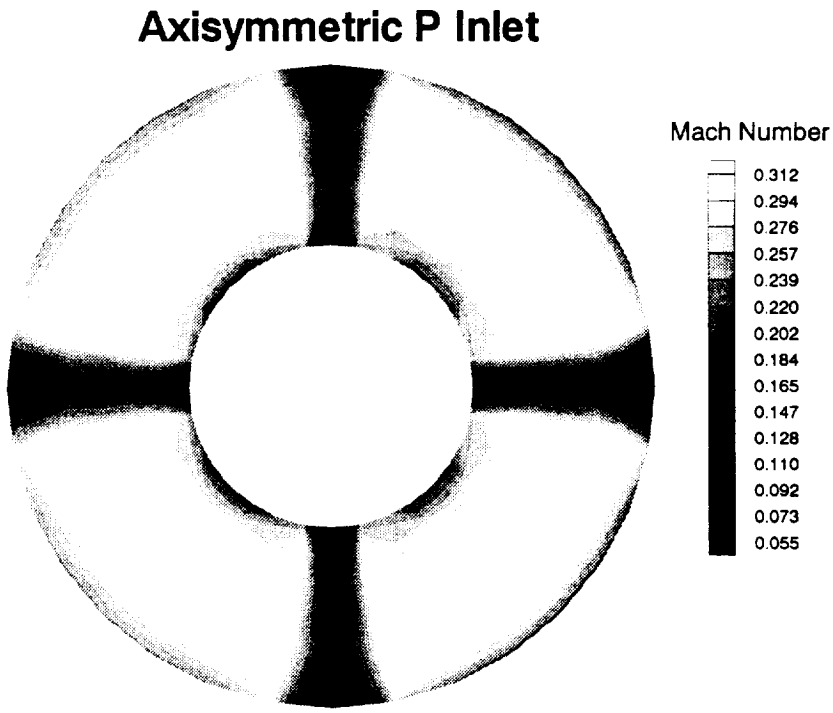


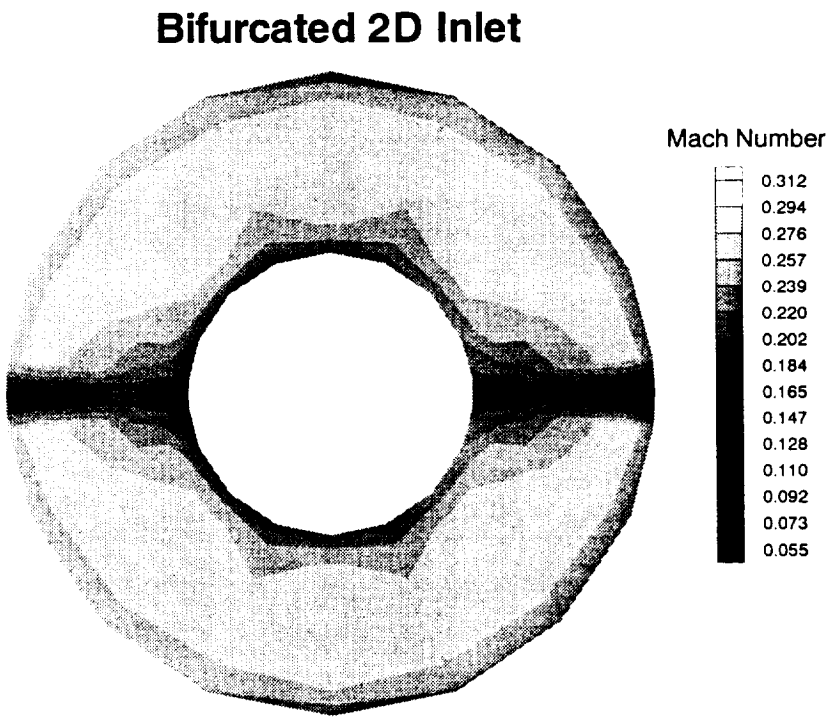


**Figure 4.7 Mach Number Distribution at the Fan Face, 60 PNC**

inlets. The low Mach number on both inlets at the tip region is a result of boundary layer growth as the flow travels down the inlet from the cowl lip.

Figure 4.8 shows the Mach number contours of the bifurcated two-dimensional inlet and axisymmetric P inlet for a test speed of 88 PNC. These contours are very similar to the ones at 60 PNC. The only significant difference in the plots is the increasing regions of low velocities at the tip and hub wall passages. The core flow Mach numbers have increased on both inlets when compared to 60 PNC test speed. The wakes behind the struts seem to grow larger and deeper. The P inlet Mach number drops from 0.52 in the core flow to 0.16 directly behind the strut. The 2D inlet Mach number drops from 0.40 in the core flow to 0.28 behind the trailing edge of the centerbody. The P inlet has a sharper velocity gradient change as the fan blades pass through the slow flow region.

It was necessary to measure the wake profiles behind the centerbody support struts in order to determine if the shape of the profile had any effect on the noise generation. Figure 4.9 gives an illustration of the measurement locations on both inlet. Figure 4.10 compares the wake profiles shed from the support struts of the P inlet and the centerbody of the 2D inlet at 60 PNC and 88 PNC. Theses figures show the inlets have sharp velocity changes as the measurement crosses the trailing edge of the strut. The P inlet has a much steeper change as the profile crosses the trailing edge of the strut when compared to the 2D inlet. The width of the wake profile seems to very similar for both inlets at the different speeds. The biggest difference is the depth of the wake. For the test condition

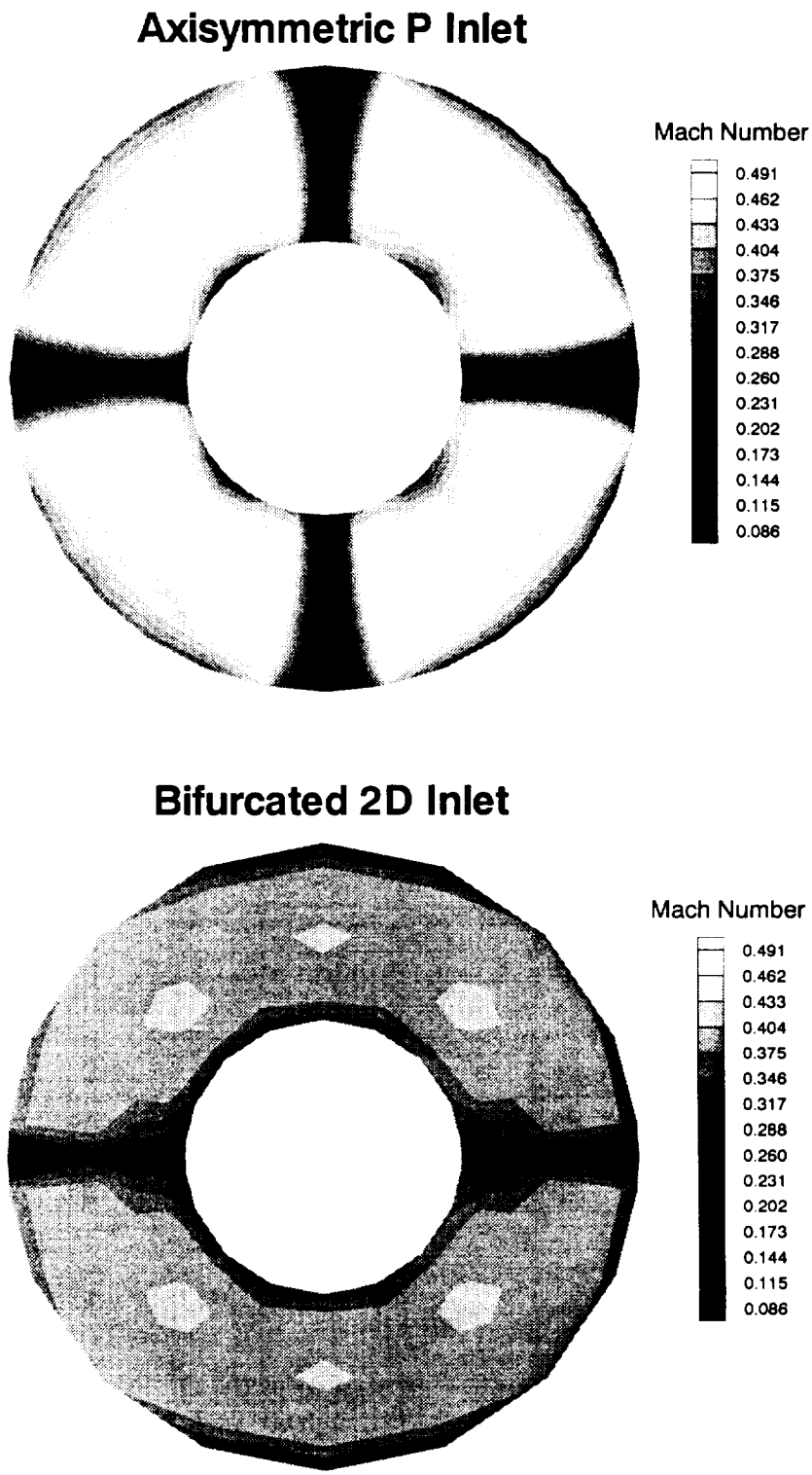


**Figure 4.8 Mach Number Distribution at the Fan Face, 88 PNC**

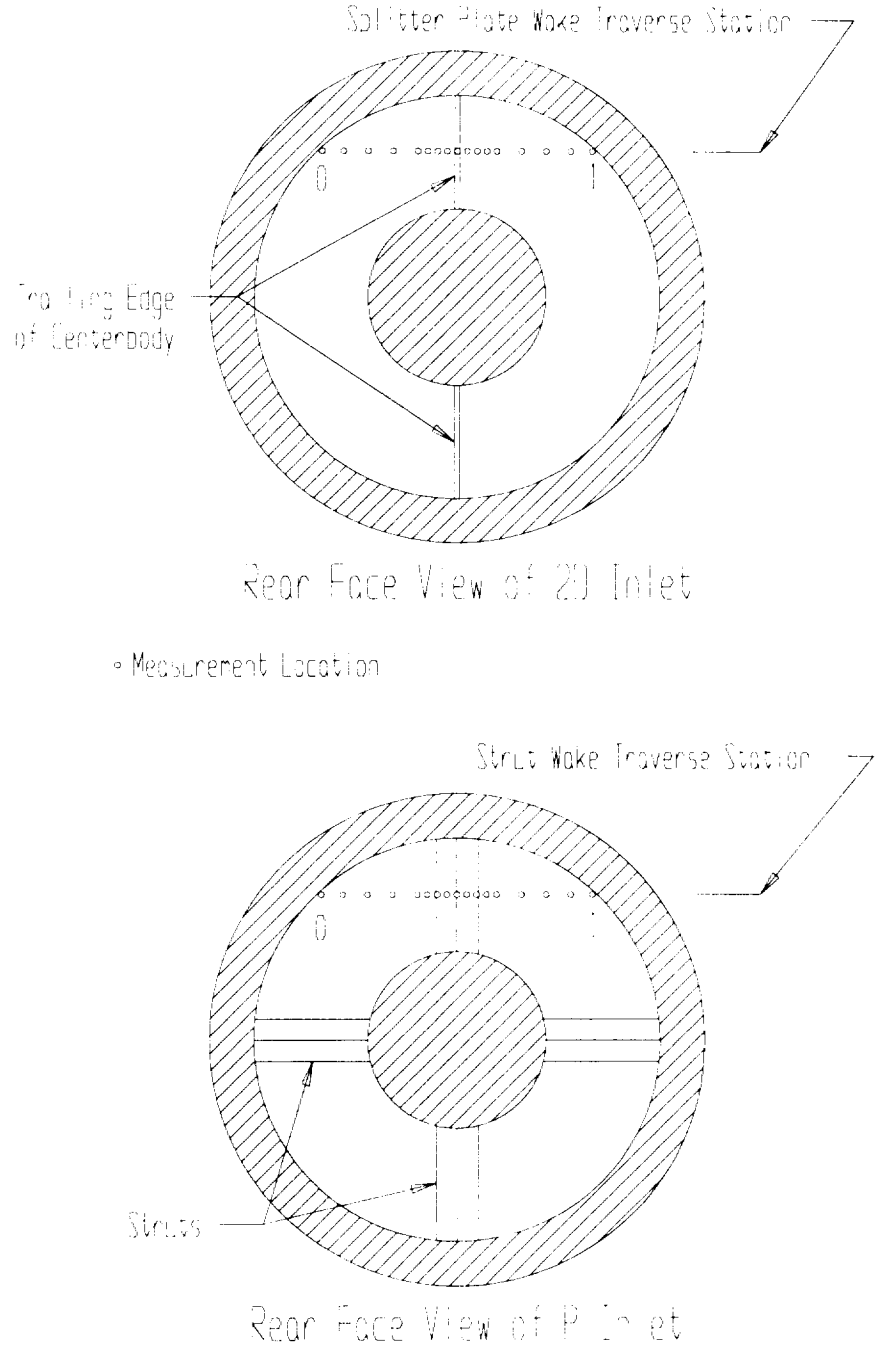


**Figure 4.9 Wake Profile Traverse Stations**

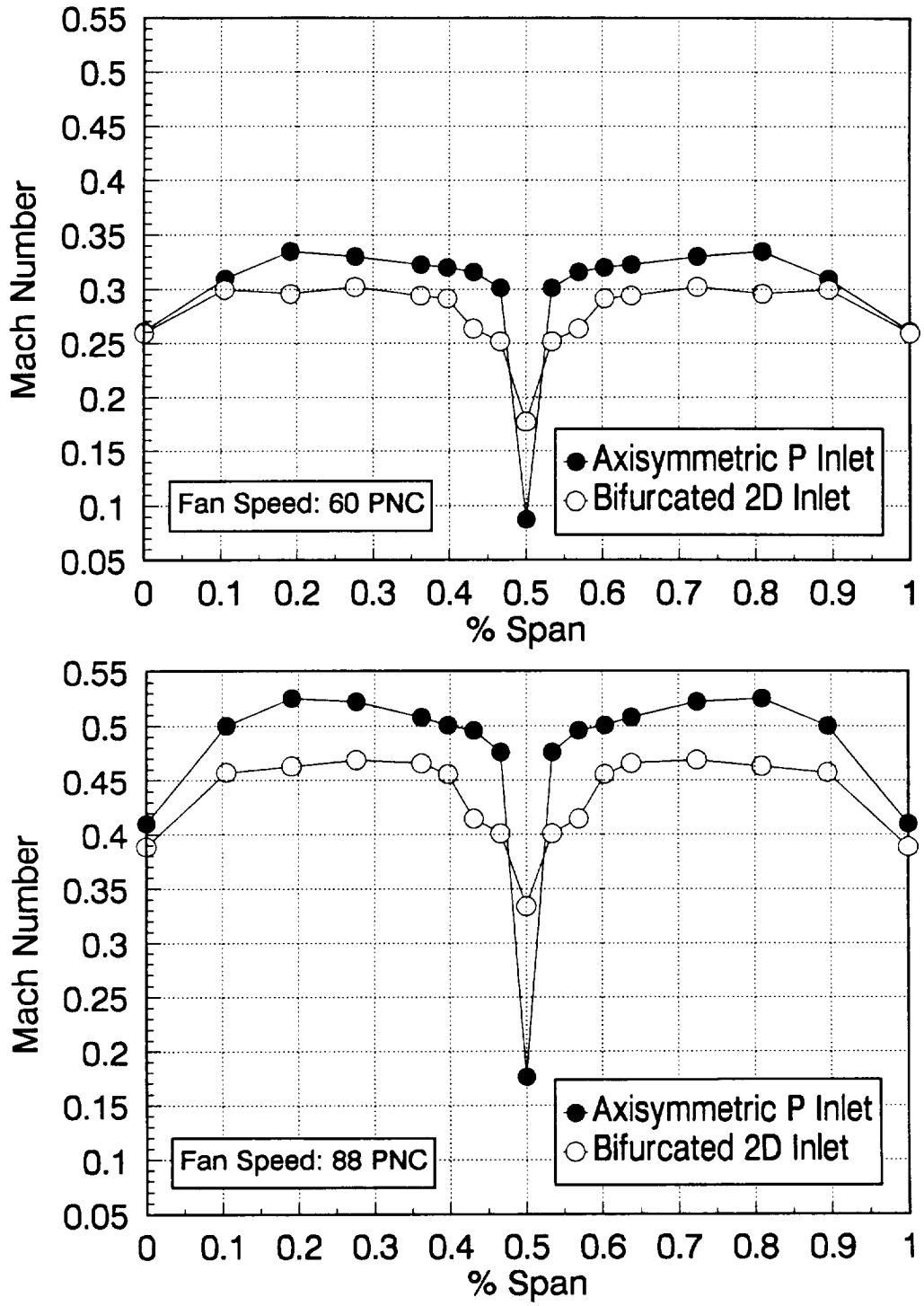


**Figure 4.10 Wake Profile Behind Strut, 60 PNC and 88 PNC**

of 60 PNC, the P inlet drops from a Mach number of 0.3 at the last measurement position before getting directly behind the strut to 0.08 directly behind the strut and the 2D inlet from 0.25 to 0.18. For the test condition of 88 PNC, the P inlet drops from a Mach number of 0.47 at the last measurement position before getting directly behind the strut to 0.17 directly behind the strut and the 2D inlet from 0.4 to 0.28. It is also important to notice how the profile for the P inlet curves from the tip walls all the way down to the slow flow behind the strut. The wake in the 2D inlet instead has an indention right before the profile gets behind the strut. This may be attributed to the boundary layer on the centerbody and its interference with the centerbody nose cone. The same effect can be see in Figures 4.7 and 4.8 for the 2D inlet around the nose cone and splitter plate intersection. Even though the P inlet wake was deeper than the 2D inlet wake, the radiated noise levels discussed in Section 4.2.2 were not increased at 60 PNC. The reasons for this are not yet fully understood and more research should focus on measuring how the wake profile shape effects the noise generation of the fan.

### 4.1.5 Inlet Pressure Recovery

The aerodynamic performance of the two inlets can be quantified by obtaining the total pressure recovery of each inlet at the fan face of the simulator. Figure 4.11 shows the pressure recovery contours at the fan face for the 2D inlet and the P inlet at 60 PNC. The P inlet shows an almost unnoticeable boundary layer in the core flow region or at the

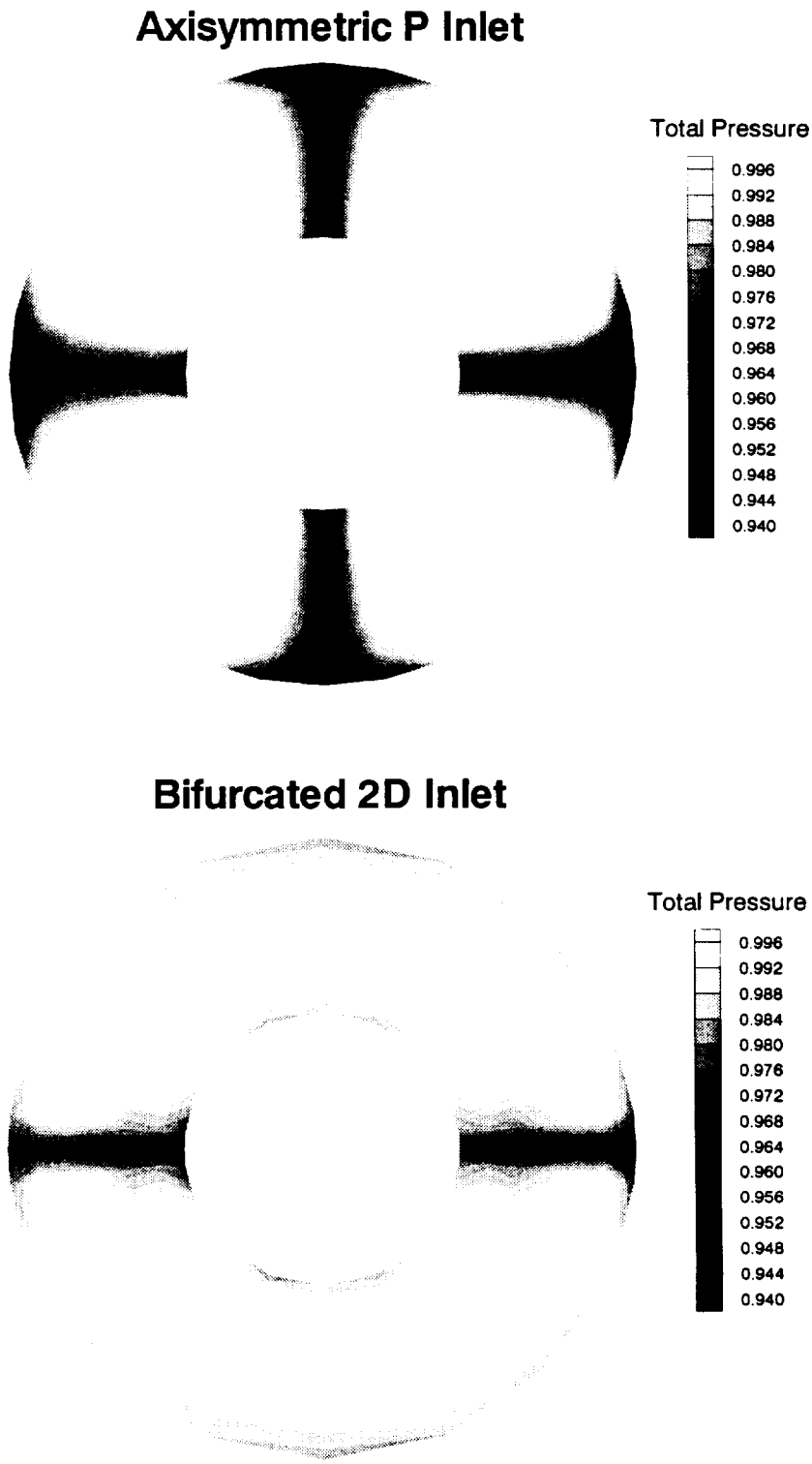


**Figure 4.11 Total Pressure Recovery Distribution at the Fan Face, 60 PNC**

45° circumferential position. The core flow is very uniform until it encounters the struts. The four centerbody support struts create a low pressure recovery region directly behind each of them. This low pressure recovery is caused by the large wakes the struts create in the flow approaching the simulator. Boundary layer buildup is evident at the tip wall near the struts because of a vortex/boundary layer interaction in the corner flow region. The reason the hub wall region does not show any signs of large boundary layers is not yet known. The 2D inlet contour shows small boundary layer growth along the tip and hub walls. This separation region is larger than the boundary layer on the P inlet. The boundary layer on the cowl wall of the 2D inlet is a result of the transition section from a rectangle at the front of the inlet to a circular shape at the fan face. Boundary layer fluid can also be seen accumulating at the hub of the trailing edge of the centerbody indicating the interaction with the nose cone. As the boundary layer grows on the centerbody it encounters the nose cone right before the fan face and is pushed out into the core flow. This increases the losses seen around the trailing edge of the centerbody at the hub wall. The 2D inlet only has two low pressure region because of the centerbody having a splitter plate trailing edge. These wakes cause a low pressure region, however they are not as severe as the wakes shed from the support struts in the P inlet.

Figure 4.12 illustrates the total pressure recovery contours of the two inlets at 88 PNC. The P inlet contour is very similar to the contour at 60 PNC except for the loses behind the struts. The velocity has increased, and as a result the wakes have deepened and the loses have increased. The boundary layer region in the core flow areas has

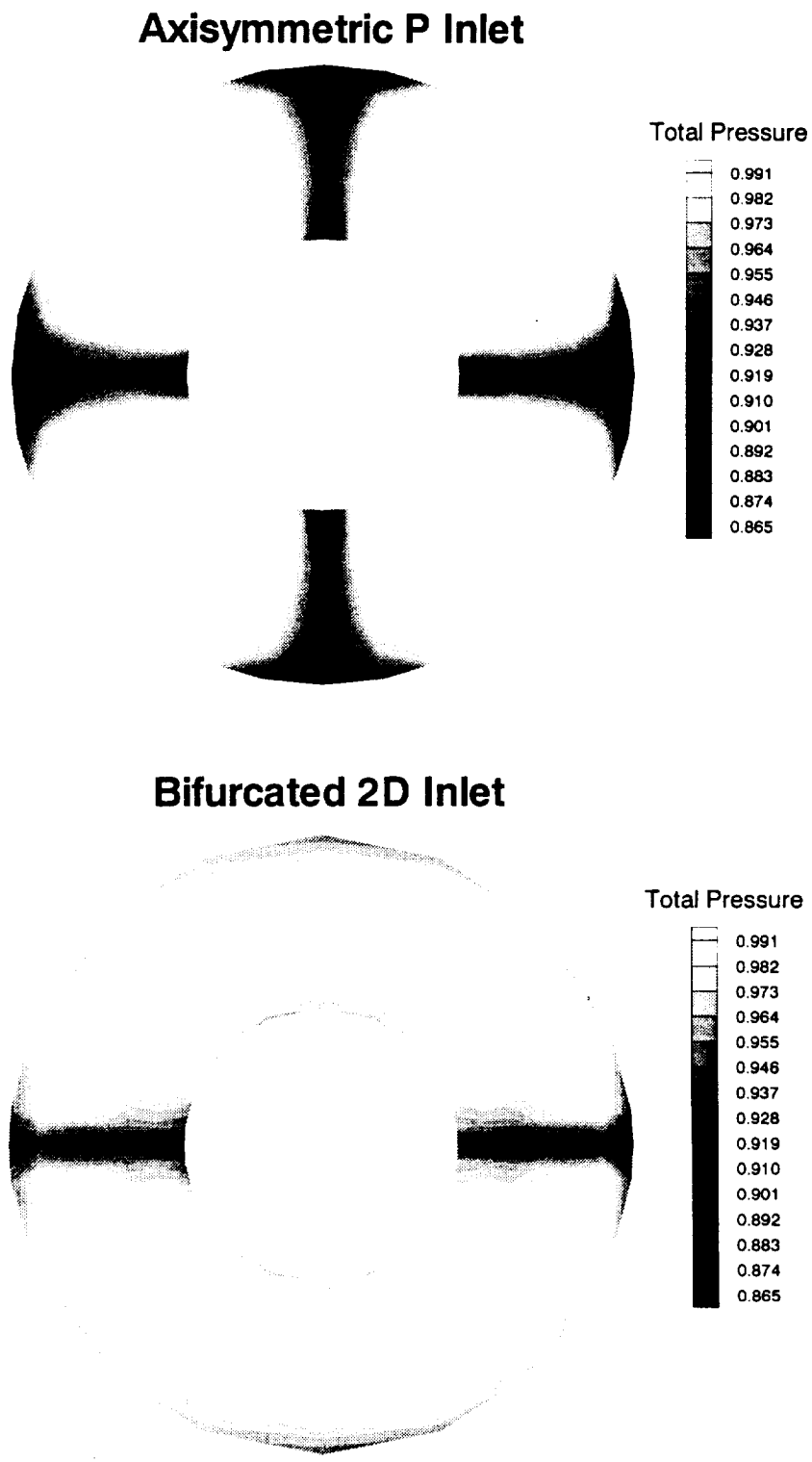


**Figure 4.12 Total Pressure Recovery Distribution at the Fan Face, 88 PNC**

increased slightly. The 2D inlet contour is very similar to the contour at 60 PNC as well. The boundary layer regions have increased slightly and the loses behind the trailing edge of the centerbody have also increased.

Table 4.3 presents the area averaged pressure recovery of the 2D inlet and the P inlet at both test speeds. Since the wake depth and the boundary layer thickness both increase with flow velocity it is expected that the pressure recovery at 88 PNC will be lower than that of 60 PNC. The average pressure recovery at the fan face is very similar for the two inlets at the approach and takeoff flight conditions. The P inlet has more losses behind the struts, however the 2D inlet has a larger tip and hub boundary layer giving each inlet a comparable pressure recovery. The average total pressure recovery is calculated by averaging the pressure recovery over the seven radial positions over the entire circumferential span. The individual radial measurements are then averaged together weighted on the area of the radial region. These results demonstrate the aerodynamic performance of both inlets and that neither inlet has a distinct advantage over the other.

**Table 4.3 Fan Face Area Averaged Total Pressure Recovery**

| Inlet Type | Pressure Recovery 50,000 RPM (60 PNC) | Pressure Recovery 70,000 RPM (88 PNC) |
|---|---|---|
| Bifurcated 2D Inlet | 0.992 | 0.981 |
| Axisymmetric P Inlet | 0.991 | 0.979 |

A circumferential distortion intensity parameter was developed the quantify the gradient differences of the flow loses in the circumferential direction. This parameter is defined in the Aerospace Recommended Practice (ARP 1420) by the Society of Automotive Engineers. The ARP provides guidelines by which gas turbine engine aerodynamic stability and performance, as affected by the quality of the airflow delivered to the engine, can be evaluated consistently. This specific parameter permits the representation and evaluation of the total pressure effects on the system stability and performance. The distortion intensity is described as the magnitude of the pressure defect for each radial ring of measurements spanning the entire 360° annulus. The distortion intensity was determined over the radial positions and then area averaged to determine the overall circumferential distortion for the entire fan face. A detailed description and computer code explaining how the parameter was calculate for each inlet is contained in Appendix C. Table 4.4 list the distortion intensities for both inlets at 60 PNC and 88 PNC. The 2D inlet and the P inlet show the pressure distortion increasing as the flow velocity increased. The increase is a result of the wakes becoming deeper and the boundary layer growth increasing.

**Table 4.4 Total Pressure Circumferential Distortion Intensities**

| Inlet Type | Distortion 50,000 RPM (60 PNC) | Distortion 70,000 RPM (88 PNC) |
|---|---|---|
| Bifurcated 2D Inlet | 0.009 | 0.020 |
| Axisymmetric P Inlet | 0.022 | 0.050 |

## 4.2 Acoustic Results

Three sections will be used to present the acoustic performance of the 2D inlet and P inlet. The first section explains the soft choking effect that influenced the noise levels of the P inlet. The second section shows the radiated noise patterns of the tone and overall sound pressure levels. The tone sound pressure level may also be referred to as the blade passing tone (BPT). These measurements are used to map out the acoustic performance of the forward propagating fan noise coming from the inlet. The acoustic measurements are presented in a directivity plot format containing all 12 circumferential locations from 0° to 110° at 10° increments at a radius of 48 in (122 cm). The center of the radius of measurement was the center of each inlet's capture area. The acoustic results presented here are the radiated noise levels from the two inlets at a single measurement plane. The primary acoustic planes are used for this comparison; however, all the planes for an individual inlet are shown to have the same trends (See Appendix D). A comparison between the radiated fan noise patterns of the 2D inlet and P inlet will

show which inlet has the best acoustic performance. The third section uses the sample narrowband spectra to explain the characteristics of the radiated noise from the inlets.

### 4.2.1 Soft Choking Effect

The tone and overall sound pressure levels were measured versus the blade tip speeds at the 20° microphone location to illustrate what happens to the radiated noise levels as the fan speed is increased for both inlets. Figure 4.13 presents the throat Mach numbers and tone sound pressure level for the 2D inlet and P inlet at the 20° microphone position as a function of the blade tip speed of the fan. At 50,000 RPM (895 ft/s), the BPT for the P inlet is louder by 1 dB. At 54,000 RPM (966 ft/s), the BPT for the 2D inlet dropped to its lowest value. The reason for this is possibly due to the shifting of the acoustic lobes being radiated from the inlet. As the speed of the simulator increases, the radiated lobes will move according to Homicz and Lordi (1974). The lobes will shift toward the centerline of the inlet and the measurement location could possibly fall in between two primary lobes. The lobe radiation patterns will be discussed in Section 4.2.4. As the speed approached 70,000 RPM (1250 ft/s), the P inlet noise level dropped significantly as soft choking began to occur. The soft choking effect was influenced by the throat Mach number associated with the particular inlet. The throat Mach number graph shows the large difference in the Mach numbers between the two inlets as the speed increases. The BPT was 16 dB higher than the 2D inlet at the takeoff speed indicating a

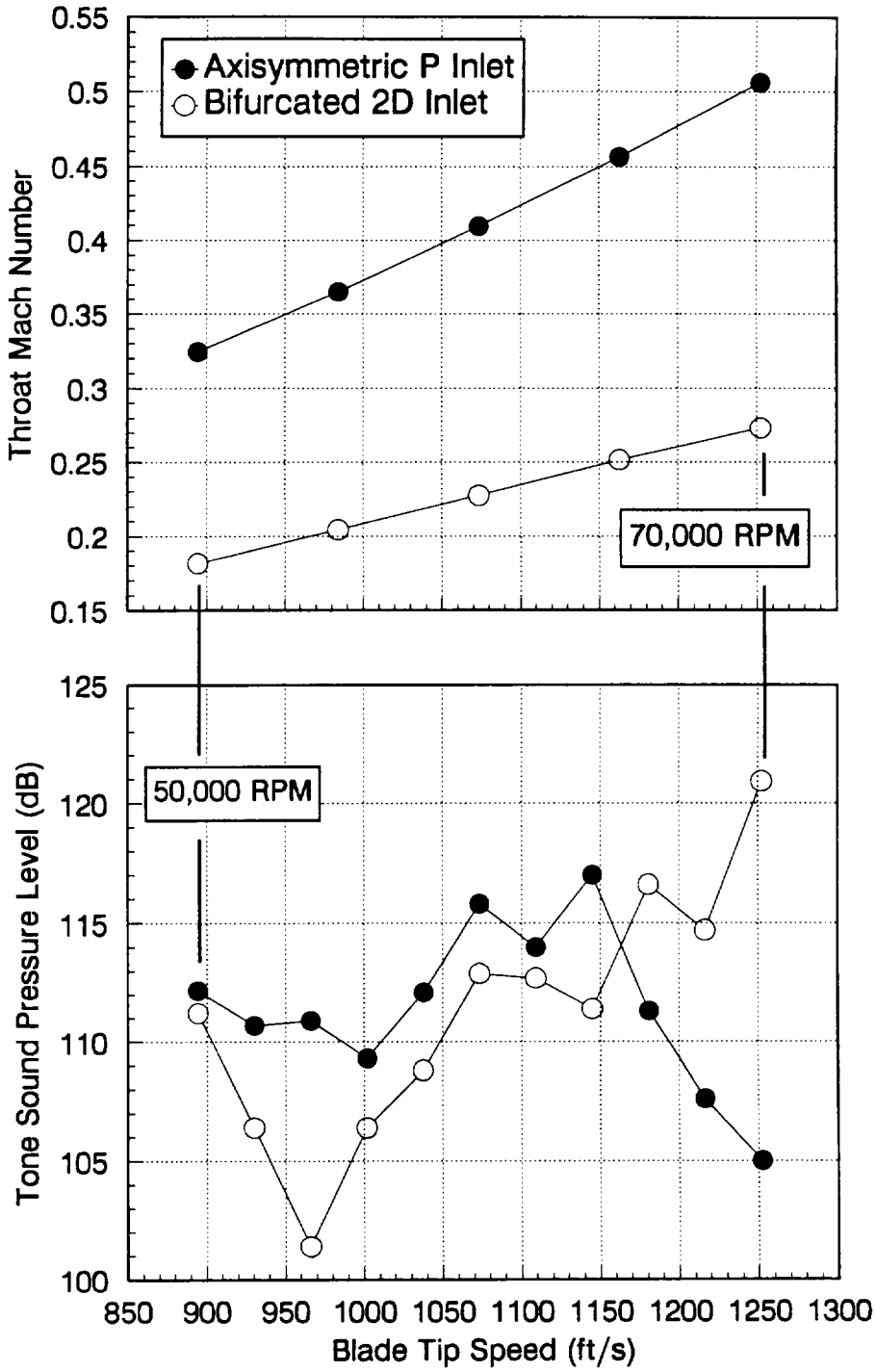


**Figure 4.13 Inlet Throat Mach Number and Tone Sound Pressure Level vs. Blade Tip Speed at the 20° Microphone Location**

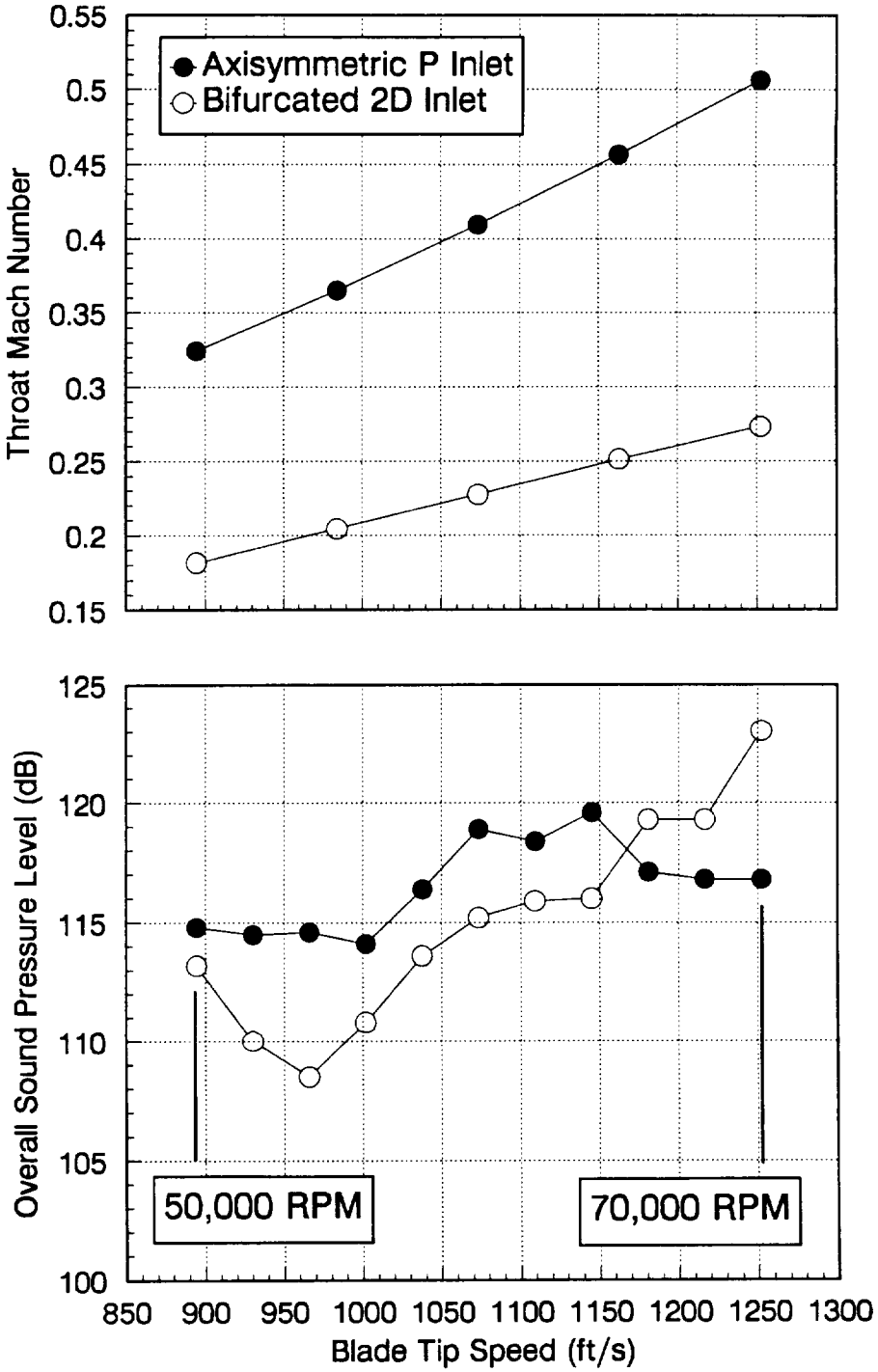


**Figure 4.14 Inlet Throat Mach Number and Overall Sound Pressure Level vs. Blade Tip Speed at the 20° Microphone Location**

better acoustic performance for the P inlet. Figure 4.14 presents the throat Mach numbers and overall sound pressure level for the 2D inlet and P inlet at the 20° microphone position as a function of the blade tip speed of the fan. The OASPL is a measurement of the contribution of the broadband noise and all tones over the frequency domain (0-25600Hz). As the fan speed increased, the same effect was seen as in the BPT graph. At approach conditions the difference was less than 2 dB, and at takeoff conditions the difference was approximately 6 dB, illustrating that the P inlet noise level dropped due to a soft choking effect at the throat.

### 4.2.2 Radiated Noise Levels

The directivity plots for the approach flight conditions are shown in Figure 4.15 comparing the radiated noise levels for both of the inlets. Each tone and overall sound pressure level value represent the average of five consecutive readings from the frequency spectra recorded with the B&K signal analyzer. The averaging helps to eliminate the influences of atmospheric disturbances and the fluctuating fan speeds on the measurements. The fan speed fluctuated a maximum of 2% of the test speed for both inlets at 60 PNC and 88 PNC for this research. The error in the acoustic measurements was ±1.5 dB for the P inlet and ±2.5 dB for the 2D inlet at both test speeds. The tone sound pressure level plot illustrates both inlets having relatively the same noise levels in the 0° to 70° sector and varying between 0 and 3 dB. A maximum difference of 13 dB is

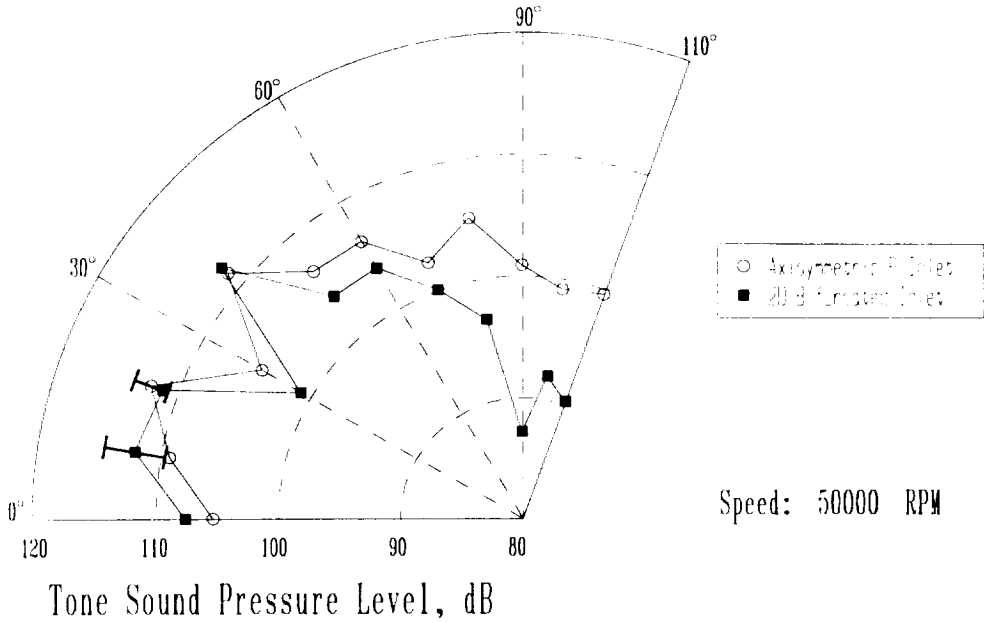


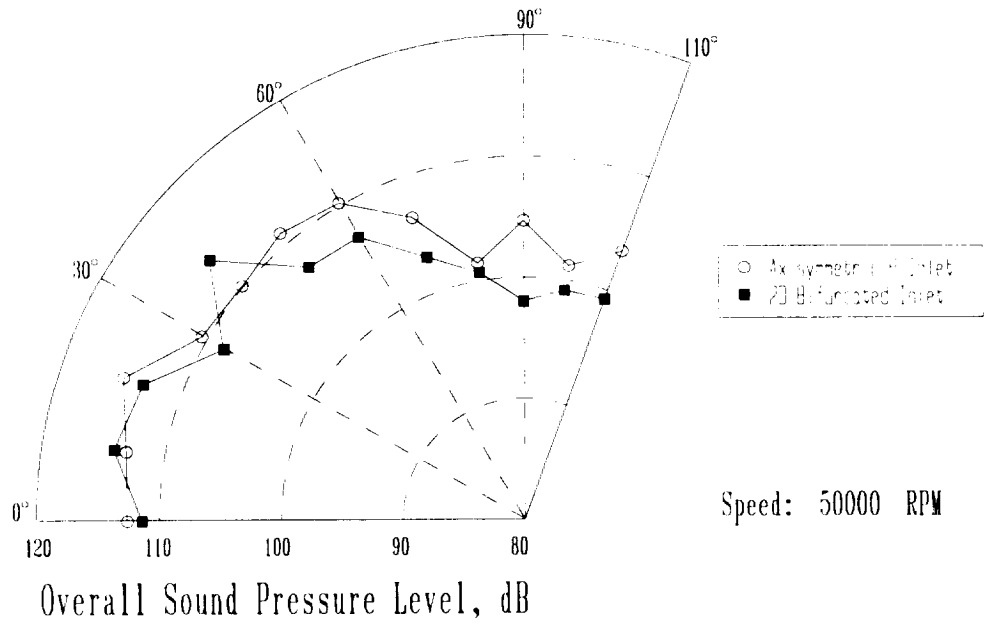


**Figure 4.15 Directivity Plots at 60 PNC (Approach Condition)**

seen in the rear sector at the 90° microphone location. The average tone sound pressure level for the entire 0° to 110° sector was calculated and the two inlets differ by less than 1 dB. The sound pressure level is defined by:

$$SPL = 10\log_{10}\left(\frac{p}{p_{ref}}\right)^2 \text{dB}$$

where $p$ is the rms pressure fluctuation and $p_{ref}$ is the reference rms pressure fluctuation equal to 20μPa. The following average SPL equation was derived from the previous definition of SPL.

$$SPL_{avg} = 10\log_{10}\left[\frac{1}{n}\sum_{i=1}^{n}10^{\left(\frac{SPL_i}{10}\right)}\right]$$

where $n$ is the number of measurement locations ($n$=12) and $SPL_i$ is the measurement at each microphone location from 0° to 110° ($i$=1…12). The overall sound pressure level plot shows both inlets are producing similar noise levels throughout the entire measurement section varying between 0 and 6 dB with maximum difference at the 90° microphone location. The average overall sound pressure level for the entire 0° to 110° sector differed by less than 1 dB and show the same conclusions as the tone sound

pressure level. For the approach conditions of 60 PNC, neither inlet has a distinct advantage over the other for the acoustic performance.

The sideline radiated noise levels are regulated by the FAA aircraft noise regulations. Figure 4.16 estimates the blade passing frequency tone sideline radiation of the 2D inlet and P inlet for 60 PNC at a distance of 48 in (122 cm) from the inlet's centerline. The results are interpolated from the far field measurements of the BPT data of Figure 4.15 for the 10° to 110° measurement locations. The guidelines for the sideline calculations are presented by Dunn and Peart. The sideline sound pressure level was calculated from the equations shown below.

$$SPL_{sideline}(x) = SPL_a(\theta) - 20\log\left\{SDx\left(\frac{\csc(\theta)}{R}\right)\right\}$$

$$x = SD\cot(\theta)$$

| | |
|---|---|
| $SPL_{sideline}$: | Sound Pressure Level at the sideline parallel to the inlets axis at a distance x from the center of the arc for acoustic measurement |
| $SPL_a$: | Sound Pressure Level at the θ angular microphone location |
| $SD$: | Distance to sideline, $SD$=48in (122cm) |
| $R$: | Radius of arc for acoustic measurement, $R$=48in (122cm) |
| $\theta$: | Angular measurement location, $\theta = 0° \ldots 110°$ |
| $x$: | Distance along the sideline from the center of the arc used for the acoustic measurement |

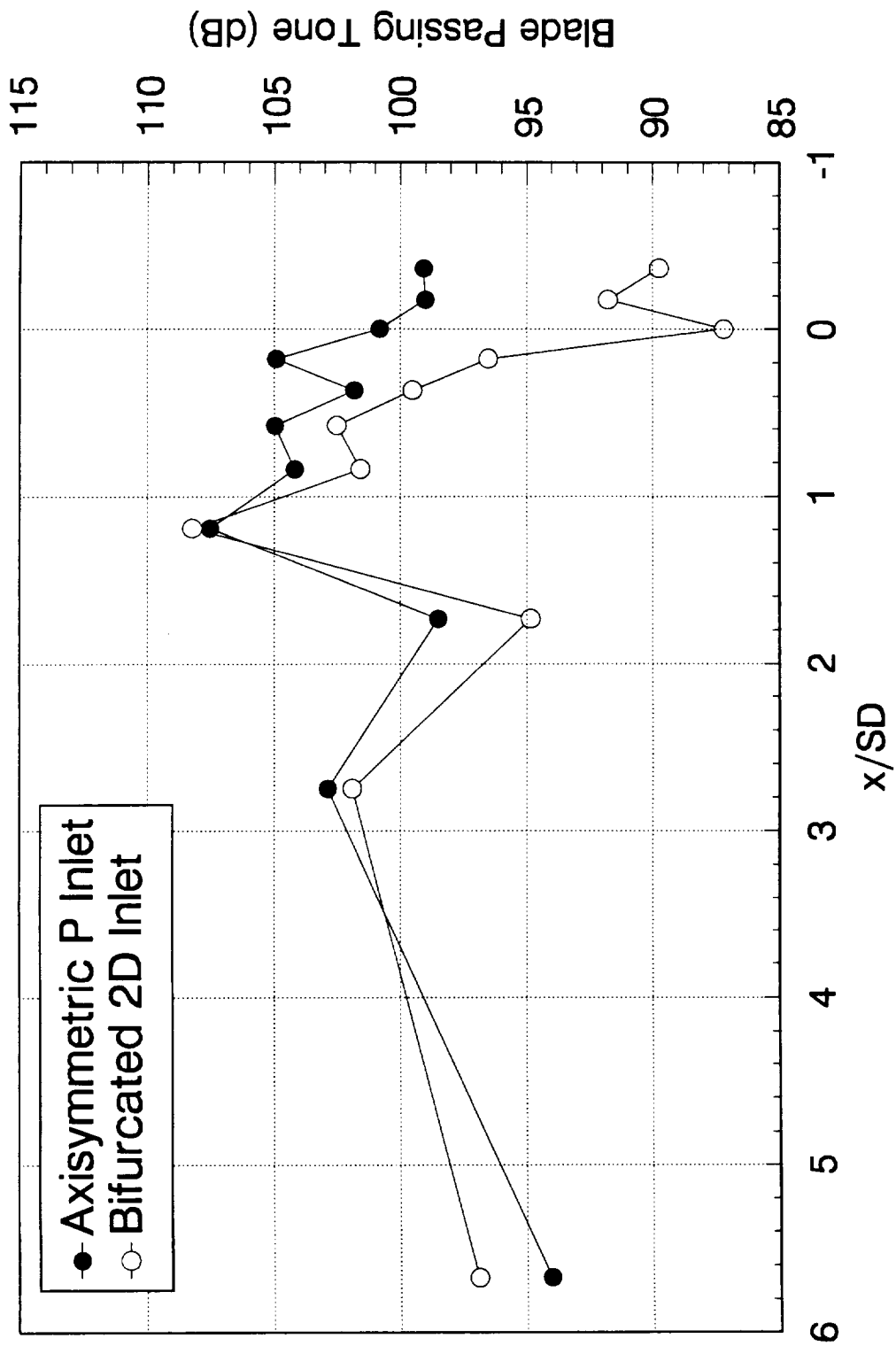


**Figure 4.16 Sideline Estimates for Blade Passing Tone, 60 PNC**

Since the sideline distance and the radius of the arc for the measurements are equal in the test setup, the above equation is reduced to:

$$SPL_{sideline}(x) = SPL_a(\theta) - 20\log\{\csc(\theta)\}$$

The graph shows the same trends as the BPT directivity plot for the approach condition giving each inlet approximately the same sideline noise levels.

Figure 4.17 shows the graphs of the radiated noise levels from both inlets at the takeoff condition of 88 PNC. The directivity plot for the tone sound pressure level shows the 2D inlet having higher noise levels in the 0° to 70° sector than the P inlet. A maximum difference of 16 dB is seen at the 20° microphone location. In the rear sector, the two inlets have only small differences. The average tone sound pressure level for the entire 0° to 110° sector differ by 9 dB. The overall sound pressure level directivity plot illustrates the same results as the tone sound pressure level directivity plot. The forward sector, from 0° to 60°, shows the 2D inlet with a louder sound pressure level with a maximum of 6 dB occurring at the 20° microphone location. The average overall sound pressure level for the entire 0° to 110° sector differs by 3 dB and show the same conclusions as the tone sound pressure level when comparing the two inlets. For the takeoff conditions of 88 PNC, the P inlet has a distinct acoustic performance advantage over the 2D inlet because the soft choking effect becomes evident due to the throat Mach

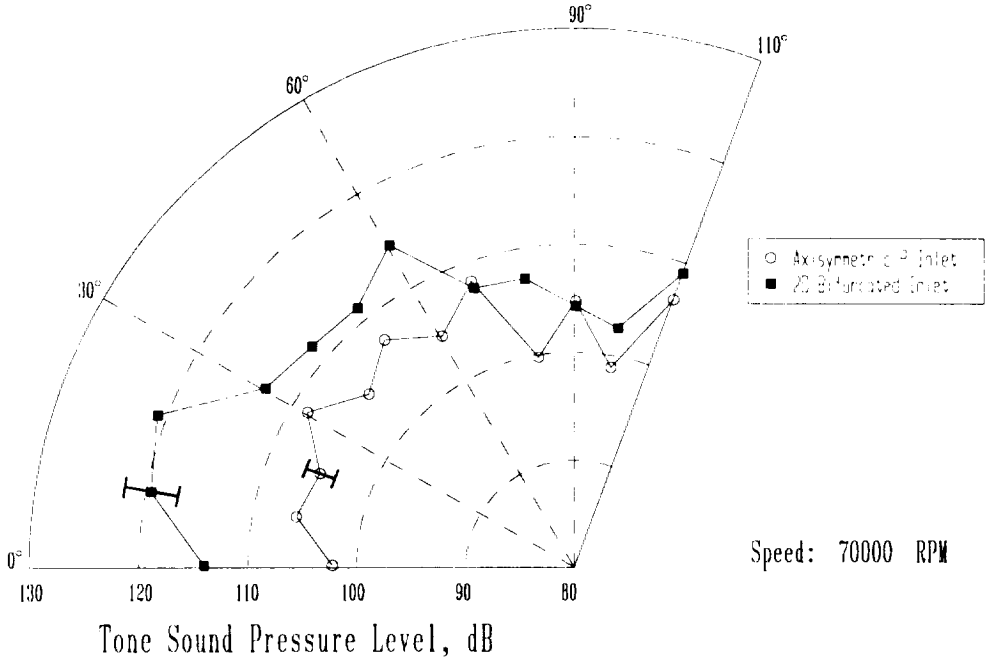


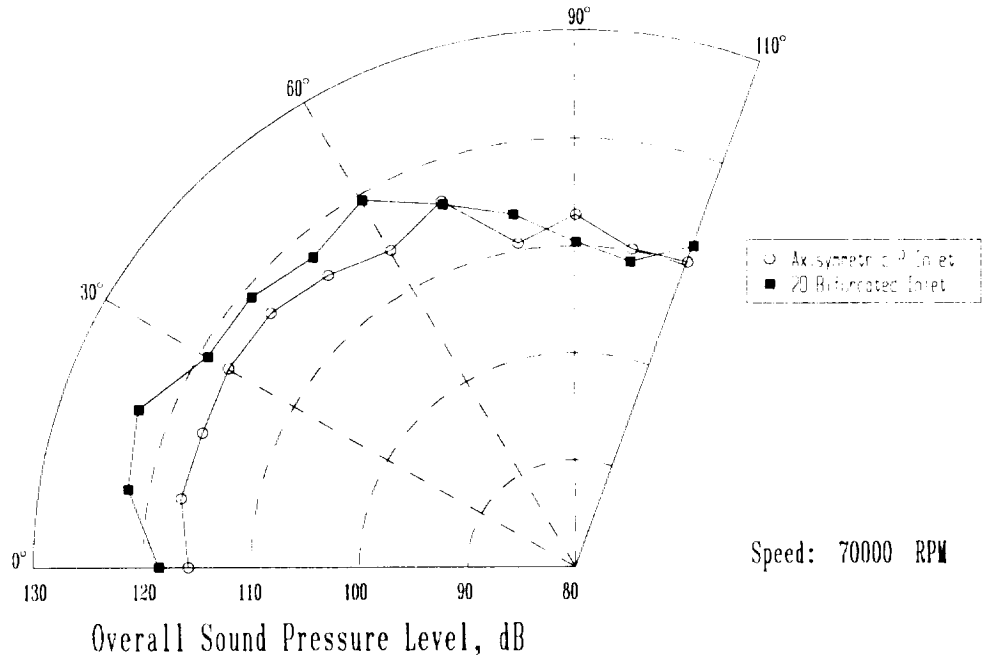


**Figure 4.17 Directivity Plots at 88 PNC (Takeoff Condition)**

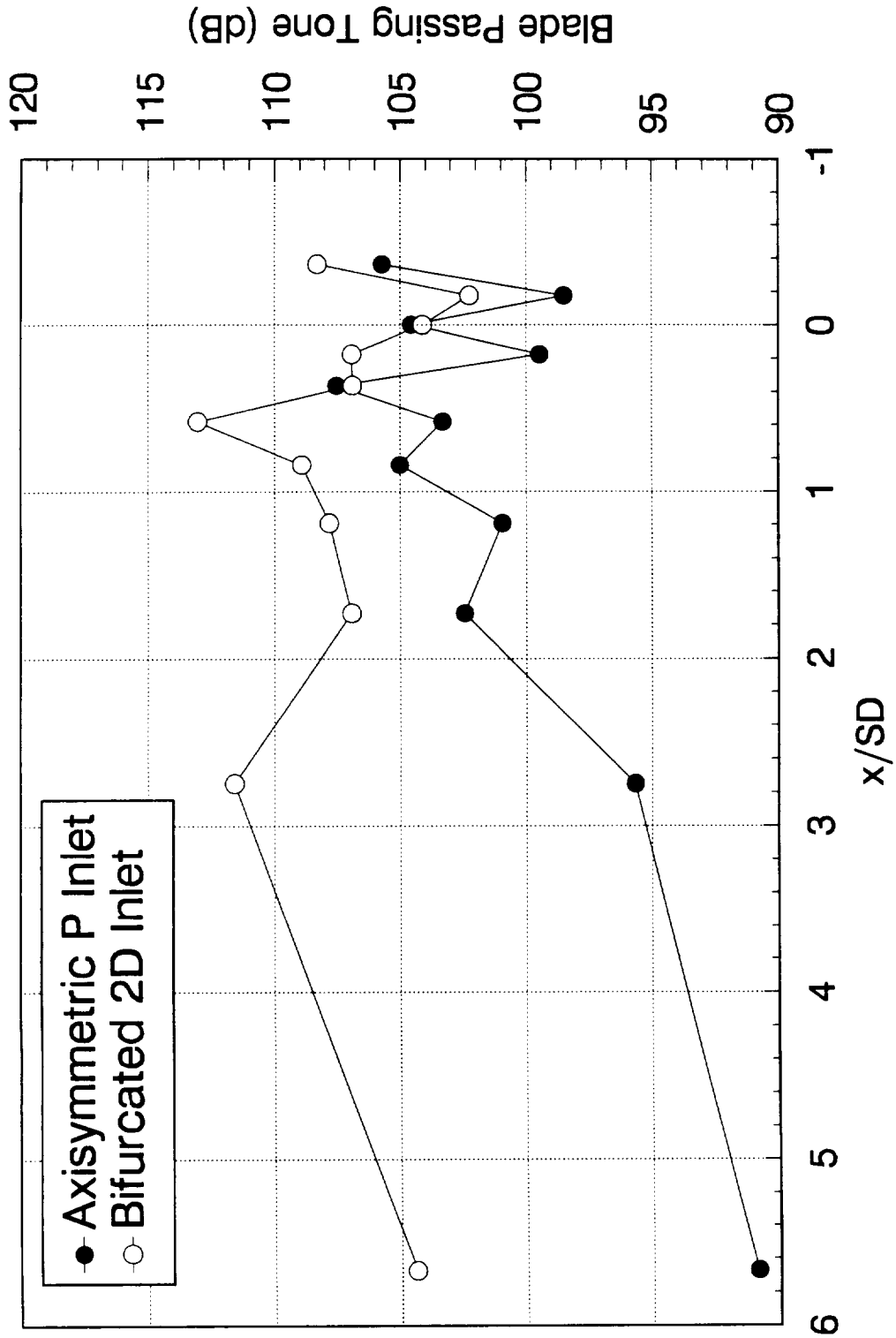


**Figure 4.18 Sideline Estimates for Blade Passing Tone, 88 PNC**

number exceeding 0.5. Figure 4.18 estimates the sideline radiation of the blade passing frequency tone at 88 PNC showing the same results as the directivity plot.

### 4.2.3 Narrowband Noise Spectra

The narrowband spectra are useful in analyzing the characteristics of the forward radiated noise from the supersonic inlets. The spectra presented in this section are a linear average of twenty samples over a frequency range of 0 to 25.6 kHz at resolution of 32 Hz. The tone and overall sound pressure levels were recorded from each of these individual spectrums and were presented in the previous section.

Figures 4.19 and 4.20 illustrate a sample spectrum for the 2D inlet and P inlet at a test speed of 60 PNC (approach conditions) at a microphone location of 0° and 20° respectively. These spectra are typical of a fan with subsonic blade tip speeds. For the approach flight conditions, the turbofan simulator was running at 50,000 RPM (60 PNC) with a blade tip speed of 895 ft/s (Mach 0.8). The blade passing frequency was at 15 kHz at this test condition. Both figures show the blade passing frequency tone as the dominate noise source. The rest of the spectrum contains broadband noise. Comparing the difference in inlet spectra can point to large or small differences in the overall sound pressure levels. For this case, the OASPL measured for the two inlets differed by only 1 dB. The spectra comparison reflect these result because there are not any large differences in the spectra for either inlet at each microphone location.

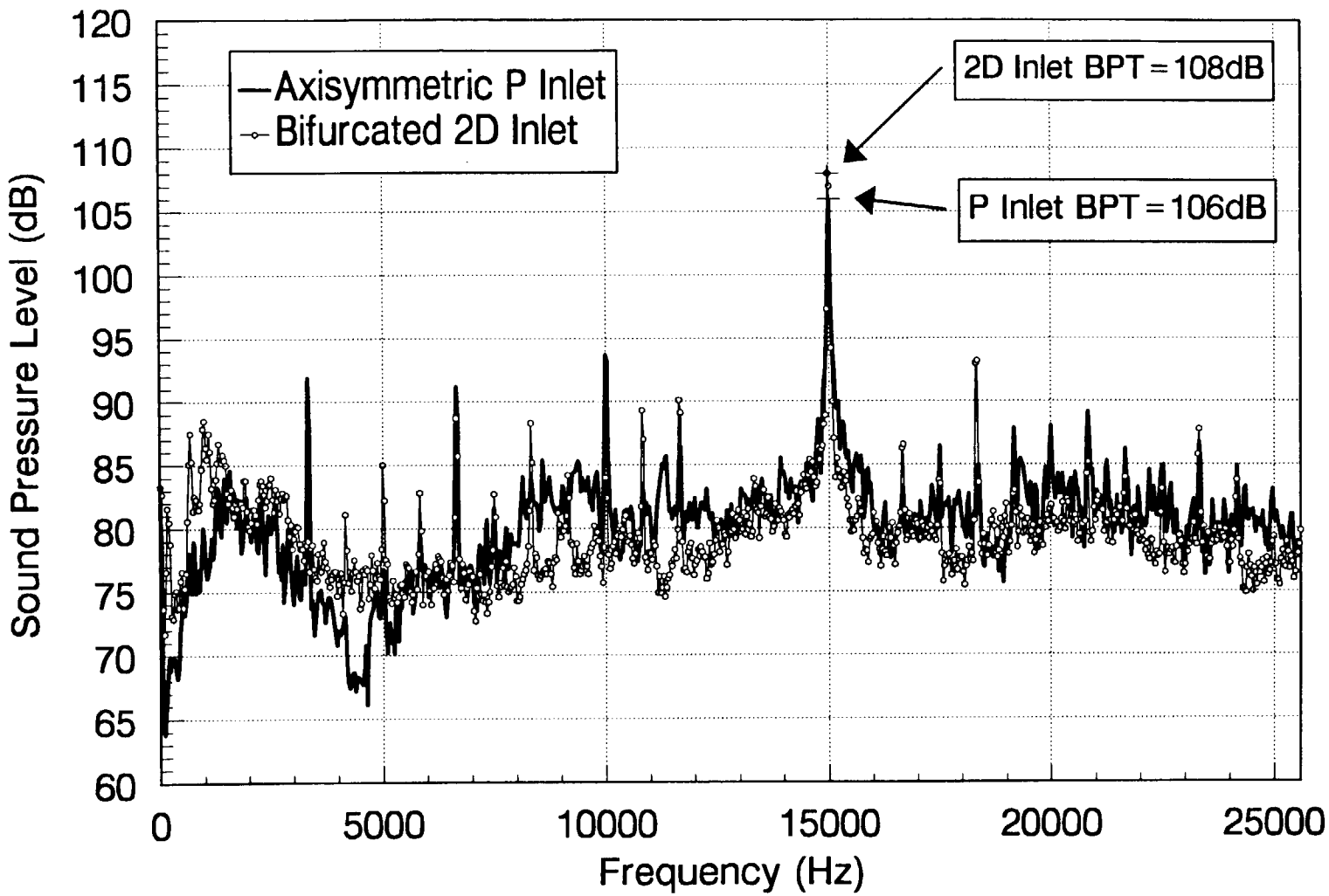


**Figure 4.19 Sample Spectra at the 0° Microphone Location, 60 PNC**

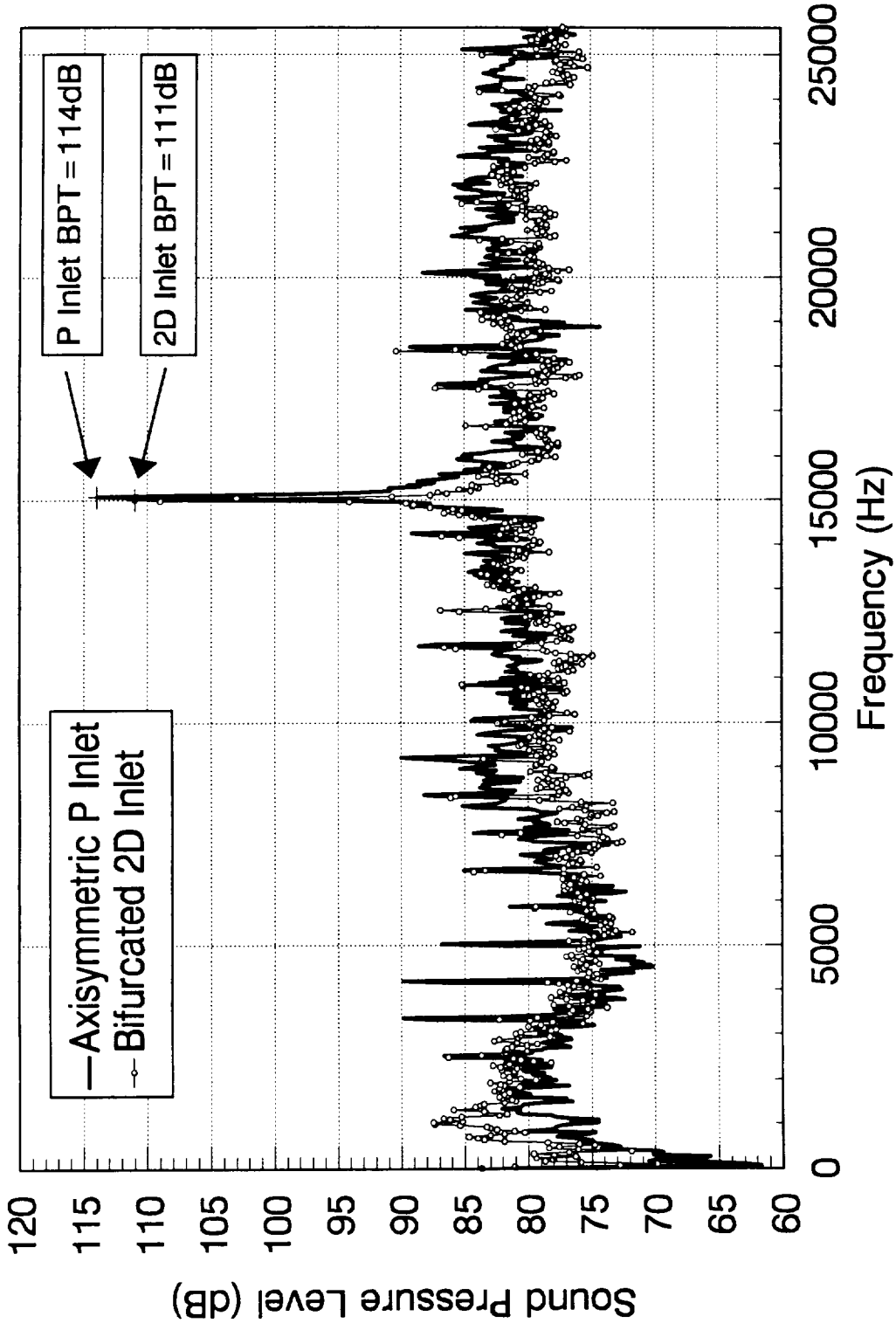


**Figure 4.20 Sample Spectra at the 20° Microphone Location, 60 PNC**

Figures 4.21 and 4.22 show sample spectra for the 2D inlet and P inlet at a test speed of 88 PNC (takeoff conditions) at microphone locations of 0° and 20° respectively. These spectra are typical of a fan with supersonic blade tip speeds. For the takeoff flight conditions, the turbofan simulator was running at 70,000 RPM (88 PNC) with a blade tip speed of 1295 ft/s (Mach 1.1). The blade passing frequency is at 21 kHz at this test condition. Both figures show the blade passing frequency tone as the dominate noise source. The onset of the combination tones can be seen at integer multiples of the fan rotational frequency (833 Hz). For this case, the OASPL measured for the 2D inlet was louder by 3 dB and 6 dB for 0° and 20° microphone location, respectively. The spectra analyses reflects these results because there are large differences in the magnitude of the combination tones and the blade passing frequency tone for the 2D inlet when compared to the P inlet. The soft choking effect, caused by the throat Mach number in the P inlet exceeding 0.5, significantly reduces the BPT and OASPL and is evident in these two sets of sample spectra. The broadband noise seems to be relatively at the same level for the two inlets. These sample spectra reflect the directivity plot comparison and indicate that the P inlet has an acoustic advantage at the takeoff flight condition.

### 4.2.4 Modal Analysis

The theory for generation and propagation of modes has been discussed in Chapter Two. It was determined that the modes due to the strut-fan and stator-fan

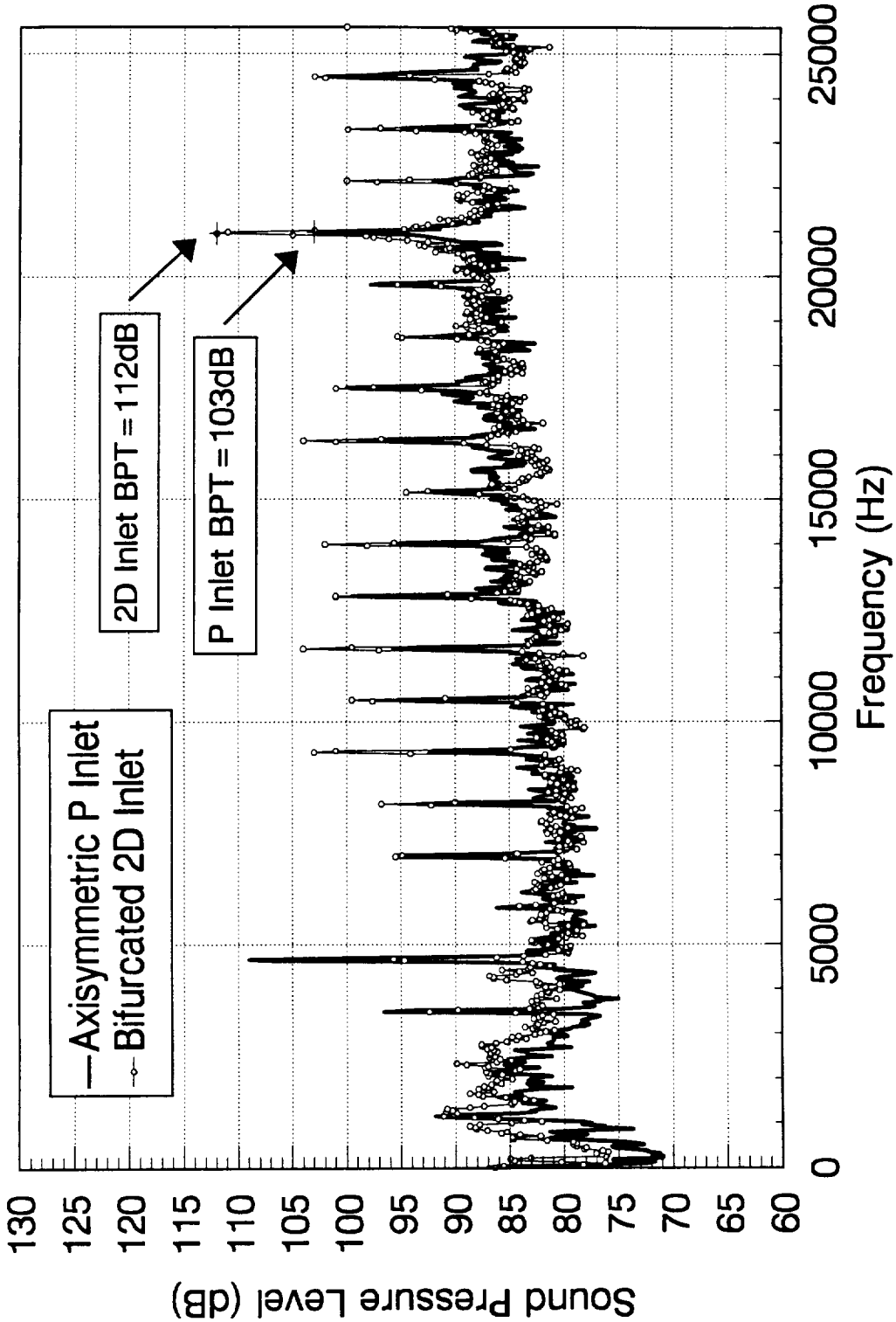


**Figure 4.21 Sample Spectra at the 0° Microphone Location, 88 PNC**

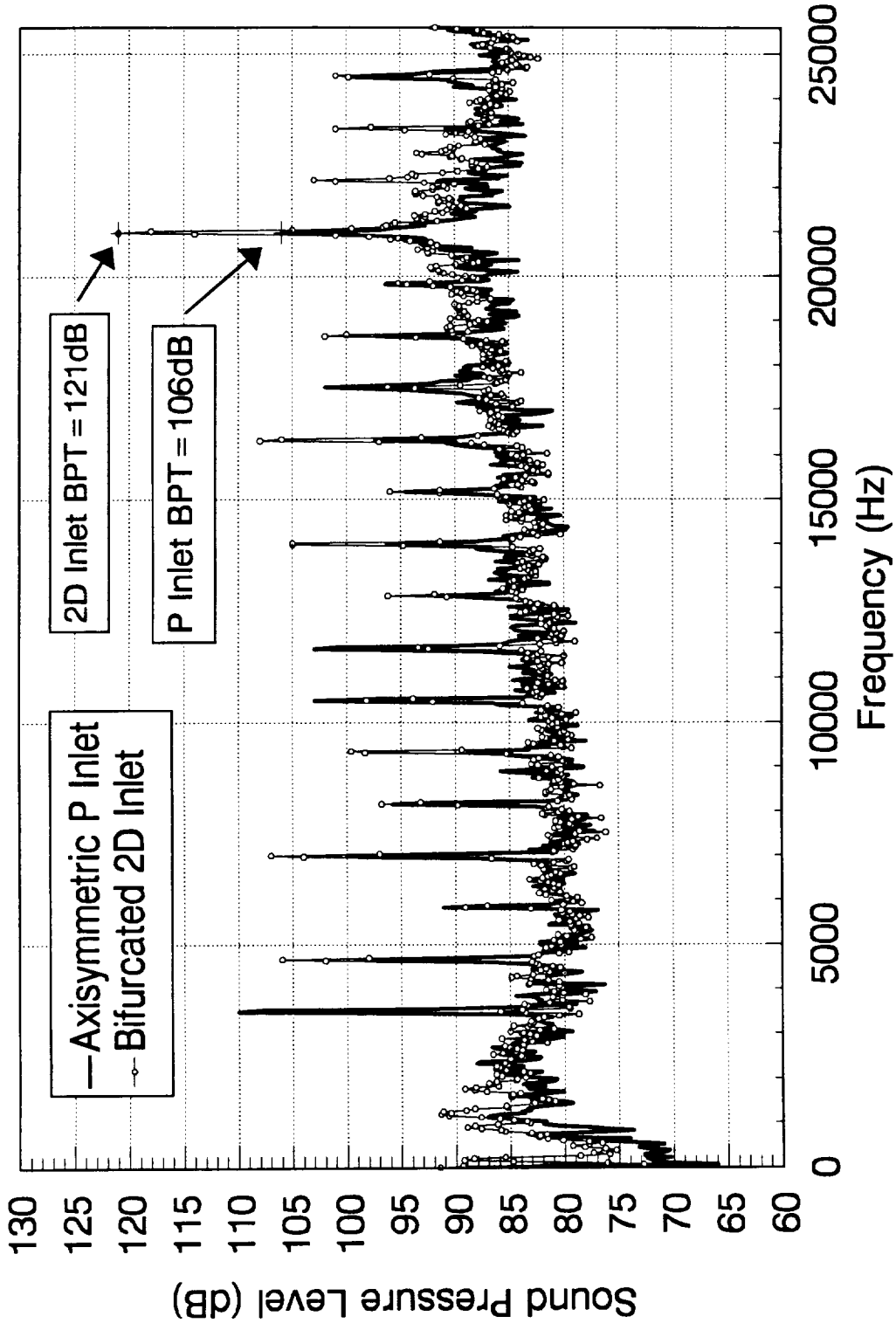


**Figure 4.22 Sample Spectra at the 20° Microphone Location, 88 PNC**

interaction will be generated at 50,000 RPM (60 PNC) and 70,000 RPM (88 PNC). At the same time it is not necessary for all modes that are generated to propagate and radiate in the far field. In this study the fan has 18 blades and 26 stators. The P inlet has four support struts and the 2D inlet has no struts. The mode cut-off ratio ($\xi$) as defined by Tyler and Sofrin decides whether a particular mode will propagate or decay.

The mode that propagates in the duct of the inlet will radiate in the far field and can be identified in the far field radiation pattern as lobe shaped amplitude variations. Homzic and Lordi have developed a simplified analytical method which can approximate the angular location of the primary lobe for a particular mode. This analytical method was developed for unflanged cylindrical ducts and hub-tip ratios of less than 0.5. This method was used to determine if the drop in the tone sound pressure level of the 2D inlet at the 20° microphone position was possibly due to the shifting lobe patterns propagating form the inlet. Table 4.5 shows the radiation angles for the 2D inlet at 50,000 RPM (895 ft/s) and 54,000 RPM (966 ft/s). These two speeds were investigated because the graph of the BPT vs. blade tip speed (Figure 4.13) showed a substantial drop in the sound pressure level from 50,000 RPM to 54,000 RPM. The angle of radiation indicates where the peak of the lobe would fall in relation to the inlet's centerline axis (0°). An example of a typical lobe radiation pattern is shown in Figure 4.23. It is important to note the lobe shapes in this illustration. In between each radiated lobe there is a region of low amplitude. If the 20° microphone measurement location fell in the low amplitude region at 54,000 RPM (966 ft/s), then the low BPT reading can be explained. Table 4.5 shows

that as the speed increased, the angle of radiation shifted towards the centerline of the inlet. The $m$=2, $\mu$=0 mode radiates at 10.6° and $m$=2, $\mu$=1 modes radiates at 24.5° at 54,000 RPM. It is possible that the 20° microphone location was in the low amplitude region between the (2,0) and (2,1) lobes at 54,000 RPM. This is an estimate of the lobe patterns because directivity plots were only take at the approach and takeoff conditions and not at 54,000 RPM.

**Table 4.5 2D Inlet Modal Analysis**

| Simulator Speed | Circumferential Order ($m$) | Radial Order ($\mu$) | Mode Cut-off Ratio (strut-fan) | Radiation Angle |
|---|---|---|---|---|
| 50,000 RPM (895 ft/s) | 2 | 0 | 5.03 | 11.5° |
| | 2 | 1 | 2.23 | 26.6° |
| 54,000 RPM (966 ft/s) | 2 | 0 | 5.44 | 10.6° |
| | 2 | 1 | 2.41 | 24.5° |

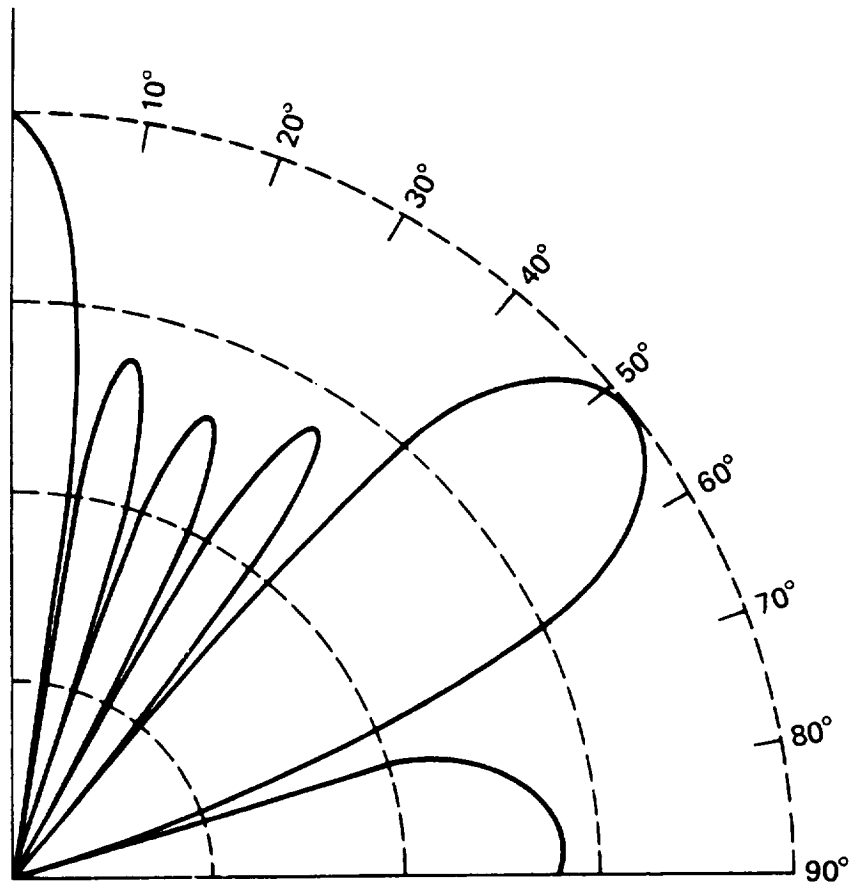


**Figure 4.23 Example of Acoustic Lobe Radiation Pattern**

# 5.0 Conclusions

The main objective of this research was to evaluate the aeroacoustic performance of two different small-scale supersonic inlets under simulated aircraft approach and takeoff flight conditions. A 1/14 model of NASA's axisymmetric supersonic P inlet and bifurcated two-dimensional supersonic inlet were tested experimentally with a 4.1 in (10.4 cm) diameter turbofan engine simulator. The results show neither inlet having a distinct aeroacoustic advantage of the other at the approach flight condition of 60 PNC (50,000 RPM). The results, at the takeoff flight condition of 88 PNC (70,000 RPM), show the P inlet having an acoustic advantage over the 2D inlet due to the soft choking effect at the throat.

The axisymmetric P inlet has a smaller throughflow area and a streamlined centerbody supported by four struts. The noise radiated from the inlet is significantly reduced because the throat Mach number exceeds 0.5. The 2D inlet has a disadvantage because the throat Mach number only reaches 0.26 at takeoff conditions, and does not benefit from the soft choking effect. The total pressure recovery for both inlets at approach conditions remains very high, indicating that each inlet would perform very

well. At the takeoff condition, the inlets see a reduction in the pressure recovery from 99% to 98%, but this does not give either inlet an aerodynamic advantage. Acoustically, the P inlet and 2D inlet differ by less than 1 dB for the tone and overall sound pressure levels at the approach condition. At the takeoff condition, the P inlet has lower tone and overall sound pressure levels by 9 dB and 3 dB, respectively. The average BPT reduction is a direct result of the throat Mach number of the P inlet being 2.0 times greater than that of the 2D inlet.

The results of this investigation illustrates how the geometry of the inlet can have an important effect on the noise propagation properties of the inlet. The smaller the throat area the higher the throat Mach number becomes and the less noise that will propagate to the far field. However, reducing the throat area limits the operating conditions of the supersonic inlet. The P inlet has the best aeroacoustic performance at takeoff fight condition, however at the approach flight condition either inlet will suit the needs of the supersonic aircraft.

From the results in this paper, it is apparent that design advantages of a supersonic inlet can be realized through the use of small-scale test programs. More importantly, small-scale test programs provide a setting for low cost experiments to develop a better understanding of the complex relationships between supersonic inlet aerodynamic and aircraft engine acoustics. Future aeroacoustic research should be directed toward understanding how the fan face distortion effects the generation of noise from the inlet. It is not clear from this research how the different wake profiles shed by the centerbody

support struts of the axisymmetric P inlet and the centerbody splitter plate of the bifurcated 2D inlet change the radiated noise levels. The wake characteristics could be changed in order to see the effects on the generated noise levels. Another area that should be investigated more thoroughly is the soft choking effect. Acoustic measurements for different throat areas could lead to a better understanding of the influence of the throat Mach number on the attenuation of noise from the supersonic inlets.

# Appendix A: Bellmouth Test

Wagner and Ng observed that the axisymmetric P inlet and the bifurcated two-dimensional inlet had large separation regions originating at the cowl lip. An effort was made to reduce the cowl lip separation on both inlets by installing a bellmouth. A bellmouth is used under static testing conditions to simulate forward movement of the engine inlet. This allows the supersonic test inlets to perform as if they were moving forward, such as in approach and takeoff flight conditions.

Figure A.1 shows total pressure recovery profiles for the P inlet and the 2D inlet. The P inlet without the bellmouth has a large losses at the tip region of the cowl lip station. When the P inlet was equipped with a bellmouth, the losses at the tip were reduced to unmeasureable values. The 2D inlet was compared at the throat station because the sharp lip 2D inlet design prevented measurements at the cowl lip. The profile adequately shows the large separation at the tip region was significantly reduced. This comparison illustrates that the bellmouth will reduce cowl lip separation when testing under static conditions.

Table A.1 presents the total pressure recovery averages at the fan face of the simulator for the two different inlets with and without the bellmouth. This shows the losses at the fan face were reduce for both inlets by using the bellmouth.

**Table A.1 Fan Face Area Averaged Total Pressure Recovery With and Without Bellmouth**

| Inlet Type<br>70,000 RPM (88 PNC) | Pressure Recovery<br>without Bellmouth | Pressure Recovery<br>with Bellmouth |
|---|---|---|
| Bifurcated 2D Inlet | 0.961 | 0.981 |
| Axisymmetric P Inlet | 0.894 | 0.979 |

There was an interest in seeing how the cowl lip separation affected the noise radiated from the inlets. Acoustic measurements were made at the takeoff condition of 70,00 RPM (88 PNC) and are presented in Figure A.2 and A.3. The tone sound pressure level increased when the bellmouth was used with the P inlet. This was a result of cleaning up the flow at the fan face of the simulator. The overall sound pressure level dropped slightly because the strong distortions at the fan face have been removed. By examining the spectrum at the 20° microphone position, the results seen on the directivity plots can be explained. The spectrum recorded without the bellmouth shows only broadband noise radiating from the inlet. However, the spectrum recorded with the bellmouth illustrates the on set of the multiple pure tones radiating from the fan blades and a drop in the broadband noise. The blade passing frequency tone also becomes very evident. This spectrum is representative of an engine operating at in flight conditions. It shows how cleaning up the inlet flow field can effect the acoustic signature of the simulator engine.

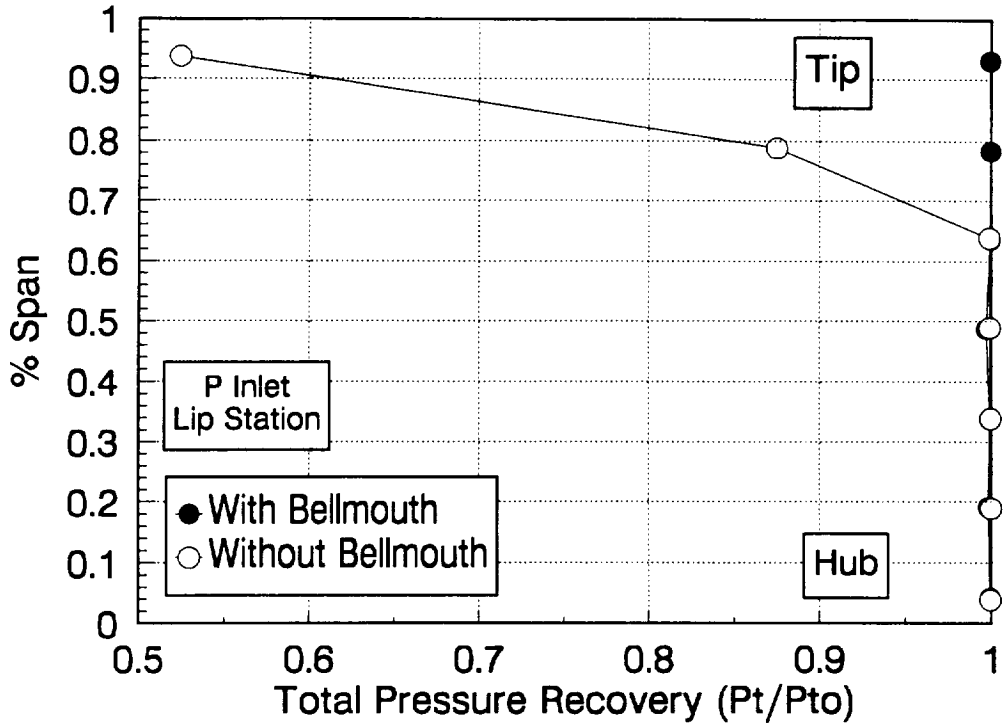


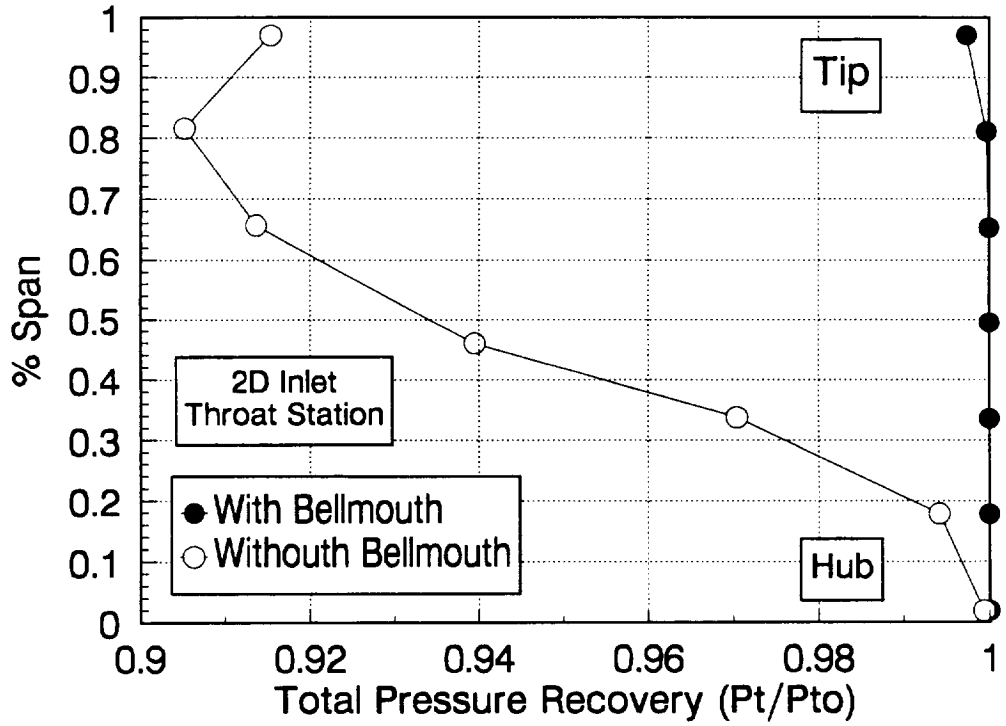


**Figure A.1 Total Pressure Recovery Profiles at the Lip Station of the P Inlet and the Throat Station of the 2D Inlet With and Without Bellmouth, 88 PNC**

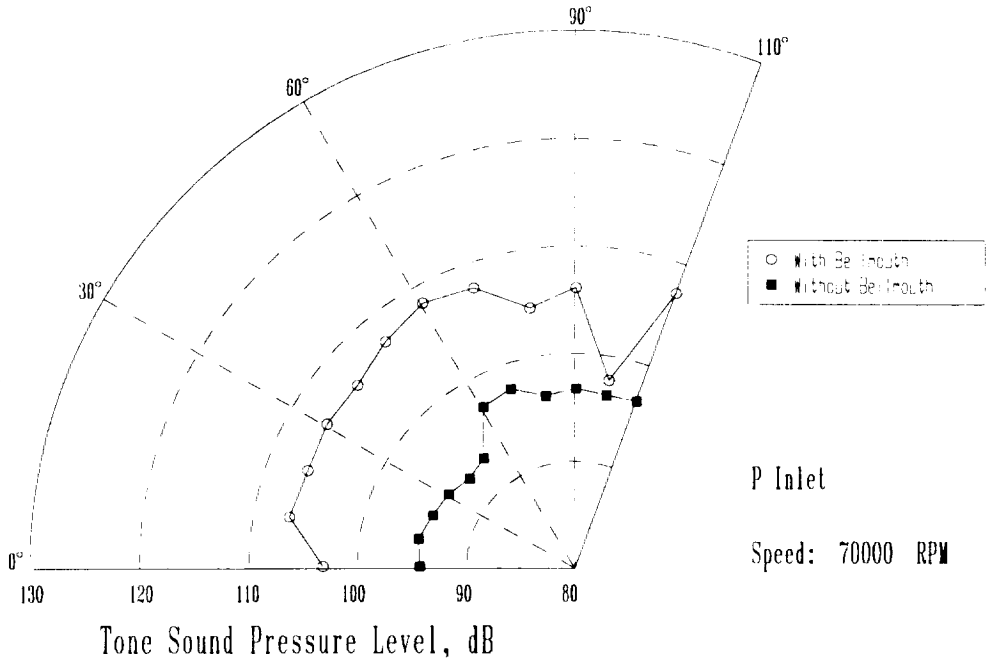


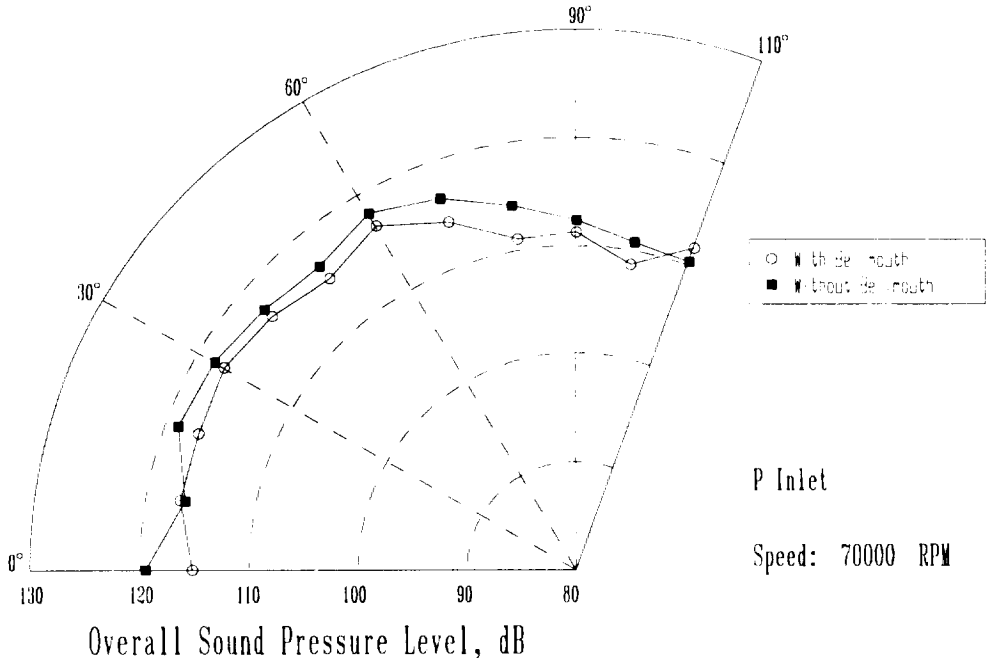


**Figure A.2 Directivity Plots of the P Inlet With and Without Bellmouth, 88 PNC**

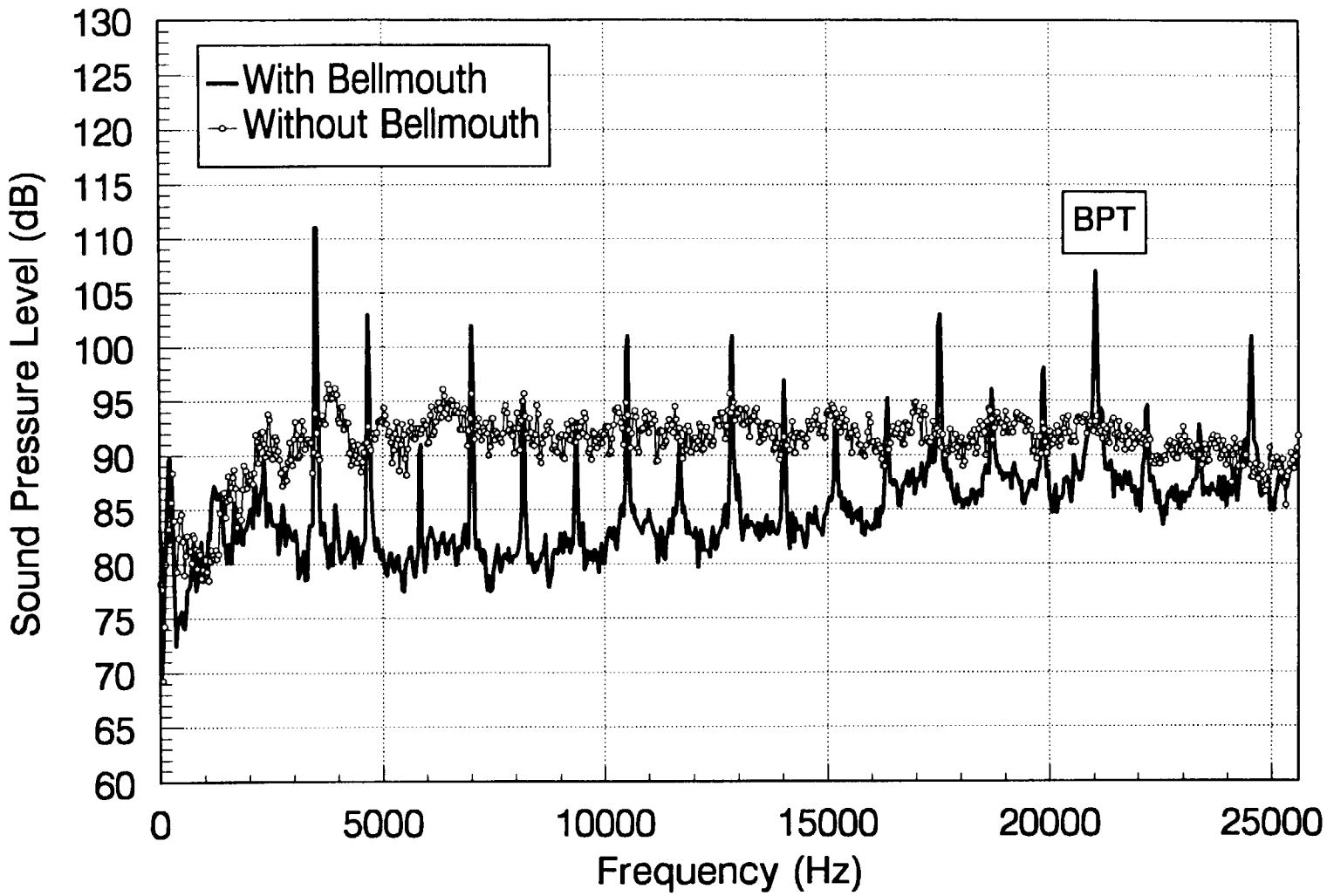


**Figure A.3 Sample Spectra at the 20° Microphone Location of the P Inlet With and Without Bellmouth, 88 PNC**

# Appendix B: Fan Exit Area Test

The fan exit area is crucial to the fan operating condition of the Model 460 turbofan simulator engine used in this research. It was determined before this experiment that the fan exit area was too large, therefore the engine was not performing within the normal operating curves. The original fan exit area was 7.05 $in^2$. The fan exit area was then reduced to 5.47 $in^2$ in an attempt to force the simulator to operate normally. The original fan exit area is termed old fan exit area and the reduced fan exit area is termed new fan exit area in Appendix B. Tables B.1 and B.2 show how the fan exit area change increased the fan pressure ratio of the turbofan simulator for both inlets. Figure 4.2 in Section 4.1.2 shows the turbofan simulator performance map.

**Table B.1 Fan Pressure Ratios for the Bifurcated Two-Dimensional Inlet, Old and New Fan Exit Area**

| Fan Speed 50,000 RPM (60 PNC) | Fan Pressure Ratio |
|---|---|
| Old Fan Exit Area | 1.14 |
| New Fan Exit Area | 1.18 |
| **Fan Speed 70,000 RPM (88 PNC)** | **Fan Pressure Ratio** |
| Old Fan Exit Area | 1.26 |
| New Fan Exit Area | 1.35 |

**Table B.2 Fan Pressure Ratios for the Axisymmetric P Inlet, Old and New Fan Exit Area**

| Fan Speed 50,000 RPM (60 PNC) | Fan Pressure Ratio |
|---|---|
| Old Fan Exit Area | 1.10 |
| New Fan Exit Area | 1.17 |
| **Fan Speed 70,000 RPM (88 PNC)** | **Fan Pressure Ratio** |
| Old Fan Exit Area | 1.21 |
| New Fan Exit Area | 1.34 |

Figure B.1 illustrates the Mach number and total pressure recovery profiles at the 45° circumferential fan face station for the new and old fan exit areas at 88 PNC for the P inlet. The profiles show the Mach number slowing and the pressure recovery increasing. This is evident because the flow at the exit of the fan is being restricted due to the smaller fan exit area. The tone sound pressure level directivity plot in Figure B.2 does not show any large changes in the radiated noise. However, the overall plot has approximately a 5 to 8 dB difference throughout the measurements. The reason for this can be seen in the spectrum at the 20° microphone position (Figure B.3). The entire spectrum has been pushed up as a result of the fan loading being increased. This change in fan performance will not have any bearing on the acoustic outcome of the inlet comparison because each inlet was test with the new fan exit area.

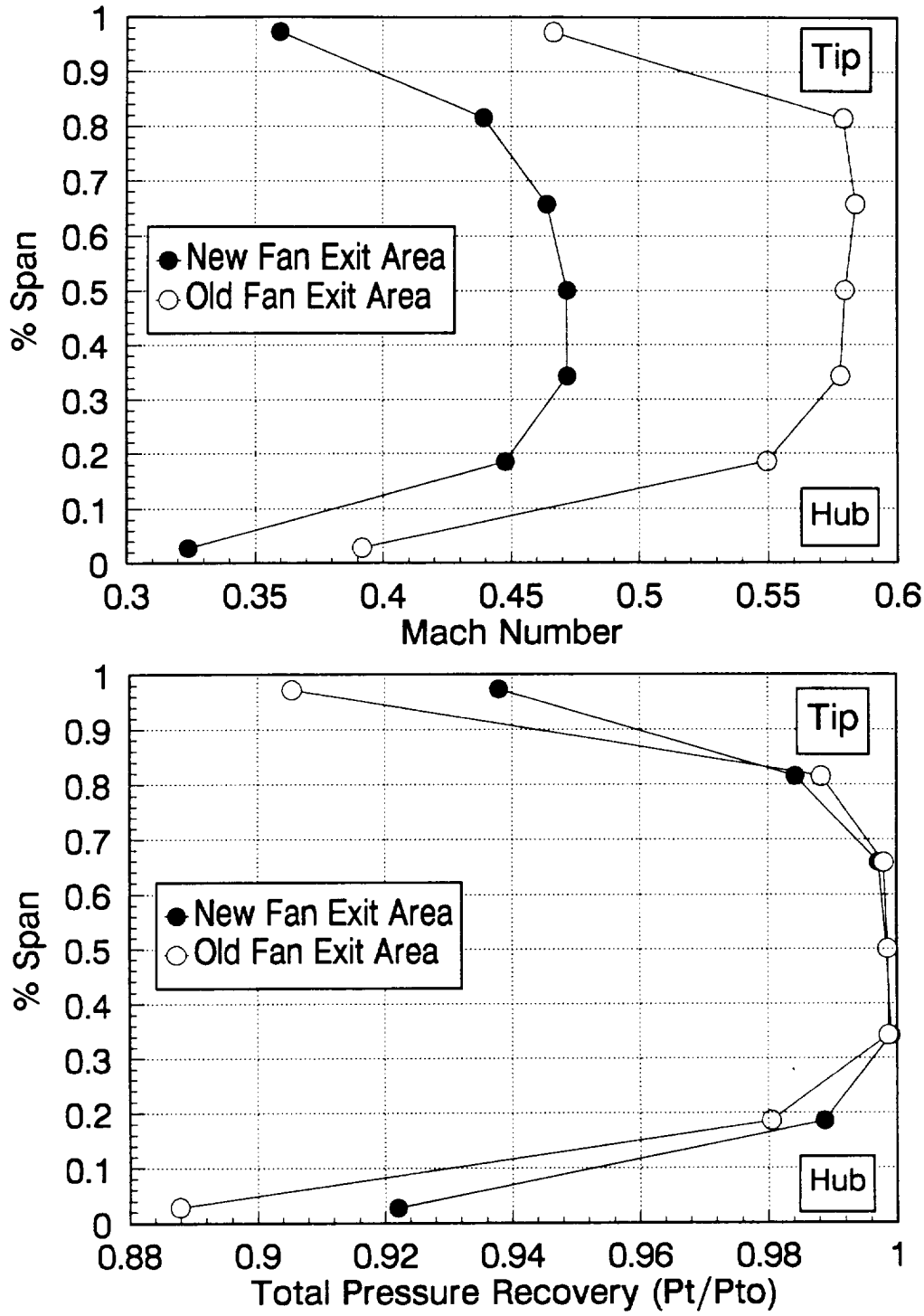


**Figure B.1 Mach Number and Total Pressure Recovery Profiles for P inlet at the 45° Circumferential Fan Face Station Comparing New and Old Fan Exit Area, 88 PNC**

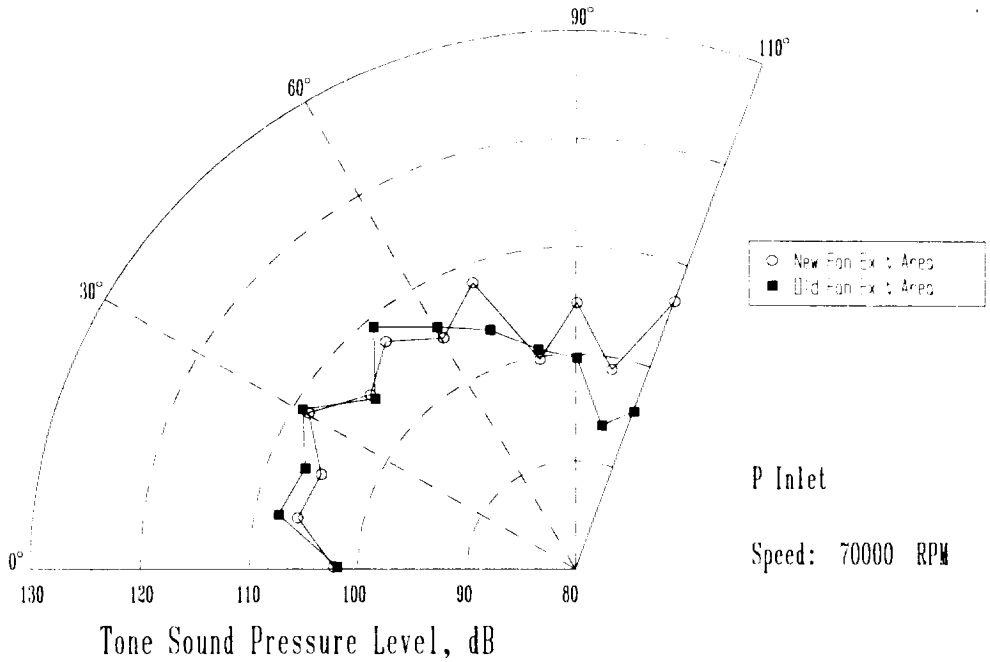


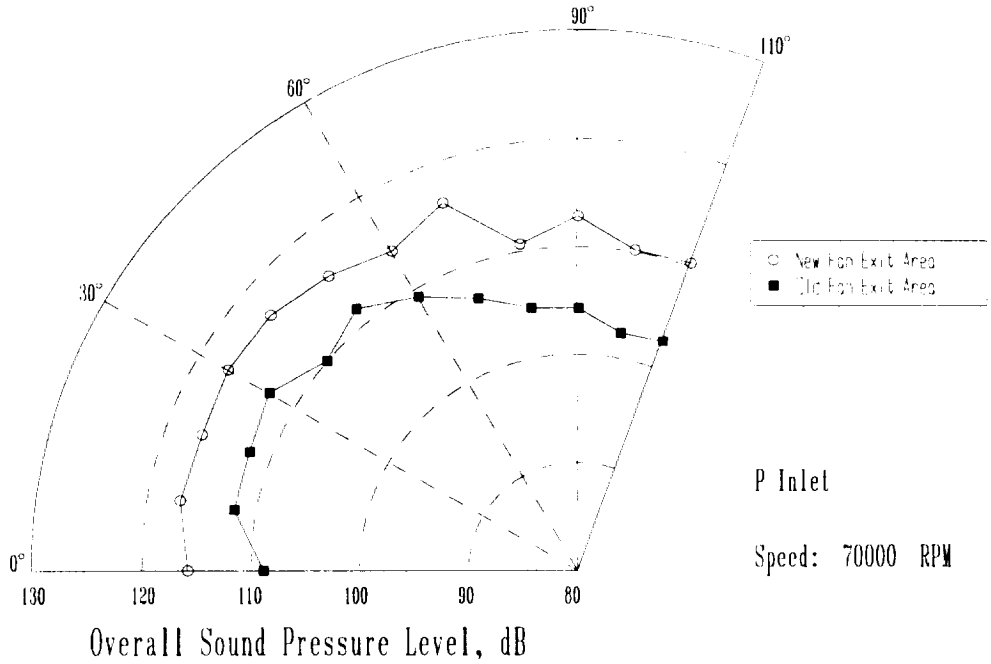


**Figure B.2 Directivity Plots of the P Inlet Comparing New and Old Fan Exit Area, 88 PNC**

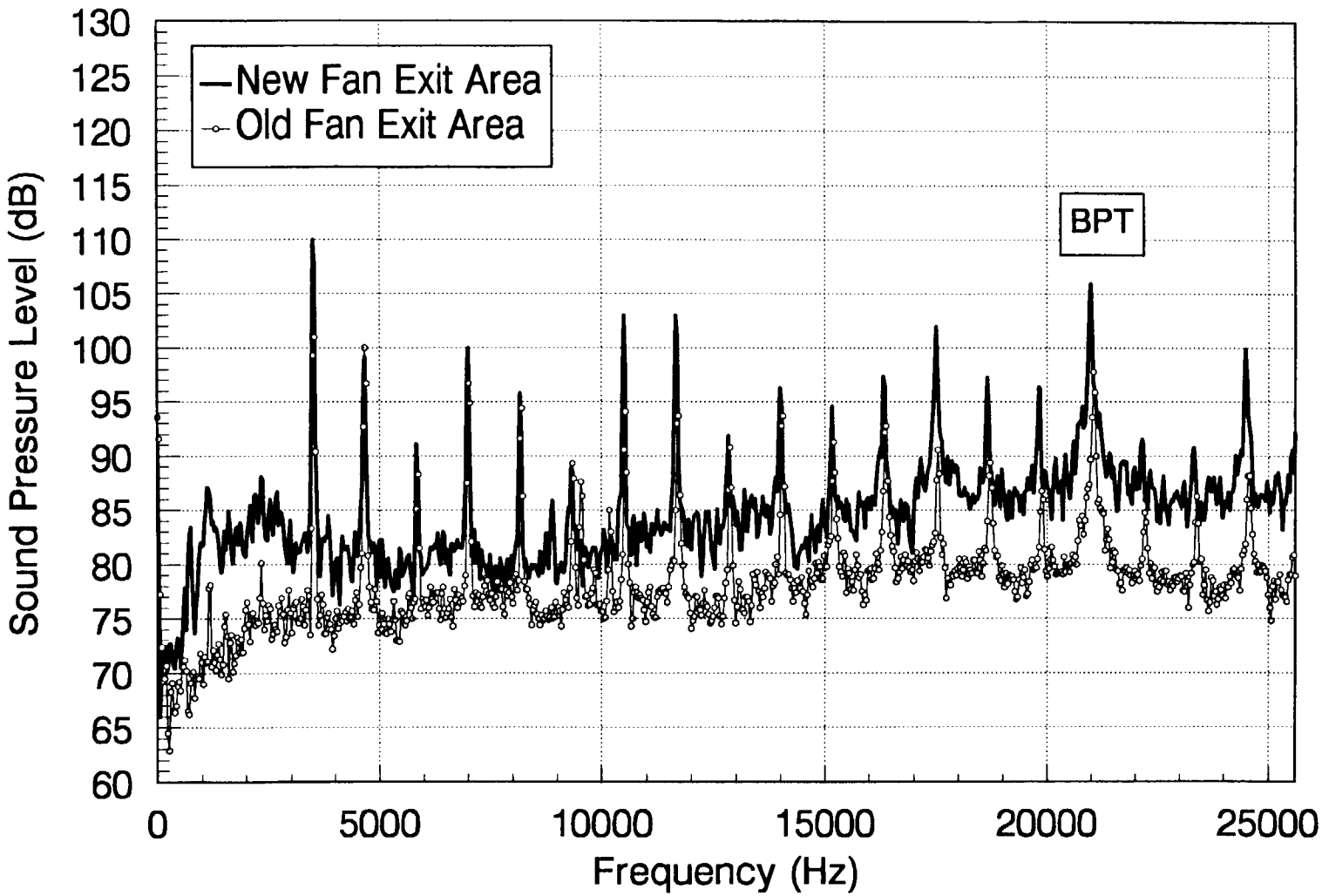


**Figure B.3 Sample Spectra at the 20° Microphone Location of the P Inlet Comparing New and Old Fan Exit Areas, 88 PNC**

# Appendix C: Circumferential Distortion Method

The gas turbine engine inlet flow distortion guidelines are presented in ARP 1420. Distortion-descriptor elements are used to describe the distortion at the fan face of an engine. In this thesis, the circumferential distortion intensity (CDI) was calculated for the axisymmetric P inlet and the bifurcated two-dimensional inlet. The CDI is described as the magnitude of the pressure defect for each ring of measurements around the fan face. For this experiment there were seven radial measurement positions, therefore seven different CDI's had to be calculated and then area averaged in order to get the CDI for the entire fan face. The CDI is defined below:

$$Intensity = \left(\frac{\Delta PC}{P}\right)_i = \frac{(PAV)_i - (PAVLOW)_i}{(PAV)}$$

where:

$$(PAV)_i = \frac{1}{360}\int_0^{360} P(\theta)_i d\theta$$

$P(\theta)_i$ is a function resulting from a linear fit between the data points

$$(PAVLOW)_i = \frac{1}{\theta_i^-}\int_{\theta_i^-} P(\theta)_i d\theta$$

$P(\theta)$: Total pressure at any angle θ for a given ring at constant radius

$PAV$: Ring average pressure

| | |
|---|---|
| *PAVLOW*: | Average total pressure of low total-pressure region for a ring |
| $\theta^{-}$: | Extent of the low-pressure region |
| *i*: | Ring number (seven radial measurement rings at the fan face) |

The above equations where used in a FORTRAN Computer Program to calculate the average circumferential distortion intensity at the fan face. The program code is listed on the following pages of Appendix C. At this point, it is still unclear as to how the circumferential distortion effects the generation of noise from the fan. Further studies need to be conducted in this area.

```
C*********************************************************************
C*          CIRCUMFERENTIAL DISTORTION INTENSITY PROGRAM             *
C*                          MAIN PROGRAM                             *
C*********************************************************************
      DIMENSION M(50,50),P(50,50),E(50)
      REAL M,P,CDI,E
      CHARACTER TYPE,INLET*5,RPM*10,DATA*50,OUT*50,CASE,FLAG
C*********************************************************************
5     WRITE (*,10) 'CIRCUMFERENTIAL DISTORTION PROGRAM'
      WRITE (*,*) 'TEST CASE OR REAL CASE (T,R)?'
      READ (*,20) CASE
      IF (CASE.EQ.'R')THEN
         WRITE (*,*) 'USING MACH OR PRES (M,P)?'
         READ (*,20) TYPE
         WRITE (*,*) 'ENTER INLET TYPE (P,2D):'
         READ (*,20) INLET
         WRITE (*,*) 'ENTER SPEED (50K,70K):'
         READ (*,20) RPM
      ENDIF
10    FORMAT (1X,A/)
11    FORMAT (1X,A)
20    FORMAT (A)
30    FORMAT (1X,A)
35    FORMAT (1X,2A)
40    FORMAT (/1X,A,F12.8)
C*********************************************************************
C* TEST CASE                                                         *
C*********************************************************************
      IF (CASE.EQ.'T')THEN
         WRITE (*,*) 'ENTER DATA FILE NAME:'
         READ (*,20) DATA
         WRITE (*,*) 'ENTER OUTPUT FILE NAME:'
         READ (*,20) OUT
         OPEN (UNIT = 1, FILE = DATA)
         OPEN (UNIT = 2, FILE = OUT)
         WRITE (2,10) 'TEST CASE'
         WRITE (*,10) 'TEST CASE'
         WRITE (2,35) 'DATAFILE= ',DATA
         WRITE (*,35) 'DATAFILE= ',DATA
         WRITE (2,35) 'OUTPUT FILE= ',OUT
         WRITE (*,35) 'OUTPUT FILE= ',OUT
         CALL TEST(CDI,DATA,OUT)
         WRITE (*,40) 'CDI =',CDI
         TYPE = 'X'
         INLET = 'X'
         RPM = 'X'
      ENDIF
C*********************************************************************
C* MACH NUMBER - P INLET - 50,000 RPM - 70,000 RPM                   *
C*********************************************************************
      IF ((TYPE.EQ.'M').AND.(INLET.EQ.'P').AND.(RPM.EQ.'50K'))THEN
         OPEN (UNIT = 1, FILE = 'C:\KMILLER\CDI\DATA\P50KM.TXT')
         OPEN (UNIT = 2, FILE = 'C:\KMILLER\CDI\DATA\P50KM.CDI')
         DATA = 'C:\KMILLER\CDI\DATA\P50KM.TXT'
         OUT = 'C:\KMILLER\CDI\DATA\P50KM.CDI'
         WRITE (2,10) 'P INLET - MACH NUMBER - 50,000 RPM - DISTORTION'
         WRITE (*,10) 'P INLET - MACH NUMBER - 50,000 RPM - DISTORTION'
         WRITE (2,30) 'DATAFILE = P50KM.TXT'
         WRITE (*,30) 'DATAFILE = P50KM.TXT'
         WRITE (2,30) 'OUTPUT FILE = P50KM.CDI'
         WRITE (*,30) 'OUTPUT FILE = P50KM.CDI'
         CALL PINLET(CDI,DATA,OUT)
         WRITE (*,40) 'CDI =',CDI
```

```
      ENDIF
C*********************************************************************
      IF ((TYPE.EQ.'M').AND.(INLET.EQ.'P').AND.(RPM.EQ.'70K'))THEN
         OPEN (UNIT = 1, FILE = 'C:\KMILLER\CDI\DATA\P70KM.TXT')
         OPEN (UNIT = 2, FILE = 'C:\KMILLER\CDI\DATA\P70KM.CDI')
         DATA = 'C:\KMILLER\CDI\DATA\P70KM.TXT'
         OUT = 'C:\KMILLER\CDI\DATA\P70KM.CDI'
         WRITE (2,10) 'P INLET - MACH NUMBER - 70,000 RPM - DISTORTION'
         WRITE (*,10) 'P INLET - MACH NUMBER - 70,000 RPM - DISTORTION'
         WRITE (2,30) 'DATAFILE = P70KM.TXT'
         WRITE (*,30) 'DATAFILE = P70KM.TXT'
         WRITE (2,30) 'OUTPUT FILE = P70KM.CDI'
         WRITE (*,30) 'OUTPUT FILE = P70KM.CDI'
         CALL PINLET(CDI,DATA,OUT)
         WRITE (*,40) 'CDI =',CDI
      ENDIF
C*********************************************************************
C* MACH NUMBER - 2D INLET - 50,000 RPM - 70,000 RPM                  *
C*********************************************************************
      IF ((TYPE.EQ.'M').AND.(INLET.EQ.'2D').AND.(RPM.EQ.'50K'))THEN
         OPEN (UNIT = 1, FILE = 'C:\KMILLER\CDI\DATA\2D50KM.TXT')
         OPEN (UNIT = 2, FILE = 'C:\KMILLER\CDI\DATA\2D50KM.CDI')
         DATA = 'C:\KMILLER\CDI\DATA\2D50KM.TXT'
         OUT = 'C:\KMILLER\CDI\DATA\2D50KM.CDI'
         WRITE (2,11) '2D INLET - MACH NUMBER - 50,000 RPM - DISTORTION'
         WRITE (*,10) '2D INLET - MACH NUMBER - 50,000 RPM - DISTORTION'
         WRITE (2,30) 'DATAFILE = 2D50KM.TXT'
         WRITE (*,30) 'DATAFILE = 2D50KM.TXT'
         WRITE (2,30) 'OUTPUT FILE = 2D50KM.CDI'
         WRITE (*,30) 'OUTPUT FILE = 2D50KM.CDI'
         CALL BINLET(CDI,DATA,OUT)
         WRITE (*,40) 'CDI =',CDI
      ENDIF
C*********************************************************************
      IF ((TYPE.EQ.'M').AND.(INLET.EQ.'2D').AND.(RPM.EQ.'70K'))THEN
         OPEN (UNIT = 1, FILE = 'C:\KMILLER\CDI\DATA\2D70KM.TXT')
         OPEN (UNIT = 2, FILE = 'C:\KMILLER\CDI\DATA\2D70KM.CDI')
         DATA = 'C:\KMILLER\CDI\DATA\2D70KM.TXT'
         OUT = 'C:\KMILLER\CDI\DATA\2D70KM.CDI'
         WRITE (2,11) '2D INLET - MACH NUMBER - 70,000 RPM - DISTORTION'
         WRITE (*,10) '2D INLET - MACH NUMBER - 70,000 RPM - DISTORTION'
         WRITE (2,30) 'DATAFILE = 2D70KM.TXT'
         WRITE (*,30) 'DATAFILE = 2D70KM.TXT'
         WRITE (2,30) 'OUTPUT FILE = 2D70KM.CDI'
         WRITE (*,30) 'OUTPUT FILE = 2D70KM.CDI'
         CALL BINLET(CDI,DATA,OUT)
         WRITE (*,40) 'CDI =',CDI
      ENDIF
C*********************************************************************
C* PRESSURE - P INLET - 50,000 RPM - 70,000 RPM                      *
C*********************************************************************
      IF ((TYPE.EQ.'P').AND.(INLET.EQ.'P').AND.(RPM.EQ.'50K'))THEN
         OPEN (UNIT = 1, FILE = 'C:\KMILLER\CDI\DATA\P50KP.TXT')
         OPEN (UNIT = 2, FILE = 'C:\KMILLER\CDI\DATA\P50KP.CDI')
         DATA = 'C:\KMILLER\CDI\DATA\P50KP.TXT'
         OUT = 'C:\KMILLER\CDI\DATA\P50KP.CDI'
         WRITE (2,10) 'P INLET - PRESSURE - 50,000 RPM - DISTORTION'
         WRITE (*,10) 'P INLET - PRESSURE - 50,000 RPM - DISTORTION'
         WRITE (2,30) 'DATAFILE = P50KP.TXT'
         WRITE (*,30) 'DATAFILE = P50KP.TXT'
         WRITE (2,30) 'OUTPUT FILE = P50KP.CDI'
         WRITE (*,30) 'OUTPUT FILE = P50KP.CDI'
         CALL PINLET(CDI,DATA,OUT)
```

```
         WRITE (*,40) 'CDI =',CDI
      ENDIF
C*********************************************************************
      IF ((TYPE.EQ.'P').AND.(INLET.EQ.'P').AND.(RPM.EQ.'70K'))THEN
         OPEN (UNIT = 1, FILE = 'C:\KMILLER\CDI\DATA\P70KP.TXT')
         OPEN (UNIT = 2, FILE = 'C:\KMILLER\CDI\DATA\P70KP.CDI')
         DATA = 'C:\KMILLER\CDI\DATA\P70KP.TXT'
         OUT = 'C:\KMILLER\CDI\DATA\P70KP.CDI'
         WRITE (2,10) 'P INLET - PRESSURE - 70,000 RPM - DISTORTION'
         WRITE (*,10) 'P INLET - PRESSURE - 70,000 RPM - DISTORTION'
         WRITE (2,30) 'DATAFILE = P70KP.TXT'
         WRITE (*,30) 'DATAFILE = P70KP.TXT'
         WRITE (2,30) 'OUTPUT FILE = P70KP.CDI'
         WRITE (*,30) 'OUTPUT FILE = P70KP.CDI'
         CALL PINLET(CDI,DATA,OUT)
         WRITE (*,40) 'CDI =',CDI
      ENDIF
C*********************************************************************
C* PRESSURE - 2D INLET - 50,000 RPM - 70,000 RPM                     *
C*********************************************************************
      IF ((TYPE.EQ.'P').AND.(INLET.EQ.'2D').AND.(RPM.EQ.'50K'))THEN
         OPEN (UNIT = 1, FILE = 'C:\KMILLER\CDI\DATA\2D50KP.TXT')
         OPEN (UNIT = 2, FILE = 'C:\KMILLER\CDI\DATA\2D50KP.CDI')
         DATA = 'C:\KMILLER\CDI\DATA\2D50KP.TXT'
         OUT = 'C:\KMILLER\CDI\DATA\2D50KP.CDI'
         WRITE (2,11) '2D INLET - PRESSURE - 50,000 RPM - DISTORTION'
         WRITE (*,10) '2D INLET - PRESSURE - 50,000 RPM - DISTORTION'
         WRITE (2,30) 'DATAFILE = 2D50KP.TXT'
         WRITE (*,30) 'DATAFILE = 2D50KP.TXT'
         WRITE (2,30) 'OUTPUT FILE = 2D50KP.CDI'
         WRITE (*,30) 'OUTPUT FILE = 2D50KP.CDI'
         CALL BINLET(CDI,DATA,OUT)
         WRITE (*,40) 'CDI =',CDI
      ENDIF
C*********************************************************************
      IF ((TYPE.EQ.'P').AND.(INLET.EQ.'2D').AND.(RPM.EQ.'70K'))THEN
         OPEN (UNIT = 1, FILE = 'C:\KMILLER\CDI\DATA\2D70KP.TXT')
         OPEN (UNIT = 2, FILE = 'C:\KMILLER\CDI\DATA\2D70KP.CDI')
         DATA = 'C:\KMILLER\CDI\DATA\2D70KP.TXT'
         OUT = 'C:\KMILLER\CDI\DATA\2D70KP.CDI'
         WRITE (2,11) '2D INLET - PRESSURE - 70,000 RPM - DISTORTION'
         WRITE (*,10) '2D INLET - PRESSURE - 70,000 RPM - DISTORTION'
         WRITE (2,30) 'DATAFILE = 2D70KP.TXT'
         WRITE (*,30) 'DATAFILE = 2D70KP.TXT'
         WRITE (2,30) 'OUTPUT FILE = 2D70KP.CDI'
         WRITE (*,30) 'OUTPUT FILE = 2D70KP.CDI'
         CALL BINLET(CDI,DATA,OUT)
         WRITE (*,40) 'CDI =',CDI
      ENDIF
C*********************************************************************
      WRITE (*,*)
      WRITE (*,*) 'DO ANOTHER (Y,N)?'
      READ (*,20) FLAG
      IF (FLAG.EQ.'Y') THEN
         GOTO 5
      ENDIF
C*********************************************************************
      END
C*********************************************************************
C****************   -   END OF MAIN PROGRAM    -   *********************
C*********************************************************************
C
C*********************************************************************
```

```
C* SUBROUTINE FOR P INLET                                                *
C***********************************************************************
      SUBROUTINE PINLET(CDI,DATA,OUT)
      REAL G(50,50),CDI,E(50)
      DIMENSION GAV(10),D(50),S(10),GAVLOW(10),GC(10)
      DIMENSION SAREA(10),MD(10),R(10)
      REAL H,A,SLOPE,B,THETA,AREA,LAREA,LH,GAV,D,GAVLOW,GC
      REAL SAREA,MD,R
      CHARACTER*50 DATA,OUT
      OPEN (UNIT = 1,FILE = DATA)
      OPEN (UNIT = 2,FILE = OUT)
C***********************************************************************
      DO I=1,33
         D(I)=(I-1)*11.25
      ENDDO
C***********************************************************************
      DO J=1,35
         READ (1,*) E(J)
      ENDDO
      K=0
      L=2
      DO J=1,5
         DO I=1,7
            G(I,J+(L*2)) = E(I+(K*7))
         ENDDO
         K=K+1
         L=L-1
      ENDDO
      DO J=9,13
         DO I=1,7
            G(I,J) = G(I,J-8)
         ENDDO
      ENDDO
      DO J=17,21
         DO I=1,7
            G(I,J) = G(I,J-16)
         ENDDO
      ENDDO
      DO J=25,29
         DO I=1,7
            G(I,J) = G(I,J-24)
         ENDDO
      ENDDO
      K=2
      DO J=6,8
         DO I=1,7
            G(I,J) = G(I,J-K)
         ENDDO
         K=K+2
      ENDDO
      K=10
      DO J=14,16
         DO I=1,7
            G(I,J) = G(I,J-K)
         ENDDO
         K=K+2
      ENDDO
      K=18
      DO J=22,24
         DO I=1,7
            G(I,J) = G(I,J-K)
         ENDDO
         K=K+2
```

```
      ENDDO
      K=26
      DO J=30,32
         DO I=1,7
            G(I,J) = G(I,J-K)
         ENDDO
         K=K+2
      ENDDO
      DO I=1,7
         G(I,33) = G(I,1)
      ENDDO
      WRITE (2,15) 'DATA'
      WRITE (2,17) 'ANGLE','HUB','TIP'
      DO J=1,33
         WRITE (2,5) D(J),(G(I,J), I=1,7)
      ENDDO
5     FORMAT (F7.2,7F10.6)
15    FORMAT (/1X,A/)
17    FORMAT (1X,A,6X,A,57X,A)
C*********************************************************************
      DO I=1,7
         S(I)=0.0
         DO J=1,32
            H=ABS(D(I)-D(I+1))
            A=(ABS(G(I,J)-G(I,J+1)))*0.5*H
            B=H*G(I,J)
            IF (G(I,J).GT.G(I,J+1)) THEN
              S(I)=S(I)-A+B
            ENDIF
            IF (G(I,J).LT.G(I,J+1)) THEN
              S(I)=S(I)+A+B
            ENDIF
              IF (G(I,J).EQ.G(I,J+1)) THEN
            S(I)=S(I)+B
            ENDIF
         ENDDO
         GAV(I)=S(I)/D(33)
      ENDDO
      WRITE (2,25) 'AVERAGE'
25    FORMAT (/,1X,A,/)
      DO I=1,7
         WRITE (2,30) 'GAV(',I,') =',GAV(I)
      ENDDO
30    FORMAT (1X,A,I1,A,F10.7)
C*********************************************************************
      LH=0.0
      LAREA=0.0
      WRITE (2,70) 'AVERAGE OF POINTS BELOW THE AVERAGE'
      DO I=1,7
         DO J=1,32
            IF ((G(I,J).GT.GAV(I)).AND.(G(I,J+1).LT.GAV(I))) THEN
              SLOPE=(G(I,J)-G(I,J+1))/(D(J)-D(J+1))
              B=G(I,J)-(SLOPE*D(J))
              THETA=(GAV(I)-B)/SLOPE
              H=ABS(THETA-D(J+1))
              LH=LH+H
              A=G(I,J+1)*H
              B=((GAV(I)-G(I,J+1))*H)*0.5
              AREA=A+B
              LAREA=LAREA+AREA
            ENDIF
            IF ((G(I,J).LT.GAV(I)).AND.(G(I,J+1).GT.GAV(I))) THEN
              SLOPE=(G(I,J)-G(I,J+1))/(D(J)-D(J+1))
```

```
              B=G(I,J)-(SLOPE*D(J))
              THETA=(GAV(I)-B)/SLOPE
              H=ABS(THETA-D(J))
              LH=LH+H
              A=G(I,J)*H
              B=((GAV(I)-G(I,J))*H)*0.5
              AREA=A+B
              LAREA=LAREA+AREA
            ENDIF
            IF ( ( G(I,J).LE.GAV(I) ).AND.( G(I,J+1).LE.GAV(I) )
     *      .AND.( G(I,J).GT.G(I,J+1) ) )  THEN
              H=ABS(D(J+1)-D(J))
              LH=LH+H
              A=G(I,J+1)*H
              B=((ABS(G(I,J)-G(I,J+1)))*H)*0.5
              AREA=A+B
              LAREA=LAREA+AREA
            ENDIF
            IF ( ( G(I,J).LE.GAV(I) ).AND.( G(I,J+1).LE.GAV(I) )
     *      .AND.( G(I,J).LT.G(I,J+1) ) ) THEN
              H=ABS(D(J+1)-D(J))
              LH=LH+H
              A=G(I,J+1)*H
              B=((ABS(G(I,J)-G(I,J+1)))*H)*0.5
              AREA=A-B
              LAREA=LAREA+AREA
            ENDIF
          ENDDO
          GAVLOW(I)=LAREA/LH
          WRITE (2,60) 'GAVLOW(',I,') =',GAVLOW(I)
60     FORMAT (1X,A,I1,A,F10.7)
          LAREA=0.0
          LH=0.0
       ENDDO
       WRITE (2,70) 'CIRCUMFERENTIAL DISTORTION ELEMENT'
70     FORMAT (/,1X,A,/)
       C=0.0
       DO I=1,7
          GC(I)=(GAV(I)-GAVLOW(I))/GAV(I)
          WRITE (2,80) 'GC/G(',I,') =',GC(I)
       ENDDO
80     FORMAT (1X,A,I1,A,F12.9)
C*********************************************************************
       R(1)=0.9
       R(7)=2.05
       DO I=2,6
          R(I)=((R(7)-R(1))/6.0) + R(I-1)
       ENDDO
       DO I=1,6
          MD(I)=(R(I+1)-R(I))/2.0+R(I)
       ENDDO
       SAREA(1)=(MD(1)**2.0-R(1)**2.0)*3.141592654
       SAREA(7)=(R(7)**2.0-MD(6)**2.0)*3.141592654
       DO I=2,6
          SAREA(I)=(MD(I)**2.0-MD(I-1)**2.0)*3.141592654
       ENDDO
       STOTAL=0.0
       DO I=1,7
          STOTAL=STOTAL+SAREA(I)
       ENDDO
C*********************************************************************
       DTOTAL=0.0
       DO I=1,7
```

```
         DTOTAL=DTOTAL+(SAREA(I)*GC(I))
      ENDDO
C*********************************************************************
      CDI=DTOTAL/STOTAL
      WRITE (2,90) 'CIRCUMFERENTIAL DISTORTION = ',CDI
90    FORMAT (/,1X,A,F10.6,A)
      END
C*********************************************************************
C* END SUBROUTINE FOR P INLET                                        *
C*********************************************************************
C
C*********************************************************************
C* SUBROUTINE FOR 2D INLET                                           *
C*********************************************************************
      SUBROUTINE BINLET(CDI,DATA,OUT)
      REAL G(50,50),CDI,E(50)
      DIMENSION GAV(10),D(50),S(10),GAVLOW(10),GC(10)
      DIMENSION SAREA(10),MD(10),R(10)
      REAL H,A,SLOPE,B,THETA,AREA,LAREA,LH,GAV,GAVLOW,GC
      REAL SAREA,MD,R
      CHARACTER*50 DATA,OUT
      OPEN (UNIT = 10, FILE = 'C:\KMILLER\CDI\DATA\2-ANGLES.TXT')
      OPEN (UNIT = 1, FILE = DATA)
      OPEN (UNIT = 2, FILE = OUT)
C*********************************************************************
      DO I=1,21
         READ (10,*) D(I)
      ENDDO
C*********************************************************************
      DO J=1,42
         READ (1,*) E(J)
      ENDDO
      K=0
      DO J=1,6
         DO I=1,7
            G(I,J) = E(I+(K*7))
         ENDDO
         K=K+1
      ENDDO
      K=2
      DO J=7,10
         DO I=1,7
            G(I,J) = G(I,J-K)
         ENDDO
         K=K+2
      ENDDO
      K=0
      DO J=11,16
         DO I=1,7
            G(I,J) = E(I+(K*7))
         ENDDO
         K=K+1
      ENDDO
      K=2
      DO J=17,20
         DO I=1,7
            G(I,J) = G(I,J-K)
         ENDDO
         K=K+2
      ENDDO
      DO I=1,7
         G(I,21) = G(I,1)
      ENDDO
```

```
      WRITE (2,15) 'DATA'
      WRITE (2,17) 'ANGLE','HUB','TIP'
      DO J=1,21
         WRITE (2,5) D(J),(G(I,J), I=1,7)
      ENDDO
5     FORMAT (F7.2,7F10.6)
15    FORMAT (/1X,A/)
17    FORMAT (1X,A,6X,A,57X,A)
C***********************************************************************
      DO I=1,7
         S(I)=0.0
         DO J=1,20
            H=ABS(D(J)-D(J+1))
            A=(ABS(G(I,J)-G(I,J+1)))*0.5*H
            B=H*G(I,J)
            IF (G(I,J).GT.G(I,J+1)) THEN
              S(I)=S(I)-A+B
            ENDIF
            IF (G(I,J).LT.G(I,J+1)) THEN
              S(I)=S(I)+A+B
            ENDIF
              IF (G(I,J).EQ.G(I,J+1)) THEN
            S(I)=S(I)+B
            ENDIF
         ENDDO
         GAV(I)=S(I)/360.0
      ENDDO
      WRITE (2,25) 'AVERAGE'
25    FORMAT (/,1X,A,/)
      DO I=1,7
         WRITE (2,30) 'GAV(',I,') =',GAV(I)
      ENDDO
30    FORMAT (1X,A,I1,A,F10.7)
C***********************************************************************
      LH=0.0
      LAREA=0.0
      WRITE (2,70) 'AVERAGE OF POINTS BELOW THE AVERAGE'
      DO I=1,7
         DO J=1,20
            IF ((G(I,J).GT.GAV(I)).AND.(G(I,J+1).LT.GAV(I))) THEN
              SLOPE=(G(I,J)-G(I,J+1))/(D(J)-D(J+1))
              B=G(I,J)-(SLOPE*D(J))
              THETA=(GAV(I)-B)/SLOPE
              H=ABS(THETA-D(J+1))
              LH=LH+H
              A=G(I,J+1)*H
              B=((GAV(I)-G(I,J+1))*H)*0.5
              AREA=A+B
              LAREA=LAREA+AREA
            ENDIF
            IF ((G(I,J).LT.GAV(I)).AND.(G(I,J+1).GT.GAV(I))) THEN
              SLOPE=(G(I,J)-G(I,J+1))/(D(J)-D(J+1))
              B=G(I,J)-(SLOPE*D(J))
              THETA=(GAV(I)-B)/SLOPE
              H=ABS(THETA-D(J))
              LH=LH+H
              A=G(I,J)*H
              B=((GAV(I)-G(I,J))*H)*0.5
              AREA=A+B
              LAREA=LAREA+AREA
            ENDIF
            IF ( ( G(I,J).LE.GAV(I) ).AND.( G(I,J+1).LE.GAV(I) )
     *      .AND.( G(I,J).GT.G(I,J+1) ) )  THEN
```

```
              H=ABS(D(J+1)-D(J))
              LH=LH+H
              A=G(I,J+1)*H
              B=((ABS(G(I,J)-G(I,J+1)))*H)*0.5
              AREA=A+B
              LAREA=LAREA+AREA
            ENDIF
            IF ( ( G(I,J).LE.GAV(I) ).AND.( G(I,J+1).LE.GAV(I) )
     *      .AND.( G(I,J).LT.G(I,J+1) ) ) THEN
              H=ABS(D(J+1)-D(J))
              LH=LH+H
              A=G(I,J+1)*H
              B=((ABS(G(I,J)-G(I,J+1)))*H)*0.5
              AREA=A-B
              LAREA=LAREA+AREA
            ENDIF
         ENDDO
         GAVLOW(I)=LAREA/LH
         WRITE (2,60) 'GAVLOW(',I,') =',GAVLOW(I)
60    FORMAT (1X,A,I1,A,F10.7)
         LAREA=0.0
         LH=0.0
      ENDDO
      WRITE (2,70) 'CIRCUMFERENTIAL DISTORTION ELEMENT'
70    FORMAT (/,1X,A,/)
      C=0.0
      DO I=1,7
         GC(I)=(GAV(I)-GAVLOW(I))/GAV(I)
         WRITE (2,80) 'GC/G(',I,') =',GC(I)
      ENDDO
80    FORMAT (1X,A,I1,A,F12.9)
C*********************************************************************
      R(1)=0.9
      R(7)=2.05
      DO I=2,6
         R(I)=((R(7)-R(1))/6.0) + R(I-1)
      ENDDO
      DO I=1,6
         MD(I)=(R(I+1)-R(I))/2.0+R(I)
      ENDDO
      SAREA(1)=(MD(1)**2.0-R(1)**2.0)*3.141592654
      SAREA(7)=(R(7)**2.0-MD(6)**2.0)*3.141592654
      DO I=2,6
         SAREA(I)=(MD(I)**2.0-MD(I-1)**2.0)*3.141592654
      ENDDO
      STOTAL=0.0
      DO I=1,7
         STOTAL=STOTAL+SAREA(I)
      ENDDO
C*********************************************************************
      DTOTAL=0.0
      DO I=1,7
         DTOTAL=DTOTAL+(SAREA(I)*GC(I))
      ENDDO
C*********************************************************************
      CDI=DTOTAL/STOTAL
      WRITE (2,90) 'CIRCUMFERENTIAL DISTORTION = ',CDI
90    FORMAT (/,1X,A,F10.6,A)
      END
C*********************************************************************
C* END SUBROUTINE FOR 2D INLET                                       *
C*********************************************************************
C
```

```
C*********************************************************************
C* SUBROUTINE FOR TEST CASES                                         *
C*********************************************************************
      SUBROUTINE TEST(CDI,DATA,OUT)
      REAL G(50),CDI,E(50),D(50),S
      REAL H,A,SLOPE,B,THETA,AREA,LAREA,LH,GAV,GAVLOW,GC
      CHARACTER*50 DATA,OUT
      OPEN (UNIT = 1,FILE = DATA)
      OPEN (UNIT = 2,FILE = OUT)
C*********************************************************************
      DO I=1,33
         D(I)=(I-1)*11.25
      ENDDO
C*********************************************************************
      DO I=1,33
         READ (1,*) G(I)
      ENDDO
      WRITE (2,15) 'DATA'
      WRITE (2,17) 'ANGLE'
      DO J=1,33
         WRITE (2,5) D(J),G(J)
      ENDDO
5     FORMAT (F7.2,F10.6)
15    FORMAT (/1X,A/)
17    FORMAT (1X,A)
C*********************************************************************
      S=0.0
      DO J=1,32
            H=ABS(D(J)-D(J+1))
            A=(ABS(G(J)-G(J+1)))*0.5*H
            B=H*G(J)
            IF (G(J).GT.G(J+1)) THEN
              S=S-A+B
            ENDIF
            IF (G(J).LT.G(J+1)) THEN
              S=S+A+B
            ENDIF
              IF (G(J).EQ.G(J+1)) THEN
            S=S+B
            ENDIF
      ENDDO
      GAV=S/D(33)
      WRITE (2,25) 'AVERAGE'
25    FORMAT (/,1X,A,/)
      WRITE (2,30) 'GAV =',GAV
30    FORMAT (1X,A,F10.7)
C*********************************************************************
      LH=0.0
      LAREA=0.0
      WRITE (2,70) 'AVERAGE OF POINTS BELOW THE AVERAGE'
      DO J=1,32
            IF ((G(J).GT.GAV).AND.(G(J+1).LT.GAV)) THEN
              SLOPE=(G(J)-G(J+1))/(D(J)-D(J+1))
              B=G(J)-(SLOPE*D(J))
              THETA=(GAV-B)/SLOPE
              H=ABS(THETA-D(J+1))
              LH=LH+H
              A=G(J+1)*H
              B=((GAV-G(J+1))*H)*0.5
              AREA=A+B
              LAREA=LAREA+AREA
            ENDIF
            IF ((G(J).LT.GAV).AND.(G(J+1).GT.GAV)) THEN
```

```
            SLOPE=(G(J)-G(J+1))/(D(J)-D(J+1))
            B=G(J)-(SLOPE*D(J))
            THETA=(GAV-B)/SLOPE
            H=ABS(THETA-D(J))
            LH=LH+H
            A=G(J)*H
            B=((GAV-G(J))*H)*0.5
            AREA=A+B
            LAREA=LAREA+AREA
          ENDIF
          IF ( ( G(J).LE.GAV ).AND.( G(J+1).LE.GAV )
     *    .AND.( G(J).GT.G(J+1) ) )  THEN
            H=ABS(D(J+1)-D(J))
            LH=LH+H
            A=G(J+1)*H
            B=((ABS(G(J)-G(J+1)))*H)*0.5
            AREA=A+B
            LAREA=LAREA+AREA
          ENDIF
          IF ( ( G(J).LE.GAV ).AND.( G(J+1).LE.GAV )
     *    .AND.( G(J).LT.G(J+1) ) ) THEN
            H=ABS(D(J+1)-D(J))
            LH=LH+H
            A=G(J+1)*H
            B=((ABS(G(J)-G(J+1)))*H)*0.5
            AREA=A-B
            LAREA=LAREA+AREA
          ENDIF
      ENDDO
      GAVLOW=LAREA/LH
      WRITE (2,60) 'GAVLOW =',GAVLOW
60    FORMAT (1X,A,F10.7)
      WRITE (2,70) 'CIRCUMFERENTIAL DISTORTION ELEMENT'
70    FORMAT (/,1X,A,/)
      CDI=(GAV-GAVLOW)/GAV
      WRITE (2,90) 'CIRCUMFERENTIAL DISTORTION = ',CDI
90    FORMAT (/,1X,A,F10.6)
      END
C*********************************************************************
C* END SUBROUTINE FOR TEST CASES                                     *
C*********************************************************************
```

# Appendix D: Acoustic Measurement Plane Comparison

The acoustic results presented in this thesis represent the inlet's acoustic radiation field on a single measurement plane. However, the radiation fields are three-dimensional in nature. Each acoustic plane had to be measured individually, in order to verify that of all the measurement planes were similar. The axisymmetric P inlet was measured on two planes (See Figure 3.16 in Section 3.5.2), the horizontal/vertical plane (0°) and the mid plane (45°). The bifurcated two-dimensional inlet was measured on three planes (See Figure 3.17 in Section 3.5.2), the vertical plane (0°), mid plane (45°), and the horizontal plane (90°).

Figure D.1 shows the two acoustic measurement planes of the P inlet at the approach condition (60 PNC). The tone and overall sound pressure levels have similar trends with a maximum variation of 6 dB in each plot. The takeoff condition (88 PNC) is compared in Figure D.2 and shows the same conclusion as the approach condition. The maximum variation in the tone is 5 dB and the overall is 2 dB. This illustrated that the P inlet measurements were consistent throughout the three-dimensional acoustic field.

Figures D.3 and D.4 illustrate the three measurement planes of the 2D inlet. At the approach condition (60 PNC), the tone and overall sound pressure levels varied by a maximum of 11 dB and 7 dB, respectively. For the takeoff condition (88 PNC), the tone differed by 10 dB and the overall by 8 dB. Even though these are large differences at one angular measurement position, the overall comparison between the 2D inlet and P inlet

does not change. The trend for all the plots comparing the acoustic planes of the 2D inlet are similar. It is evident from these measurements that the three-dimensional acoustic fields are consistently similar in nature.

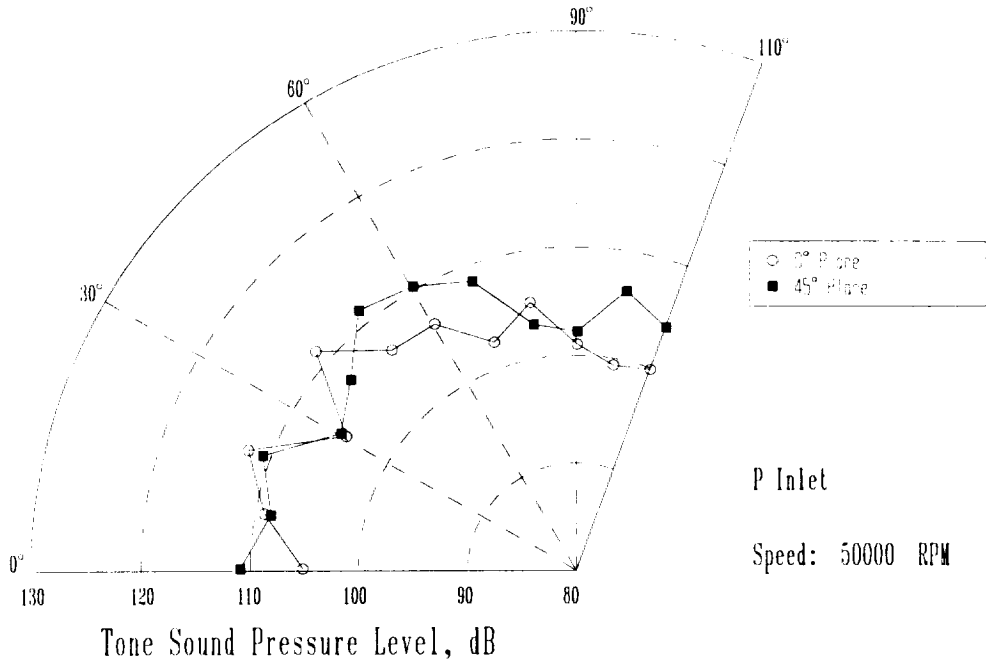


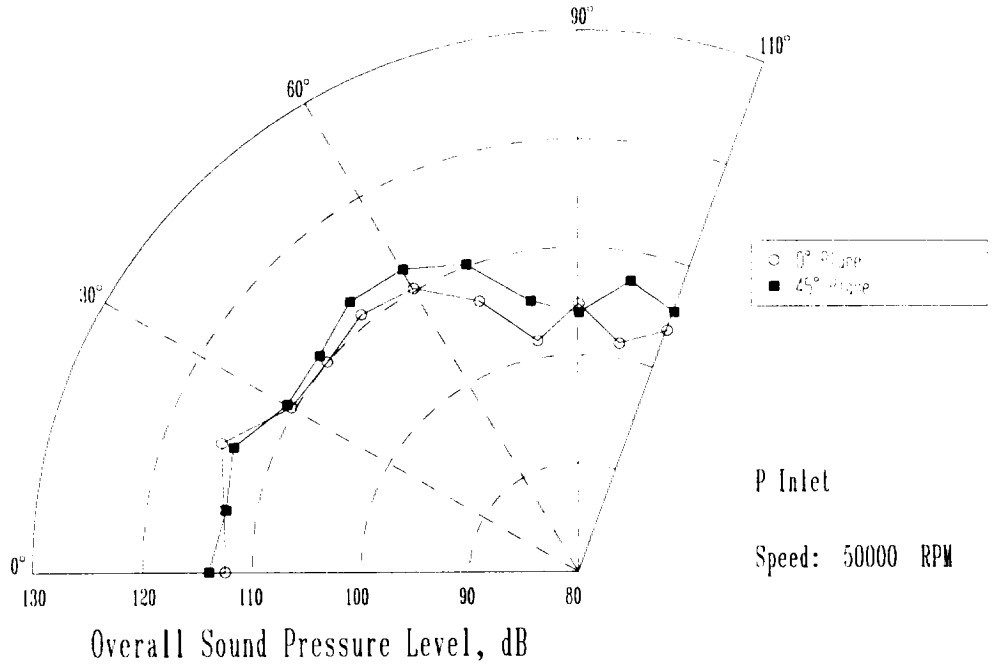


**Figure D.1 Directivity Plots of the P Inlet at 60 PNC Comparing Acoustic Planes**

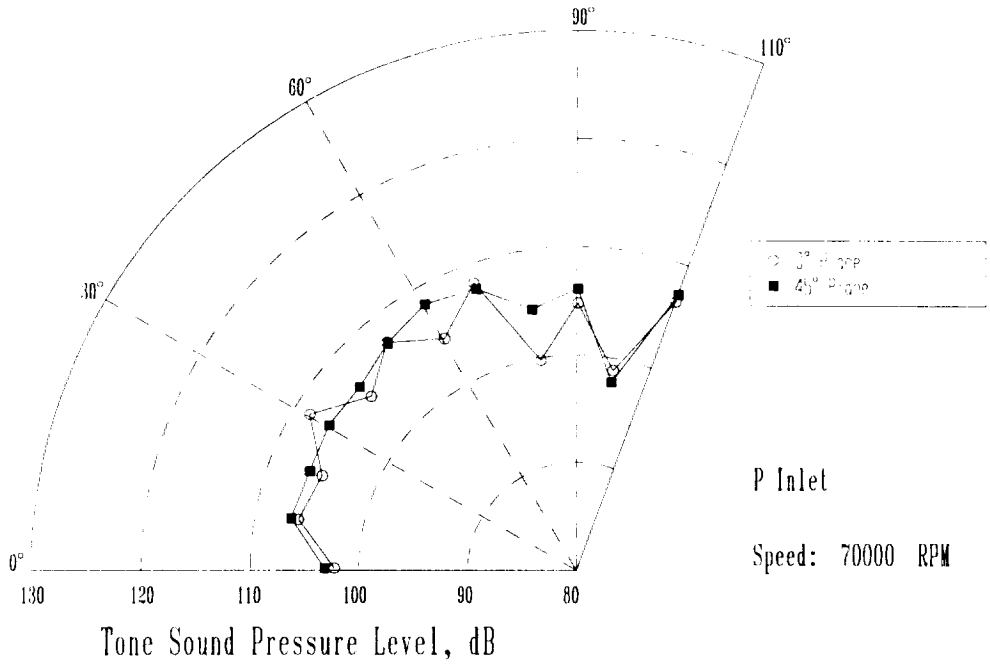


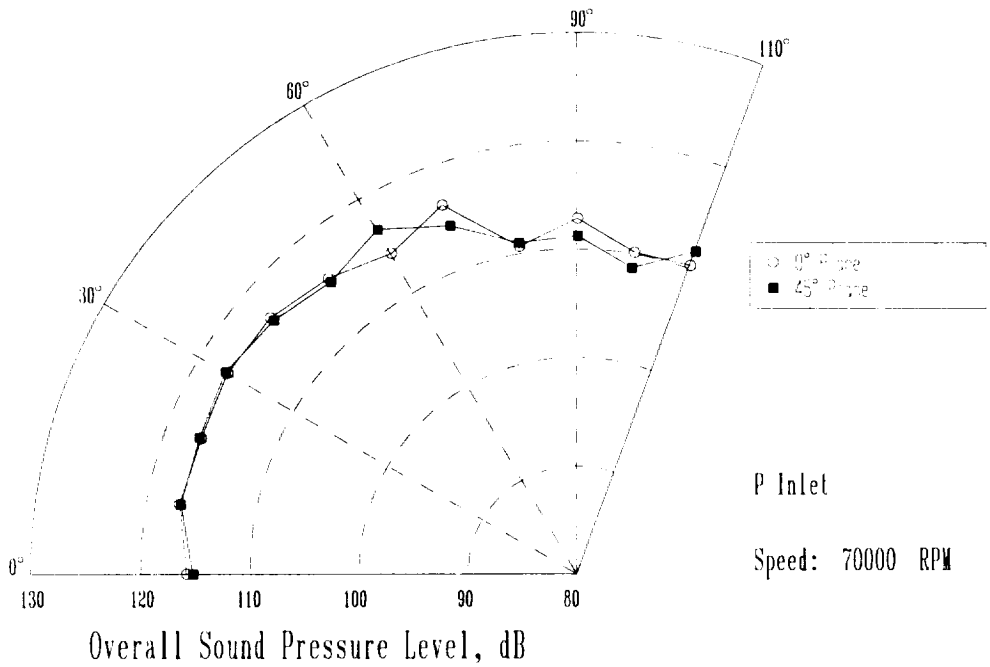


**Figure D.2 Directivity Plots of the P Inlet at 88 PNC Comparing Acoustic Planes**

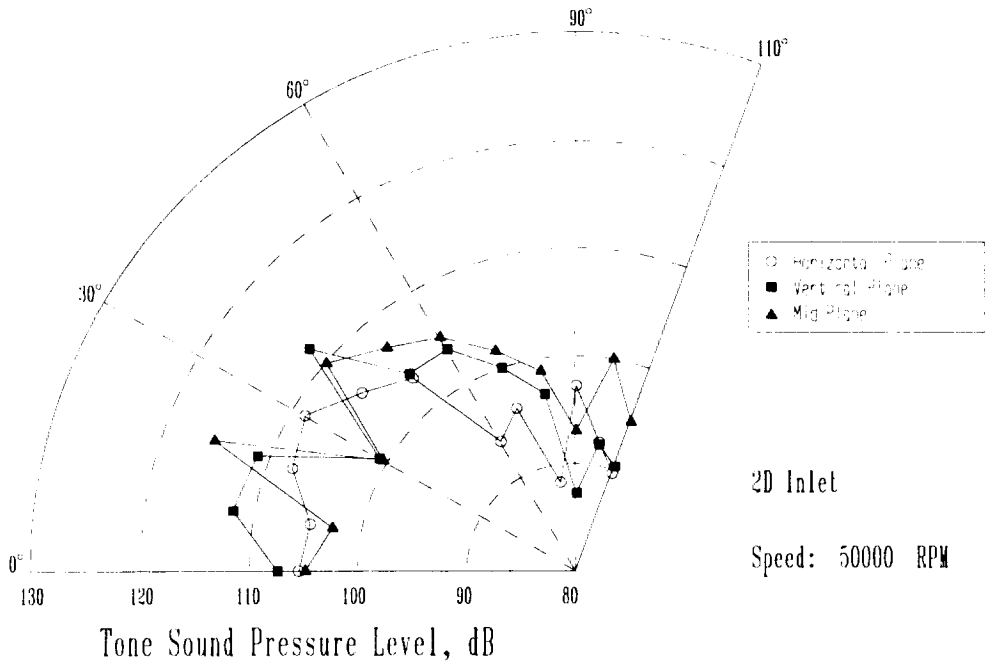


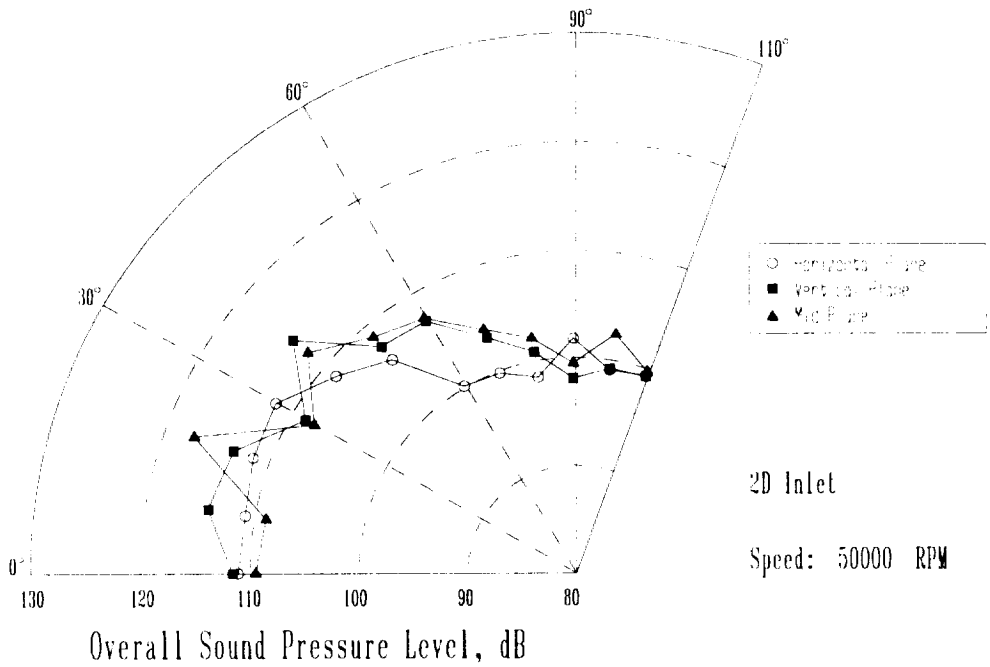


**Figure D.3 Directivity Plots of the 2D Inlet at 60 PNC Comparing Acoustic Planes**

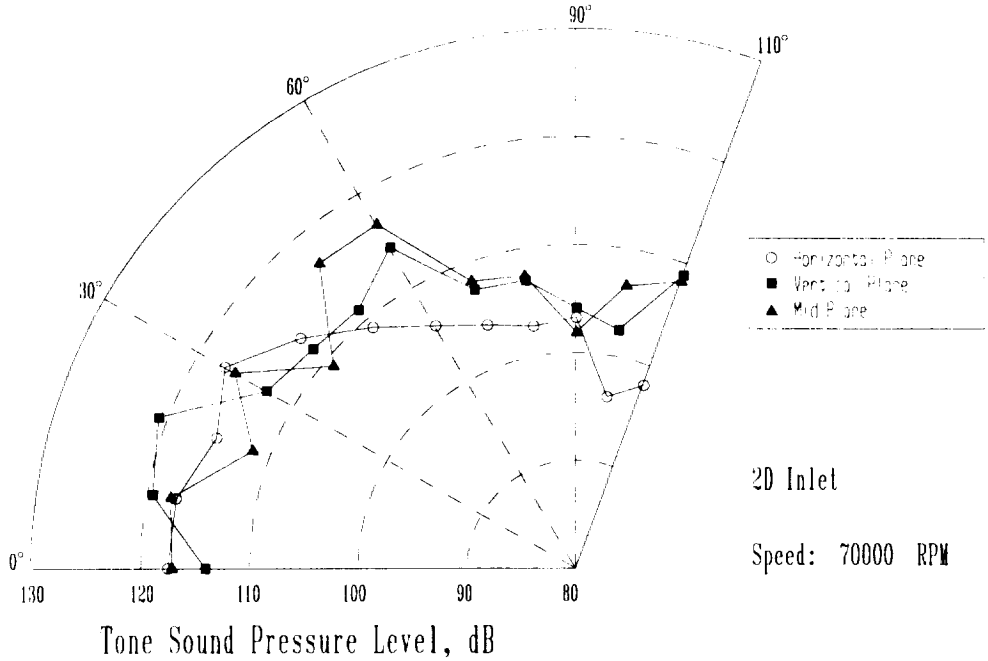


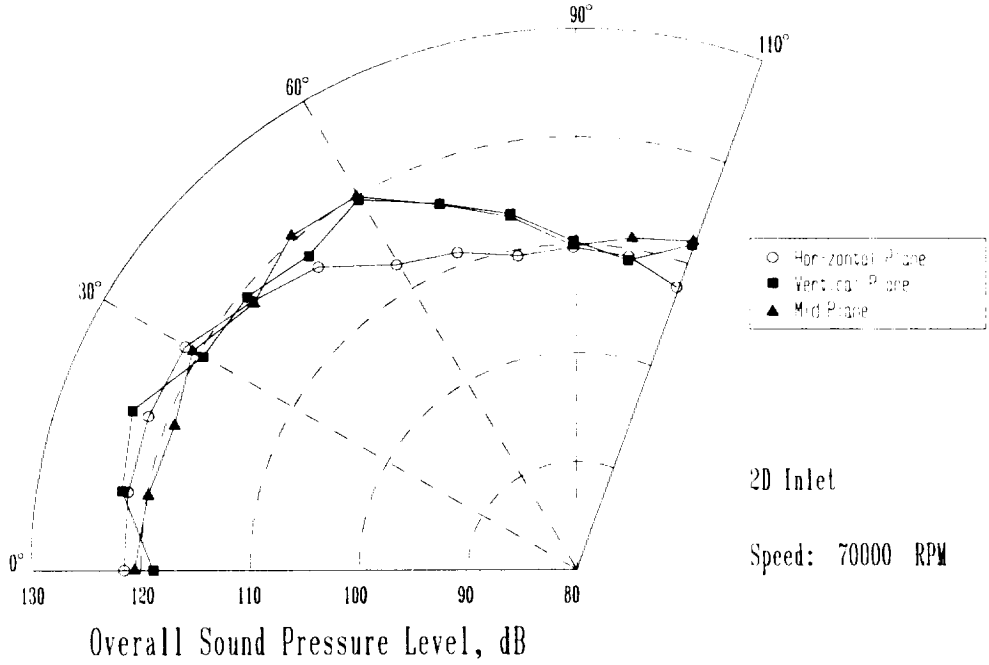


**Figure D.4 Directivity Plots of the 2D Inlet at 88 PNC Comparing Acoustic Planes**

# References


Aerospace Recommended Practice 1420, "Gas Turbine Engine Inlet Flow Distortion Guidelines," Society of Automotive Engineers, Inc., SAE International, March 1978.

Anderson, B. H., Kapoor, K., "A Study on Bifurcated Transitioning S-Ducts for High Speed Inlet Application," AIAA 94-2812, June 1994.

Ball, W.H., Pickup, N., "Low Speed Performance and Acoustic Test of an Axisymmetric Supersonic Inlet - Phase One Tests with Auxiliary Doors Closed," NASA CR-172390, October 1984.

Carden, R. O., "Nation's Largest Aircraft Firms Team Up to Develop SST Systems," The Virginia Engineer, November 1994, Vol. 33, pp. 11-12.

Criger, J. L., Copeland W. L. "Noise Studies of Inlet-Guide-Vane-Rotor Interaction of a Single Stage Axial Flow Compressor," NASA TN D-2962. September 1965.

Cumpsty, N. A., Lowrie, B.W., "The Cause of Tone Generation by Aero-Engine Fans at High Subsonic Tip Speeds and the Effect of Forward Speed," ASME 73-WA/GT-4, March 1974.

Detwiler, K. P., "Reduced Fan Noise Radiation from a Supersonic Inlet," Masters Thesis, Virginia Polytechnic Institute and State University, April 1993.

Detwiler, K., Yuan, Z., Ng, W. F., "Experimental and Numerical Studies of the Aeroacoustics of Axisymmetric Supersonic Inlets," AIAA 93-4372, October 1993.

Dunn, D. G., Peart, N. A., "Aircraft Noise Source and Contour Estimation," NASA CR-114649, July 1973.

Homicz, G. F., Lordi, J. A., "A Note on the Radiative Directivity Patterns of Duct Acoustic Modes," Journal of Sound and Vibration, December 1975 vol. 41(3) , pp. 283-290.

Feiler, C. E., Groeneweg, J. F., "Summary of Forward Velocity Effects on Fan Noise," AIAA 77-3510, 1971.

Kinsler, L. E., Frey, A. R., Coppens, A. B., Sanders, J. V., "Fundamentals of Acoustics," John Wiley & Sons, Inc., 3rd edition, 1982.

Kozak, J. D., "3-D Flow Calculation of a Bifurcated 2D Supersonic Engine Inlet at Takeoff," Masters Thesis, Virginia Polytechnic Institute and State University, August 1995.

Mathews, D. C., Nagel R. T., "Inlet Geometry and Axial Mach Number Effects on Fan Noise Propagation," AIAA 73-1022, October 1973.

Merriman, J. E., Good, R. C., "Effect of Forward Motion of Fan Noise," AIAA 75-464, 1975.

Model 460 Turbofan Propulsion Simulator Products Specification, Tech Development Inc., U.S. Patent 3434679.

Mugridge, B. D., "Axial Flow Fan Noise Caused by Inlet Flow Distortion," Journal of Sound and Vibration, August 1975, pp. 497-512.

NASA Report C-71-3510, 1971.

Nuckolls, W. E., Ng, W. F., "Fan Noise Reduction from a Supersonic Inlet during Simulated Aircraft Approach," ASME 93-gt-279, May 1993.

Oates, G. C. "Aerothermodynamics of Aircraft Engine Components," American Institute of Aeronautics and Astronautics, 1st edition, 1985, pp. 477-584.

Pande, A., Ng, W. F., "Effects of Struts on the aeroacoustics of Axisymmetric Supersonic Inlets," Virginia Polytechnic Institute and State University, November 1994.

Pande, A., Ng, W. F., "Effect of Struts on the Aeroacoustics of Axisymmetric Supersonic Inlets: Part I--Experimental Results," AIAA 95-2887, July 1995.

Saunders, J. D., Keith, T. G., "Results from Computational Analysis of a Mixed Compression Supersonic Inlet," AIAA 91-2581, June 1991.

Smelter, D. B., Sorensen, N. E., "Tests of a Mixed Compression Axisymmetric Inlet with Large Transonic Mass Flow at Mach Numbers 0.6 to 2.65," NASA TN D-6971, December 1972.

Smelter, D. B., Sorensen, N. E., "Analytic and Experimental Performance of Two Isentropic Mixed Compression Axisymmetric Inlets at Mach Numbers 0.8 to 2.65," NASA TN D-7320, June 1973.

Sorensen, N. E., Smelter, D. B., "Performance Estimate for a Supersonic Axisymmetric Inlet System," AIAA 72-45, January 1972.

Sorensen, N. E., Bencze, D. P., "Possibilities for Improved Supersonic Inlet Performance," AIAA 73-1271, November 1973.

Thomas, R. H., Gerhold, C. H., Farrasat, F., Santa Maria, O. L., Nuckolls, W. E., De Vilbiss, D. W., "Far Field Noise of the 12 inch Advanced Ducted Propeller Simulator," AIAA 95-0722, January 1995.

Tyler, J. M., Sofrin, T. G., "Axial Compressor Noise Studies," SAE Transactions, Vol. 70, 1962.

Wagner, R., "Aeroacoustics of the Bifurcated 2D Supersonic Inlet," Masters Thesis, Virginia Polytechnic Institute and State University, December 1994.

Wasserbauer, J. F., Cubbison, R. W., Trefny, C. J., "Low Speed Performance of a Supersonic Axisymmetric Mixed Compression Inlet with Auxiliary Inlets," AIAA 83-1414, 1983.

Woodward, R. P., Glaser, F. W., Lucas, J. G., "Low Flight Speed Acoustic Results for a Supersonic Inlet with Auxiliary Inlet Doors," AIAA 83-1415, June 1983.